Netherlands Enterprise Agency

Geotechnical Report Synthetic CPT Profiles

Hollandse Kust (west) Wind Farm Zone

>> *Sustainable. Agricultural. Innovative. International.*

Geotechnical Report
Synthetic CPT Profiles
Hollandse Kust (west) Wind Farm Zone
Dutch Sector, North Sea

Client Reference No. WOZ2190152
Fugro Document No. P904711/08

Issue 3

Rijksdienst voor Ondernemend Nederland

Rijksdienst voor Ondernemend Nederland (RVO)

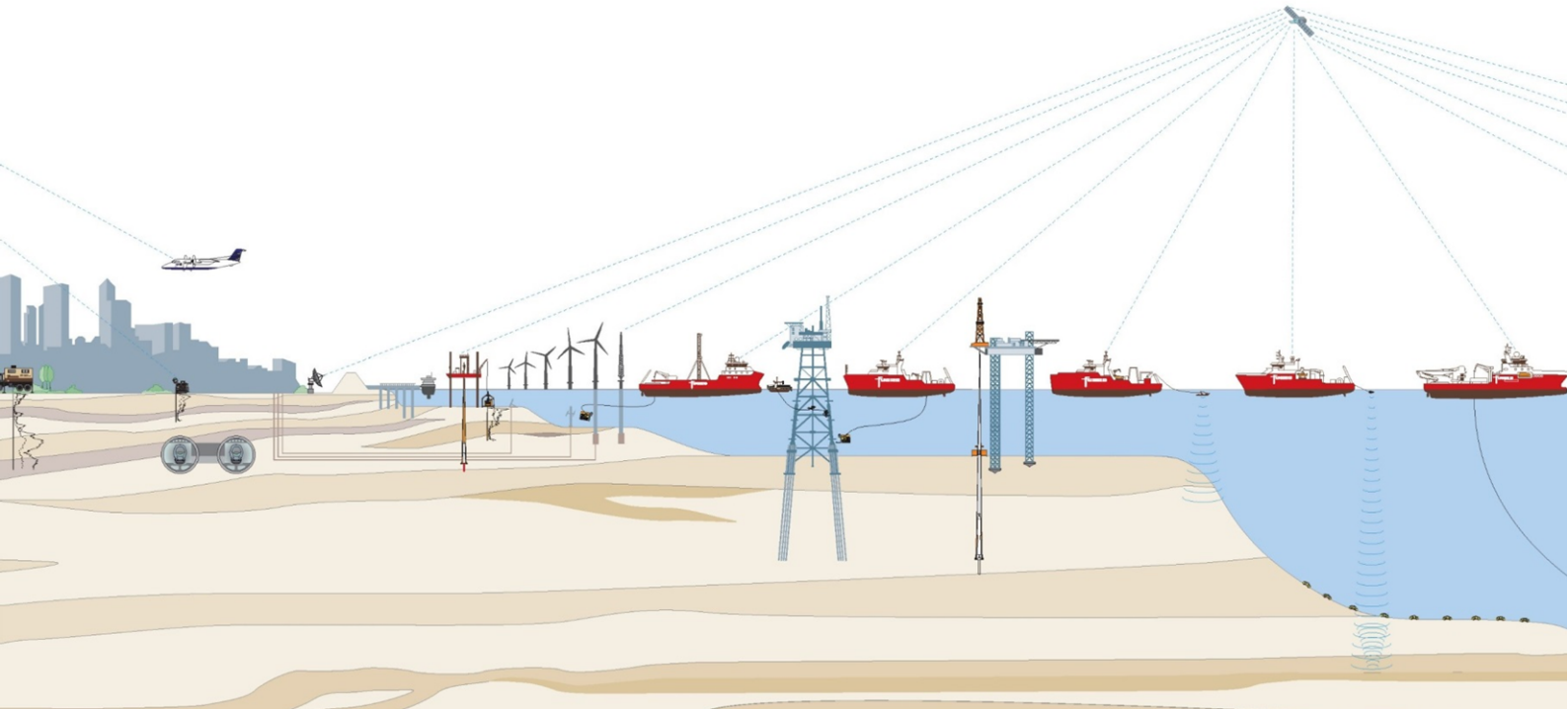

Geotechnical Report
Synthetic CPT Profiles
Hollandse Kust (west) Wind Farm Zone
Dutch Sector, North Sea

Client Reference No. WOZ2190152
Fugro Document No. P904711/08

Issue 3

Client	Rijksdienst voor Ondernemend Nederland (RVO)
Client Contact	F. van Erp
Client Address	Croeselaan 15 3521 BJ UTRECHT The Netherlands

Rijksdienst voor Ondernemend Nederland

Fugro Project Lead	J. Peuchen – Principal Geotechnical Engineer

Issue	Document Status	Date
3	Revised Final	14-Oct-2020
2	Final	9-Oct-2020
1	Complete	31-July-2020

CONTENTS

Page

MAIN TEXT:

1.	**OVERVIEW**	**1**
1.1	Purpose of Report	1
1.2	Scope of Report	1
1.3	Report Format	1
1.4	Project Responsibilities and Use of Report	2
2.	**STUDY APPROACH**	**3**
2.1	General	3
2.2	Premises and Constraints	4
2.3	CPT Parameters	5
2.4	Geotechnical Ground Model	6
3.	**RESULTS – SYNTHETIC CPT PROFILES**	**7**
3.1	Use of Results	7
3.2	Comments on Results	7
3.3	Opportunities for Enhancement	8

ISSUE 94

FNLM-GEO-REP-001

© Fugro 1998-2019

APPENDICES

APPENDIX A: PLATES REFERENCED IN MAIN TEXT
APPENDIX B: TNO REPORT
APPENDIX C: DESCRIPTIONS OF METHODS AND PRACTICES
APPENDIX D: SUPPLEMENTARY INFORMATION ABOUT DOCUMENT

1. OVERVIEW

1.1 Purpose of Report

The Netherlands Enterprise Agency (Rijksdienst voor Ondernemend Nederland, RVO), henceforth referred to as 'client', has requested Fugro to perform a geotechnical site investigation of the Hollandse Kust (west) Wind Farm Zone (WFZ). The Hollandse Kust (west) WFZ is located in the Dutch Sector of the North Sea, approximately 51 km from the coastline of Noord-Holland (refer to Plate A1).

The objective of the geotechnical site investigation and associated laboratory testing programme is to:

- Further develop and update the geological/ geophysical model for the Hollandse Kust (west) WFZ;
- Determine the vertical and lateral variation in seabed conditions;
- Provide relevant geotechnical data for the design of the Hollandse Kust (west) WFZ including, but not limited to, foundations and cables.

This report presents synthetic (predicted) cone penetration test (CPT) profiles that are supplementary to the geotechnical parameters report listed on Plate A2. The provision of synthetic CPT profiles is novel to industry and can potentially provide added value to pile foundation design of offshore wind turbines at the Hollandse Kust (west) WFZ.

1.2 Scope of Report

This report is one of a set of Fugro reports (refer to "List of Project Reports" on Plate A4). This particular report presents 1,509,783 synthetic CPT profiles for the Hollandse Kust (west) Wind Farm Zone (HKW WFZ).

The synthetic CPT profiles are for the same area (Plate A1) as considered for the companion geotechnical parameters report, i.e. Hollandse Kust (west) Geotechnical Investigation Area (HKW GIA). This area is selected within Hollandse Kust (west) Designated Wind Farm Zone (Plate A1). In this report, the Hollandse Kust (west) Geotechnical Investigation Area is referred to as the HKW WFZ or "the site". The site excludes existing jacket platforms and the related safety zones.

The synthetic CPT profiles cover the depth range of 2 m to to 50 m below seafloor (BSF). This depth range corresponds broadly with an expected depth range of primary interest for monopiles and jacket piles considered for the companion geotechnical parameters report.

1.3 Report Format

The principal sections of this report are the Main Text and Appendices A and B. This specific report also has companion digital deliverables:

- SEG-Y files for synthetic CPT profiles;
- Text file comprising synthetic CPT SEG-Y header information;
- pdfs of the SEG-Y files (i.e. with prediction results, quality indicators, and geological units);
- ascii files of synthetic CPT profiles of every 100th common depth point (CDP) location along the 2D UHR MCS lines in the site;
- GIS files, including a shapefile with the location of every 100th CDP along the 2D UHR MCS lines.

Comments are as follows.

- Section 2 describes the general study approach;
- Section 3 and Appendix B present the principal results (synthetic CPT profiles), comments on results and guide for use;
- Plates in Appendix A correspond to Main Text sections;
- Appendix C presents general practice statements and terminology that will be familiar to expert users of the types of information presented in this report;
- Appendix D provides supplementary information about this report, particularly document issue control and a quality management record.

1.4 Project Responsibilities and Use of Report

This report presents information according to a project specification determined and monitored by the client. The project specification included specific constraints, particularly on scope and schedule. Section 3 includes suggestions for further data analysis and prediction of geotechnical parameters from integrated geosciences.

This report uses and summarises information from sources listed on Plate A2. The reader should consult the source information for details. Understanding of site conditions improves upon further data analysis and interpretation. This means that some of the source interpretations may be superseded by information presented in this report.

The report was prepared in accordance with:

- Contract WOZ2190153 between Rijksdienst voor Ondernemend Nederland (RVO) and Fugro Netherlands Marine B.V., dated 1 March 2019;
- Contract supplement 20200109_HKW_Geotech_Fugro_VO-14 (03).

The report and companion digital deliverables were prepared by a team of specialists from Fugro, TNO and Delft University of Technology (Appendices B and D). The valuable input from RVO's team of specialists and consultants is acknowledged.

Read this report in its entirety. Particularly, take careful note of "Use of Geodata and Advice", presented in Appendix C. It is emphasized that the presented data are novel to industry and the reader is referred to ISO/DIS 19901-10:2018 Marine Geophysical Investigations, Chapter 10 for further specific guidance on use of *predicted* geotechnical data.

Fugro understands that this report will be used for the purpose described in this Main Text section. That purpose was a significant factor in determining the scope and level of the services. Results must not be used if the purpose for which the report was prepared or the client's proposed development or activity changes. Results may possibly suit alternative use. Suitability must be verified.

2. STUDY APPROACH

2.1 General

The general study approach is according to ISO (2018). Plates A3 and A4 summarise the principal features. Figure 1 presents a general workflow diagram, where “enhanced zonation” represents the focus of this report.

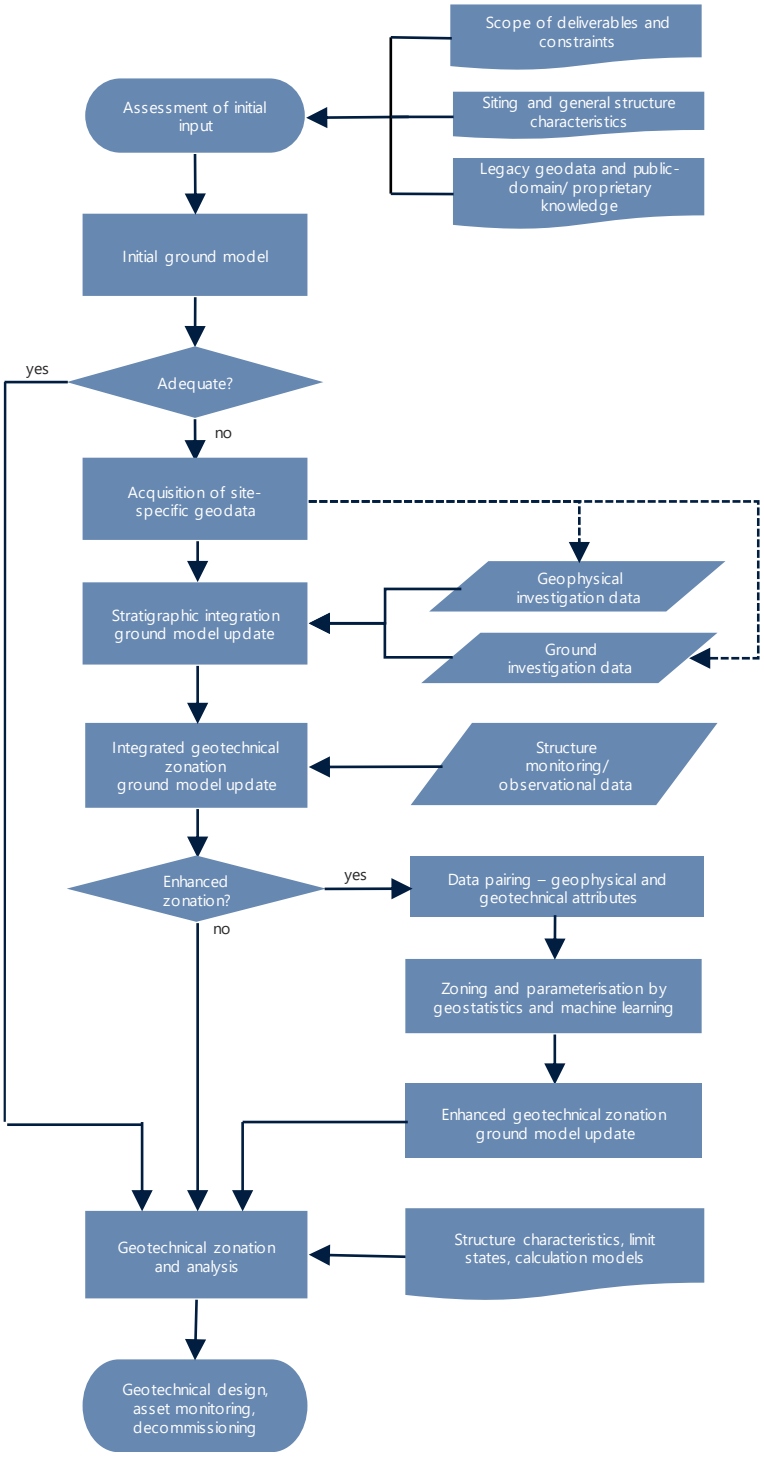

Figure 1: General procedure

2.2 Premises and Constraints

The study approach considered the following premises, including constraints on scope and schedule:

- Synthetic CPT profiles for the CDP locations of the available ultra-high resolution multichannel seismic reflection (2D UHR MCS) data within the HKW WFZ;
  - Position coordinates are according to the 2D UHR MCS data, with vertical datum (seafloor) as 2D UHR MCS seafloor pick;
  - Inclusion of approximate indicator for prediction quality of each predicted CPT data point, see Appendix B for details;
  - No synthetic CPTs are presented for the available seismic reflection data acquired by 2D UHR single channel and subbottom profiler systems;
- Synthetic CPT profiles for the depth range 2 m to 50 m BSF at a vertical data point spacing of 0.1 m;
  - The exclusion of the depth range 0 m to 2 m BSF avoids specific considerations for partial embedment effects for CPT data (refer to Appendix C, documents titled “Cone Penetration Test” and “Cone Penetration Test Interpretation”);
  - The depth range 0 m to 0.5 m BSF is outside the interpretable limits of 2D UHR MCS data (refer to Appendix C, document “Marine Reflection Seismics”);
  - Note that soils within the depth range 0 m to 2 m BSF can be subject to seabed mobility, as described in the geotechnical parameters report;
  - The selected data point spacing of 0.1 m primarily considers resolution of the available 2D UHR MCS data, averaging effects in CPT profiling and user accessibility to the large volume of synthetic CPT data;
- Prediction of a single CPT parameter, modified net cone resistance $q_n{}^*$;
  - The $q_n{}^*$ parameter serves as a primary parameter from which multiple well-known CPT parameters can be derived, as described further below;
  - The exclusion of predictions of CPT sleeve friction f_s and pore pressure u_2 (and related and/or combined CPT parameters) implies inevitable approximations, particularly when considering use of CPT data such as described in Appendix C, document “Cone Penetration Test Interpretation”;
- Use of selected CPT data available from the geotechnical parameters report (Plate A2);
  - The selection of CPT data was limited to seafloor (non-drilling) piezocone penetration tests, e.g. excluded CPT data obtained by vessel drilling deployment, seismic cone penetration tests (SCPTs) and temperature cone penetration tests (TCPTs);
  - The CPT data files included CPT-based correlations with geotechnical parameters, as used for the geotechnical parameters report.
  - Data conditioning was done as part of input preparation, as required for (i) achieving a data point spacing of 0.1 m (instead of 0.02 m), by applying a moving average algorithm over 0.1 m and (ii) for provision of $q_n{}^*$ data;
  - No further re-processing of data, e.g. no post-processing of CPT profiles for thin-layer corrections (refer to geotechnical parameters report, Plate A2);
  - Horizontal position estimate (for spatial data points) in the order of +/- 2 m;

- Use of 2D UHR MCS data as available from the geological ground model report (Plates A5 and A6);
  - Data conditioning was done as required for extraction of 2D UHR MCS attributes (Refer to Appendix B);
  - No re-processing of data and no specific analysis for the seafloor-multiples zone;
  - Seafloor as vertical datum was maintained according to the seafloor pick for the UHR MCS data, i.e. no integration with other bathymetric data;
  - Retention of the 2D UHR MCS velocity model for time-to-depth conversion;
  - Horizontal position estimate (for spatial data points) in the order of +/- 3 m;
- Data pairing and training of machine learning (ML) model;
  - Large element of existing scripting and algorithms, with no significant manual intervention;
  - Regression-type of ML (convolutional neural network) selected for high-level ML training, with checks by other ML models (refer to Appendix B for details);
  - CPT profiles for ML training were limited to one (deepest) seafloor CPT profile per location cluster (refer to Plates A5 and A6 and Appendix B) for which data above 2 m BSF and (where applicable) below 50 m BSF were clipped;
  - Extraction of seismic attributes for a 2D UHR MCS position that is closest to a CPT position for training (refer to Appendix B);
  - ML input includes selected information from the geological ground model, further described below;
- Post-processing and further interpretation
  - Post-processing steps, including quality indicators for prediction, are described in Appendix B;
  - The presented results allow post-processing and further interpretation; suggestions are included in Section 3.

2.3 CPT Parameters

The synthetic CPT profiles present $q_n{}^*$, which approximates net cone resistance q_n. The parameter $q_n{}^*$is defined as $q_n{}^* = q_c - 0.01z(a + 0.9)$ in MPa, where q_c is cone resistance in MPa, a is net area ratio (dimensionless) and z is depth below seafloor in metres. The definition of $q_n{}^*$ considers $a = 0.58$, corresponding to a of the cone penetrometers used for the seafloor CPTs selected for training.

Note that cone resistance depends on cone penetrometer design. If a is not specified otherwise, then it is suggested to estimate q_c by $q_c = q_n{}^* + 0.016z$, considering $a = 0.7$.

The $q_n{}^*$ parameter allows estimation of corrected cone resistance q_t by $q_t = q_n{}^* + 0.019z$.

The $q_n{}^*$ parameter allows estimation of normalized cone resistance $Q_t = q_n/\sigma'_{v0}$ by $Q_t = q_n{}^*/(0.009z)$, where σ'_{v0} is effective in situ vertical stress.

The parameters q_n, q_c, z, a, q_t, Q_t and σ'_{v0} are according to ISO (2014) and further explained in Appendix C, document “Cone Penetration Test”.

2.4 Geotechnical Ground Model

Information from the geotechnical ground model (geotechnical parameters report) was selectively used, i.e. limited to geological soil unit boundaries:

- Soil unit boundaries for the existing CPT profiles for training were used, as available with no adjustment(s);
- The available horizon interpretation of soil unit boundaries was used for site-wide applications, such as for generation of individual synthetic profiles and for soil unit-based estimates of soil density.

Input for the soil density estimates considered a CPT-based correlation for soil density applied to the CPT training profiles. The correlation is according to the Lengkeek method using the default parameters. Appendix C, document “Cone Penetration Test Interpretation” provides further details. The input profiles were combined with the soil unit boundaries and subsequently used in geo-statistical modelling (refer to Appendix B).

Note that the ML input excluded integration cycles for progressively updating of the geotechnical ground model based on initial generation of synthetic CPT profiles.

3. RESULTS – SYNTHETIC CPT PROFILES

3.1 Use of Results

The principal results consist of companion digital deliverables: SEG-Y files for synthetic CPT profiles and a shape file containing the locations of selected CDPs (every 100th CDP along the 2D UHR MCS lines) for which ascii files with synthetic CPT profiles area given. The results are supplementary to and must be used in conjunction of the geotechnical parameters report (Plate A2).

The $q_n{}^*$ parameter allows estimation cone resistance q_c, corrected cone resistance q_t and normalized cone resistance Q_t as described in Section 2. Estimation of other (primary) CPT parameters (i.e. sleeve friction f_s and pore pressure u_2) will require the use of correlations and approximations. No guidance on estimation of f_s and u_2 is given in this report and appropriate caution should be applied.

The SEG-Y files include quality predictors for the data points of the synthetic CPT profiles, as described in Section 2 and Appendix B. The quality predictors provide a broad indication of possible ranges of modified net cone resistance $q_n{}^*$.

The shape file includes position coordinates for the provided synthetic CPT profiles (at every 100th CDP position).

3.2 Comments on Results

The horizontal positioning uncertainty for the synthetic CPT profiles is assessed to be in the order of +/- 3 m, based on the deployed 2D UHR-MCS positioning systems and general uncertainty for points below seafloor derived from geophysical data processing. Background information is given in Appendix C, documents “Positioning Survey and Depth Measurement” and “Marine Reflection Seismics”.

The presented synthetic CPT profiles are presented relative LAT at the time of acquisition of the 2D UHR-MCS reflection data. Note that seafloor levels (relative to LAT) are expected to vary because of seabed mobility. The geological ground model report provides details on seabed mobility. The depth uncertainty (in m BSF) for the presented data points generally increases with depth below seafloor, possibly from a value of about +/- 0.3 m at seafloor to +/- 1.5 m at 50 m BSF.

The quality indicator can provide statistical values for $q_n{}^*$ that fall outside of credible ranges. For example, the quality indicator can provide a statistically calculated value of $q_n{}^* = 0.5$ MPa at 40 m BSF. This low value would be unlikely, based on the understanding of site conditions presented in the geotechnical parameters report. Figure 2 illustrates prediction zones recommended for inspection and checks.

The results within the zone of the seafloor multiple should be used with caution, as described in Appendix B. The document “Marine Reflection Seismics” (refer to Appendix C) includes background information on seafloor multiple.

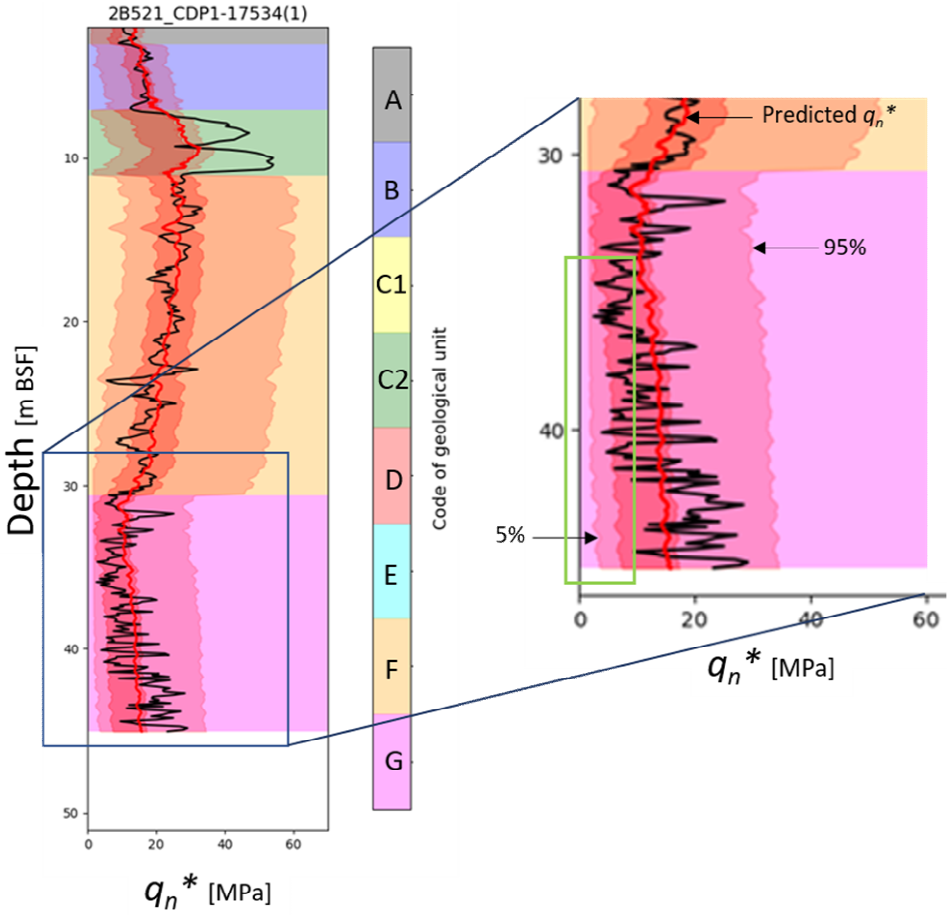

Figure 2: Example q_n* prediction and quality indicators. The green box on the right (enlarged image) illustrates an example of a prediction zone recommended for inspection and checks.

3.3 Opportunities for Enhancement

The premises and constraints summarised in Section 2 provide implicit opportunities for enhancement.

Consideration can be given to prediction of additional parameters, such as shear modulus at small strain G_{max} and soil thermal conductivity k.

The geotechnical parameters report includes a basic voxel ground model. This basic model can be enhanced by stochastic modelling that incorporates the synthetic CPT data (and other data). This could be done site-wide or for specific locations within the site (e.g. wind turbine locations and cable routes).

The quality of prediction of synthetic CPT profiles can be improved by a more integrated approach that considers additional sources of available data, e.g. data derived from sub-bottom profiler survey, single channel seismic reflection, borehole geophysical logging, seismic downhole tests (seismic cone penetration tests) and laboratory tests.

The data pairing approach described in Section 2 includes a large element of existing scripting and algorithms. Data pairing can be improved by adding manual intervention, such as:

- Manual picking of 2D UHR MCS data for CPT pairing, for best (lateral) match;
- Manual depth matching of 2D UHR MCS and CPT data – by e.g. profile smoothing/averaging, clipping, synthetic inserts, stretch/compress;
- Specific assessment of marker horizons evident in both 2D UHR MCS and CPT data.

APPENDIX A: PLATES REFERENCED IN MAIN TEXT

LIST OF PLATES IN APPENDIX A:

	Plate
Vicinity Map	A1
List of Project Reports	A2
Study Overview	A3 to A4
Bathymetry and 2D UHR MCS Track Lines	A5 to A6

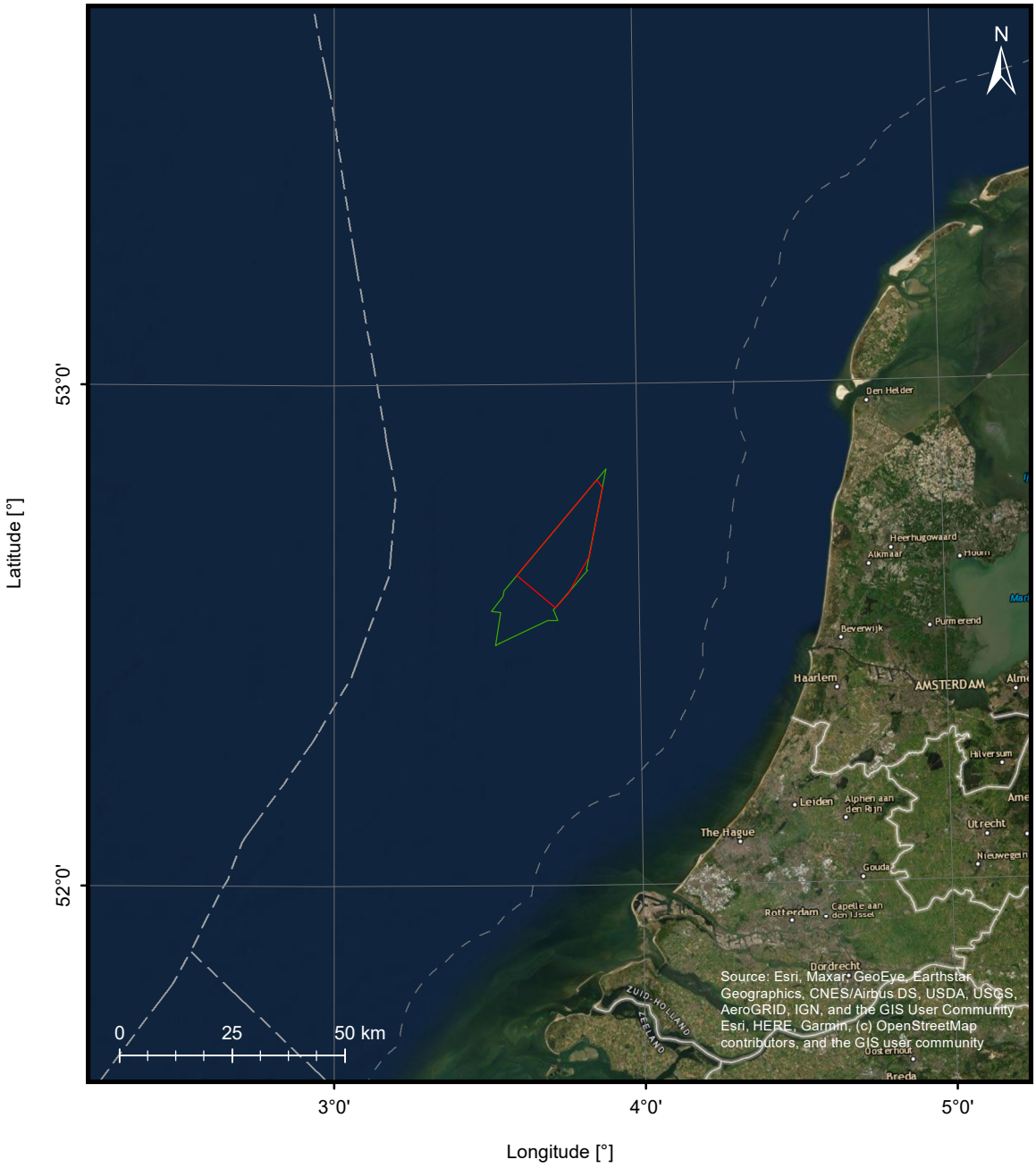

Hollandse Kust (west) - Geotechnical Investigation Area
Hollandse Kust (west) - Designated Wind Farm Zone
Maritime boundary
12 nautical mile zone

Datum : ETRS89
Spheroid : GRS80
Projection : UTM Zone 31N
Central Meridian: 3° East

Printed: 27-7-2020 14:35:35

VICINITY MAP

Report Number	Title	Contents
P904711/01	Geotechnical Report - Investigation Data – Seafloor In Situ Test Locations Hollandse Kust (west) Wind Farm Zone – Dutch Sector, North Sea	Geotechnical data including geotechnical logs, results from seafloor cone penetration tests, seafloor seismic cone penetration tests (including seismic velocity tests), seafloor temperature cone penetration tests (including temperature equilibrium tests) and pore pressure dissipation tests.
P904711/02	Geotechnical Report - Investigation Data – Seafloor Sample Locations Hollandse Kust (west) Wind Farm Zone – Dutch Sector, North Sea	Geotechnical data including geotechnical logs for vibrocore locations and results from geotechnical laboratory tests.
P904711/03	Geotechnical Report - Investigation Data – Geotechnical Borehole Locations Hollandse Kust (west) Wind Farm Zone – Dutch Sector, North Sea	Geotechnical data including geotechnical logs, results from downhole sampling and cone penetration tests, borehole geophysical logging, and results from geotechnical and biogeochemical laboratory tests.
P904711/04	Geotechnical Report - Laboratory Test Data Hollandse Kust (west) Wind Farm Zone – Dutch Sector, North Sea	Results of static, cyclic and dynamic laboratory tests.
P904711/05	Geotechnical Report - Investigation Data – Tennet Beta Platform Location Hollandse Kust (west) Wind Farm Zone – Dutch Sector, North Sea	Geotechnical data including geotechnical logs, results from downhole sampling and cone penetration tests and results from geotechnical laboratory tests.
P904711/06	Geological Ground Model Hollandse Kust (west) Wind Farm Zone – Dutch Sector, North Sea	Geological ground model including stratigraphy, geological analyses, lateral soil variability, geohazards, assessment of geotechnical suitability of selected types of structures, biostratigraphic analyses.
P904711/07	Geotechnical Report – Geotechnical Parameters Hollandse Kust (west) Wind Farm Zone – Dutch Sector, North Sea	Geotechnical parameters, including (1) geotechnical ground model focusing on monopile and jacket pile foundations, (2) selection of characteristic values of geotechnical parameters for use in selected calculation models and limit states, (3) derived values of geotechnical parameters, (4) data gap analysis, (5) seismic hazard assessment and (6) microbiologically influenced corrosion (MIC) mass loss rate assessment.
P904711/08	Geotechnical Report – Synthetic CPT Profiles Hollandse Kust (west) Wind Farm Zone – Dutch Sector, North Sea	Predicted CPT profiles (>1.5 million) for available survey lines of marine seismic reflection data.

LIST OF PROJECT REPORTS

GENERAL

Procedure:	– Integrated geoscience study according to ISO/DIS 19901-10 (2018) for synthetic (predicted) cone penetration test (CPT) profiles along survey track lines for sparker source ultra-high resolution multichannel seismic reflection (UHR MCS) profiling – Refer to documents titled "Site Characterisation" and “Marine Reflection Seismics” presented in Appendix C – Generally according to Eurocode 7 1997-1:2004 (CEN, 2009)
Premise(s):	– Scope of presented geodata according to a project specification determined and monitored by the client – Purpose of presented geodata according to description(s) given in Main Text – **Novelty of the presented data; reader is referred to (1) “Use of Geodata and Advice” presented in Appendix C and (2) ISO/DIS 19901-10:2018 Marine Geophysical Investigations, Chapter 10 for further specific guidance on use of *predicted* geotechnical data**
Type of Structure(s) and Purpose:	– Monopiles and jacket piles for support of wind turbine generators – Novel geodata (synthetic CPT profiles) that can potentially provide added value to pile foundation design of offshore wind turbines
Location:	– Hollandse Kust (west) WFZ – Refer to Main Text for definition of site location and site area – Refer to Appendix A (Plates referenced by Main Text) for geodetic parameters including vertical datum
Integration Level for Site Characterisation:	Level 2 Stratigraphic Integration; refer to document titled “Site Characterisation” in Appendix C
Site Use:	Refer to companion report on geotechnical parameters
Seafloor Conditions and Hazards:	Refer to companion report on geotechnical parameters
Stratigraphy and Ground Parameters:	– Refer to Main Text – Refer to companion report on geotechnical parameters – The reference condition for presented parameter values is the in situ state of the seabed as applicable at the time of site investigation, except where noted otherwise; any later changes to site conditions are excluded, e.g. resulting from seabed mobililty, installation of scour protection and structure(s) – Seafloor is the primary vertical datum for presented parameter values
Geotechnical Calculation(s):	Not within report scope

DATA COVERAGE

Status of Site-specific Data Acquisition:	Considered final
Information on Historic and Current Site Use:	Refer to companion report on geotechnical parameters
Information on Planned Site Use:	Refer to companion report on geotechnical parameters
Met-ocean Data:	Not applicable
Environmental Baseline:	Not applicable
UXO Information:	Not applicable
Archaeological Information:	Not applicable
Seismic (Earthquake) Data:	Not applicable
Geological Data:	– Refer to Main Text – Refer to companion report on geotechnical parameters
Geothermal Data:	Not considered: outside scope of this report

STUDY APPROACH

ISSUE 08
FNLM/GEO/SPE/102
© Fugro 2012-2020

Geophysical Survey Data:	– Refer to Main Text and plate(s) titled "Bathymetry and UHR MCS Track Lines" – Refer to companion report on geotechnical parameters
Geotechnical Data:	– Refer to Main Text and plate(s) titled " Bathymetry and UHR MCS Track Lines " – Refer to companion report on geotechnical parameters
Groundwater Data:	Refer to Main Text and companion report on geotechnical parameters
Structure/Soil Monitoring Data:	Not applicable
Physical Modelling Data:	Not applicable

INFORMATION MANAGEMENT

Data Processing:	– GeODin® software for geotechnical data processing, management and presentation – IHS Kingdom™ for seismic reflection data processing and analysis – Seisee software for viewing and editing SEG-Y data – OpenDtect seismic interpretation software for 3D imaging of seismic sections. – General purpose software, including Python™, MATLAB and ArcGIS®
Data Format(s) for Results:	– PDF for viewing and printing – SEG-Y reader/editing tool (Seisee) – SEG-Y files for – ESRI shape file for predicted CPT locations of every 100th CDP (separate deliverable, secondary to this PDF document) – SEG-Y synthetic CPT profiles (separate deliverable, secondary to this PDF document)

REFERENCES

– Computer application ESRI ArcGIS®, *Analysis and Presentation of Geo-data*, Version 10.8
– Computer application GeODin®, *Recording, Presentation and Analysis of Geo-data*
– Computer application IHS Kingdom™, *Interpretation, Analysis and Presentation of Geo-data, Version 2016/2018 (64-bit)*
– Computer application MATLAB®, *Data Processing and Analysis,* Version 2019a
– Computer application OpenDtect, Version 2019
– Computer application Python®, *Programming Language,* Version 2020
– Computer application Seisee, *SEG-Y viewer/editor, Version 2.22.6 (Jun 2017)*
– European Committee for Standardization (2009). *Eurocode 7: geotechnical design - part 1: general rules (with corrigendum EN 1997-1:2004/AC, February 2009)* (EN 1997-1:2004). https://standards.cen.eu/dyn/www/f?p=204:110:0::::FSP_PROJECT,FSP_ORG_ID:12442,6231&cs=1D03CC06CB9166EAAA1C6CE997CDA87C2
– International Organization for Standardization, 2018. *Petroleum and natural gas industries – Marine geophysical investigations.* (ISO/DIS 19901-10:2018). https://www.iso.org/standard/77017.html

© Fugro 2012-2020 FNLM/GEO/SPE/102 ISSUE 08

STUDY APPROACH

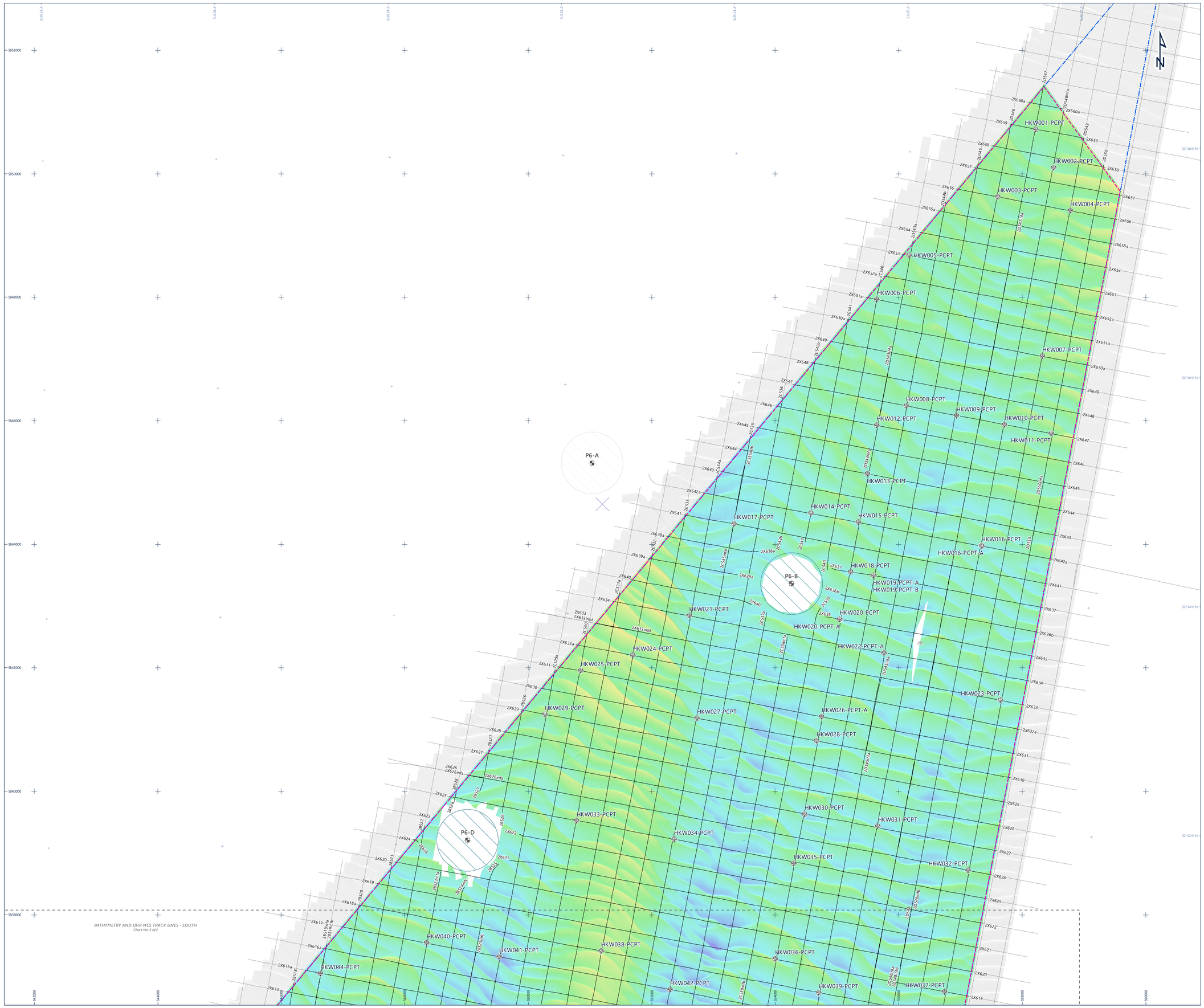

LEGEND

GEOTECHNICAL LOCATIONS

Cone penetration test point

GENERAL

Hollandse Kust (west) Wind Farm Zone (HKW WFZ)

HKW - Designated Wind Farm Zone

Structure

Buoyant waterway marking

Structure 500 m exclusion zone

Chart extent indicator

UTM grid

Geographical grid

TRACKS

UHR MCS track line

BATHYMETRY

Water depth
[m below LAT]

20
23
26
29
32
35

NOTES

1) Data aquired by multibeam echosounder (Fugro, 2019).

2) Resolution of bathymetry grid cells 0.5 m x 0.5 m.

3) Areas around platforms P6-B and P6-D are not part of HKW WFZ.

GEODETIC PARAMETERS

GEODETIC DATUM	European Terrestrial Reference System 1989
ELLIPSOID	GRS 1980
Semi-Major Axis	6,378,137.000 m
Inverse Flattening	298.257222101
PROJECTION	ETRS 1989 / UTM Zone 31N *(EPSG 25831)*
Central Meridian (CM)	03°00'00" E
Latitude of Origin	00°00'00" N
False Easting	500,000 mE
False Northing	0 mN
Scale Factor at CM	0.9996
DATUM TRANSFORMATION	ITRF2014 to ETRS89 for Epoch 2017.4959
Source	*dX=+0.05545 m dY=+0.05295 m dZ=-0.08834 m* *rX=-0.0023082 " rY=-0.0119630 " rZ=+0.0225688 " Scale=+0.00294455 ppm*
VERTICAL DATUM	Lowest Astronomical Tide (LAT)

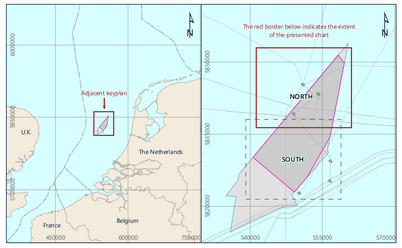

RVO
Prinses Beatrixlaan 2, 2595 AL Den Haag, The Netherlands
www.rvo.nl

Rijksdienst voor Ondernemend Nederland

Fugro
Primastraat 4, 2631 RT Nootdorp, The Netherlands
www.fugro.com

BATHYMETRY AND 2D UHR MCS TRACK LINES

NORTH

SYNTHETIC CPT PROFILES

DUTCH SECTOR - NORTH SEA

HOLLANDSE KUST (WEST) WIND FARM ZONE

Scale 1 : 20,000 at original A0 page size

0 250 500 1000 1500 2000 2500 metres

0 0.1 0.2 0.3 0.4 0.5 0.6 0.7 0.8 0.9 1 nautical mile

Fugro Document No.	Chart No.	Plate No.
P904711/08 (2)	1 of 2	A5

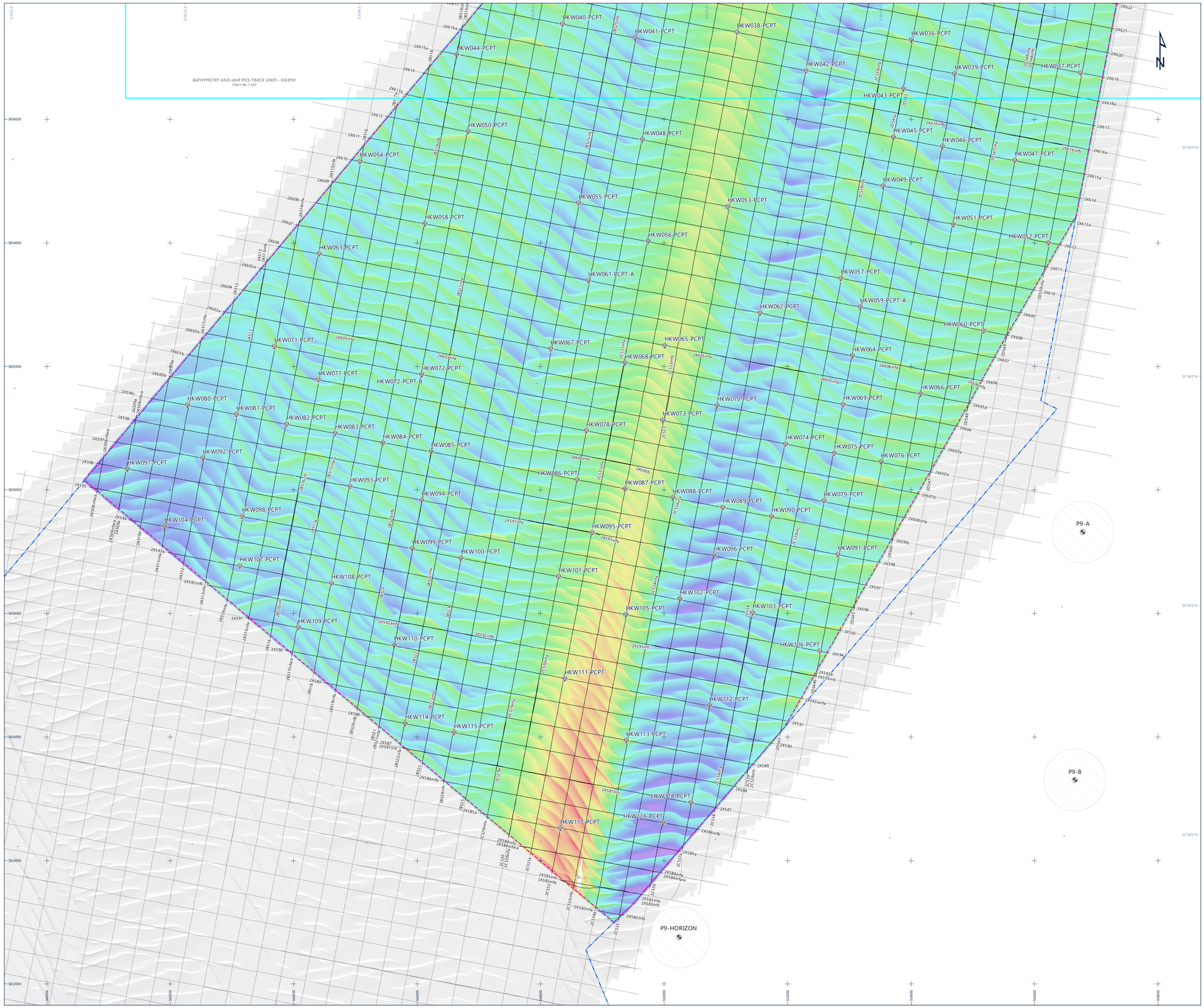

LEGEND

GEOTECHNICAL LOCATIONS

Cone penetration test point

GENERAL

Hollandse Kust (west) Wind Farm Zone (HKW WFZ)

HKW - Designated Wind Farm Zone

Structure

Buoyant waterway marking

Structure 500 m exclusion zone

Chart extent indicator

UTM grid

Geographical grid

TRACKS

UHR MCS track line

BATHYMETRY

Water depth
[m below LAT]

20
23
26
29
32
35

NOTES

1) Data aquired by multibeam echosounder (Fugro, 2019).

2) Resolution of bathymetry grid cells 0.5 m x 0.5 m.

3) Areas around platforms P6-B and P6-D are not part of HKW WFZ.

GEODETIC PARAMETERS

GEODETIC DATUM	European Terrestrial Reference System 1989
ELLIPSOID	GRS 1980
Semi-Major Axis	6,378,137.000 m
Inverse Flattening	298.257222101
PROJECTION	ETRS 1989 / UTM Zone 31N *(EPSG 25831)*
Central Meridian (CM)	03°00'00" E
Latitude of Origin	00°00'00" N
False Easting	500,000 mE
False Northing	0 mN
Scale Factor at CM	0.9996
DATUM TRANSFORMATION	ITRF2014 to ETRS89 for Epoch 2017.4959
Source	dX=+0.053045 m dY=+0.05295 m dZ= -0.08834 m rX= -0.0023082 " rY= -0.0139630 " rZ= +0.0225688 " Scale= +0.00294455 ppm
VERTICAL DATUM	Lowest Astronomical Tide (LAT)

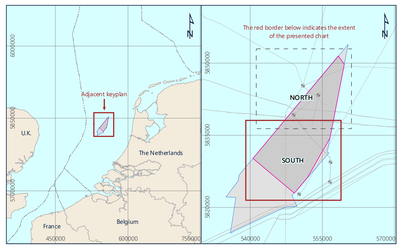

RVO
Prinses Beatrixlaan 2, 2595 AL Den Haag, The Netherlands
www.rvo.nl

Rijksdienst voor Ondernemend Nederland

Fugro
Primastraat 4, 2631 RT Nootdorp, The Netherlands
www.fugro.com

BATHYMETRY AND 2D UHR MCS TRACK LINES

SOUTH

SYNTHETIC CPT PROFILES

DUTCH SECTOR - NORTH SEA

HOLLANDSE KUST (WEST) WIND FARM ZONE

Scale 1 : 20,000 at original A0 page size

0 250 500 1000 1500 2000 2500 metres

0 0.1 0.2 0.3 0.4 0.5 0.6 0.7 0.8 0.9 1 nautical mile

Fugro Document No.	Chart No.	Plate No.
P904711/08 (2)	2 of 2	A6

APPENDIX B: TNO REPORT

TNO 2020 R11145 - Synthetic CPTs for Hollandse Kust (west) Wind Farm Zone

Princetonlaan 6
3584 CB Utrecht
P.O. Box 80015
3508 TA Utrecht
The Netherlands

www.tno.nl

T +31 88 866 42 56
F +31 88 866 44 75

TNO report

TNO 2020 R11145

Synthetic CPTs for Hollandse Kust (west) Wind Farm Zone

Date	09 October 2020
Author(s)	Stefan Carpentier, Bob Paap, Boris Boulenger, Vincent Vandeweijer, Bart Meijninger
Copy no	
No. of copies	
Number of pages	31
Number of appendices	1
Sponsor	Fugro
Project name	Synthetic CPTs
Project number	060.42051 phase 02

The ‘General Terms and Conditions for commissions to TNO’ dated July 1st, 2017 shall apply to this Report, including the following amendment thereto: “Clause 10. USE OF A FINAL REPORT”.

Fugro is allowed to use the PowerPoint presentation and the TNO report at the end of Commission for sharing with RVO and to publish on the website https://offshorewind.rvo.nl/ with the following restrictions:
- The TNO report shall be used in full and unchanged
- TNO will not be liable for any damages arising out of the public use of the TNO report and Fugro shall indemnify TNO against any claims for damages arising out of this public use
- The TNO report shall not be used for advertising or anti-advertising purposes of soliciting sales or services in a more general sense

© 2020 TNO

Contents

1 Overview ... 3

2 Methodology ... 4
2.1 General approach ... 4
2.2 Input data ... 5
2.3 Training of the CNN with supervised learning ... 14
2.4 Data processing and predictions ... 19

3 Results ... 21
3.1 Comments on results ... 21
3.2 Description of PDF files and SEG-Y files ... 27

4 Conclusions and recommendations ... 28

5 References ... 29

6 Appendix ... 30
6.1 Directory structure of the data files ... 30
6.2 How to read and use the SEGY files ... 30
6.3 How to export traces from SEGY files ... 31

1 Overview

This report describes methodology, limitations, results, conclusions and recommendations from the work involved in the prediction of 1,509,783 Cone Penetration Test (CPT) profiles along survey lines of marine seismic reflection data for the Hollandse Kust West (HKW) wind farm zone.

The scope of this report is according to project specifications determined by RVO (Rijksdienst voor Ondernemend Nederland) and Fugro.

The report describes an implementation phase of synthetic CPT prediction, in which an optimally performing Neural Network predicts CPT q_n* parameter values for each trace (approximately 1.5 million in total) of 160 2D Ultra High Resolution (UHR) multichannel seismic (MCS) reflection lines in the Geotechnical Investigation Area (GIA) of the Hollandse Kust (west) (HKW) Wind Farm Zone (Figure 2.1). This area (GIA) is selected within Hollandse Kust (west) Designated Wind Farm Zone. In this report, the Hollandse Kust (west) Geotechnical Investigation Area is referred to as the Hollandse Kust (west) Wind Farm Zone (HKW WFZ), GIA or simply “the site”.

The starting point includes 119 seafloor-based CPTs and seismic data & interpretation along 2D UHR MCS lines within the GIA. The primary output consists of ~1.5 million synthetic CPTs along track lines of seismic reflection data (at each Common Depth Point (CDP)). These constitute synthetic CPT profiles for UHR MCS data within HKW WFZ.

The CPT parameter q_n* is predicted, but not sleeve friction (f_s) and pore pressure (u_2). The depth range of predictions is 2 m to 50 m below seafloor (BSF). The top 2 m is excluded from the predictions due to unreliable data in the first 2 meters of the CPT’s. A vertical data point spacing of 0.1 m is maintained and an additional approximate indicator for prediction quality of each predicted CPT data point is supplied.

Deliverables of this project are approximately 1.5 million synthetic CPT q_n* predictions plus 5th and 95th percentile confidence intervals along the 160 2D UHR MCS lines. These data are provided as:

- Descriptions and figures in this report;
- Digital files in SEG-Y format (for each 2D UHR MCS line in the GIA);
- High-resolution plots in PDF format (for each 2D UHR MCS line in the GIA).
- Ascii files of predicted CPT profiles at selected CDPs (every 100th CDP along the 2D UHR MCS lines)
- ArcGIS shapefile containing locations of these selected CDPs

To analyse, view and plot the SEG-Y-format data, freeware software is provided.

2 Methodology

2.1 General approach

The project was split in 4 work packages and the project workplan was as follows:

WP1 – Loading and defining the input data

- Load the supplied input data: CPT data (i.e. training dataset) and the corresponding 2D UHR MCS dataset and geological soil units. The training dataset consisted of 119 seafloor-based CPTs; the 2D UHR MCS data comprised 160 lines; the geological soil unit data were provided as horizon interpretation (xyz-format). The input data were all defined in depth (z) and as much as possible with equal z-spacing
- Generate additional seismic attributes for the 2D UHR MCS dataset, including interval velocity, P-impedance, Instantaneous Amplitude as based on the results of thorough testing. Depth and geological units were supplied.
- Define the final input data consisting of seismic attribute traces
- Define the labelled dataset containing CPT q_n* and z data

WP2 – Training of a ANN (or CNN) with supervised learning

- Perform data preconditioning by synchronizing e.g. data re-sampling and tie-ins between extracted subsets of 2D UHR MCS and CPT data for the depth interval of 2 m to 50 m below seafloor
- Design a convolutional neural network (CNN) architecture that performs multi-attribute regression between UHR MCS attributes and target CPT attributes of the training data subsets
- Define a suitable training and validation/test sets
- Train the CNN using the training set and check prediction performance on the validation/test set during training
- Inspect in detail the predicted versus the training CPTs for the validation/test set
- Adjust the hyper-parameters of the CNN (hidden layers, iterations etc.) and repeat training
- Train the network on aforementioned training data sets containing inputs and targets
- Save the final trained CNN
- Perform prediction error analysis on the validation/test set
- Determine the distributions (one per geological unit) of the error misfit within the entire validation/test set and retrieve the 5th and 95th percentiles that form the quality indicator

WP3 – Predicting CPTs with the trained CNN

- Use the trained CNN consecutively on the traces of one selected in-line and one crossing x-line not being part of the training data subsets and assess the results by quantifying mismatches by (1) data driven approach and (2) sense checks by team experts
- Use the trained CNN to perform CPT predictions from the remaining ~1.5 million traces of the in-lines and x-lines and assess the results by quantifying mismatches by (1) data drive approach and (2) sense checks by team experts
- As quality indicators, generate predicted CPT q_n* and the lower and upper limits of the confidence interval corresponding to the 5th and 95th percentiles derived from the aforementioned error analysis. Do this for all Common Depth Points (CDPs) on all 2D UHR MCS lines and

- Export 1) Predicted CPTs, 2) lower (p5) and 3) upper (p95) limits of the confidence interval to a binary compressed file format (SEG-Y)
- Perform quality assessment of the predicted CPT q_n* for all CDPs on all 2D UHR MCS lines according to the official Geological Survey guidelines and standards (http://www.dinoloket.nl) for QC of delivered geological models

WP4 – Reporting

- Generate a shape file containing all line-CDP locations
- Document the methodology, results, use and limitations of the data in a concise report

2.2 Input data

The input data sets in the Geotechnical Investigation Area (GIA) (Figure 2.1) that are considered for input in the Convolutional Neural Network for prediction of synthetic CPTs are:

- 160 UHR MCS lines (2D), including the velocity model developed during UHR seismic processing
- 119 seafloor-based CPTs
- Information from the geological ground model, particularly depths of boundaries of geological soil units (at each CDP and each seafloor-based CPT)

Comments are as follows:

- UHR MCS data – no conditioning done to seismic data for attributes; no conditioning to the existing interval velocity model and no reprocessing.
- Geological soil units from integrated geophysical interpretation as per geological ground model report (Fugro, 2020a)
- Horizontal position estimates (for spatial data points) in the order of +/- 2m for CPT data and +/- 3m for UHR MCS data.

In total, 119 CPTs lead to 234 (primary and secondary) seismic CDP – CPT pairs. Many CPTs are close to seismic survey line crossings with horizontal offsets of CPTs (i.e. training locations) to nearest CDP (primary CDP) of a survey line are in order of 0 m to 16 m, Figure 2.2 illustrates this.

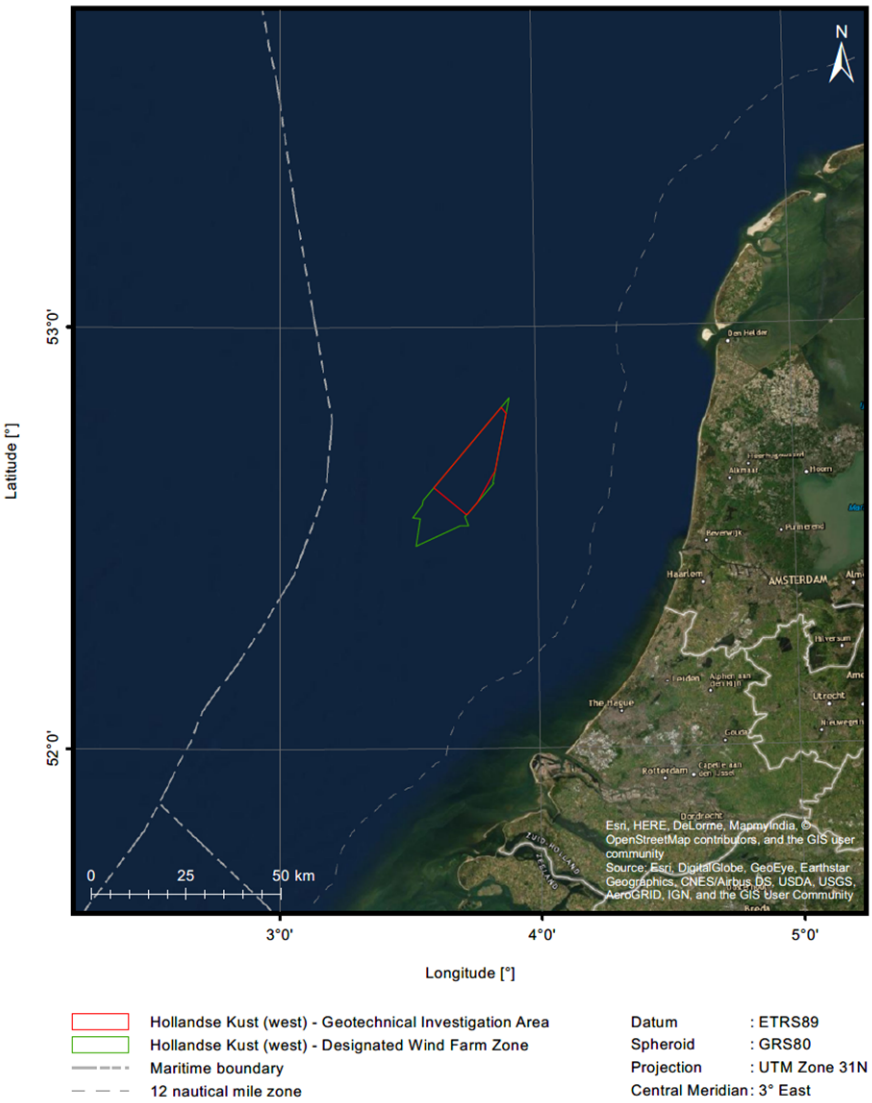

Hollandse Kust (west) - Geotechnical Investigation Area
Hollandse Kust (west) - Designated Wind Farm Zone
Maritime boundary
12 nautical mile zone

Datum : ETRS89
Spheroid : GRS80
Projection : UTM Zone 31N
Central Meridian : 3° East

Figure 2.1 Location of the Hollandse Kust West (HKW) – Geotechnical Investigation Area.

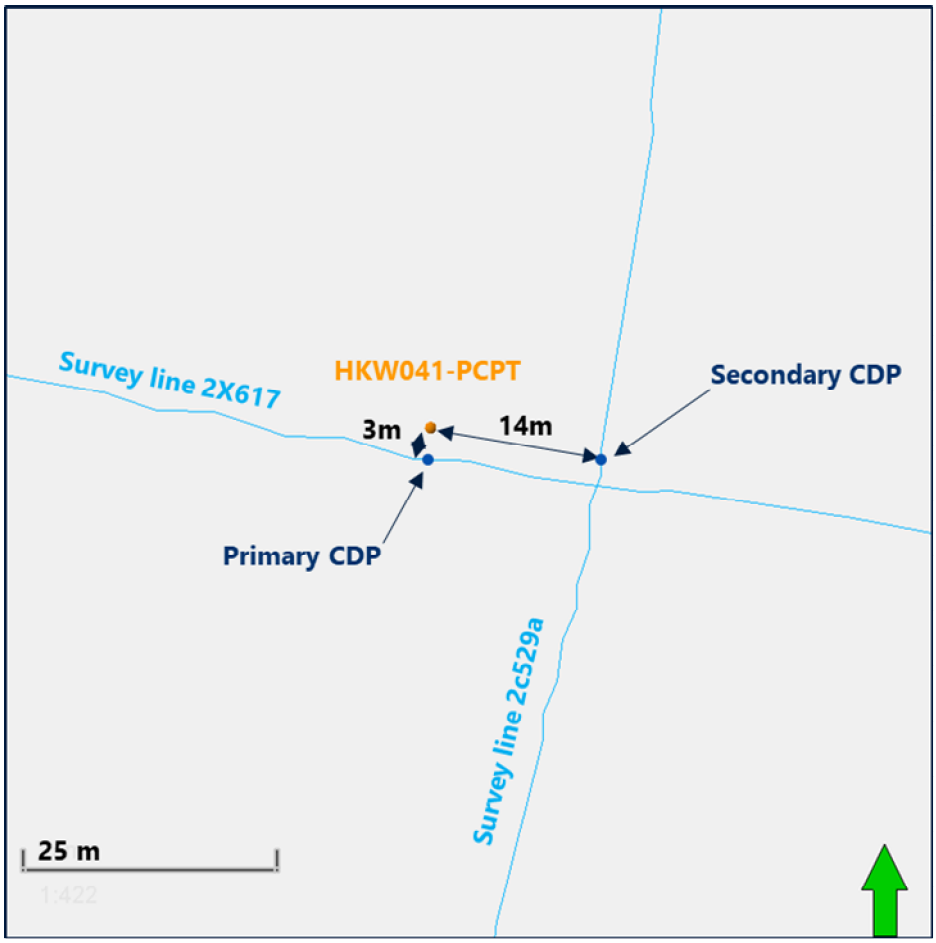

Figure 2.2 Illustration of seismic CDP locations versus their paired CPT locations. The typical closest distance between paired CDPs and CPTs is in the order of 2-3 metres, but distances up to 16 metres are not exceptional.

The choice of the optimal input seismic attributes and of the neural network architecture were made after thorough testing. The analysis of the prediction performance for a test data set led to the selection of a convolutional neural network (CNN) architecture and of the following input attributes:

- Soil units A to G (1 to 8)
- Depth in metres below seafloor
- Moving average of seismic interval velocity
- Moving average of seismic instantaneous amplitude (envelope)
- Moving average of seismic model-based impedance

The algorithm to produce the input attributes from the 162 2D UHR MCS lines with ~1.5 million traces has a large element of scripting. There was no manual picking of 2D UHR MCS data for CPT pairing for best (lateral) match. In addition there was also no manual depth matching of UHR MCS data interpretation and CPT data (e.g. by profile smoothing / averaging, clipping, synthetic inserts, stretching or compressing). Also no specific assessment of marker horizons evident in both UHR MCS and CPT data were considered. The CNN approach with parameters from thorough testing was used in this project, as well as the most optimal seismic attributes.

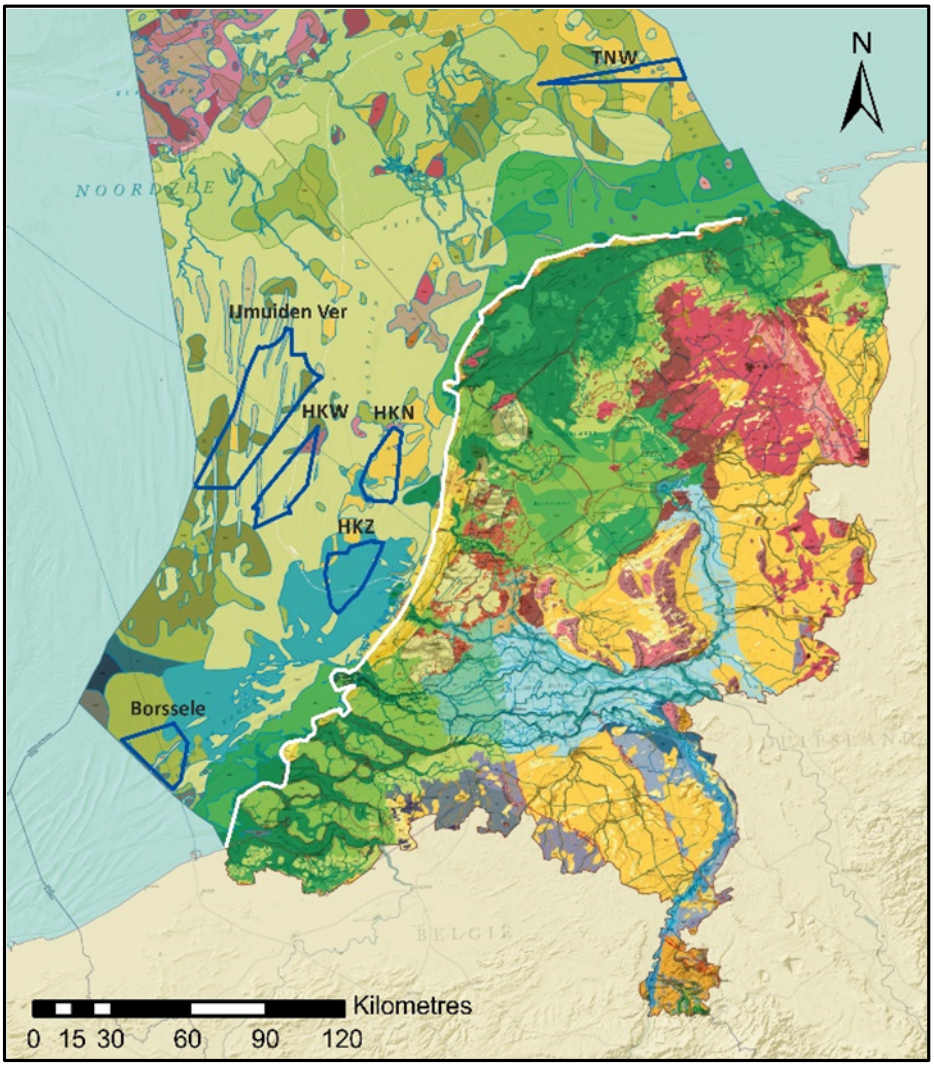

Figure 2.3 Geological map of the North Sea (Geological Survey Netherlands, 2019) with the Hollandse Kust (west) Wind Farm Zone and other wind farm zones. The high degree of geological heterogeneity is prominent.

A high degree of variability remains in the input attribute data. Figures 2.3 to 2.6 illustrate how soil heterogeneity occurs from < 1 m scale to > 1 km scale. Geological Units A to G within the lithostratigraphic framework (and in the geological ground model report (Fugro, 2020a) correspond to Geological Units 1 to 8 used in this report and accompanying digital deliverables. The lithology is dominated by sandy soils, but frequent clayey zones occur within most units.

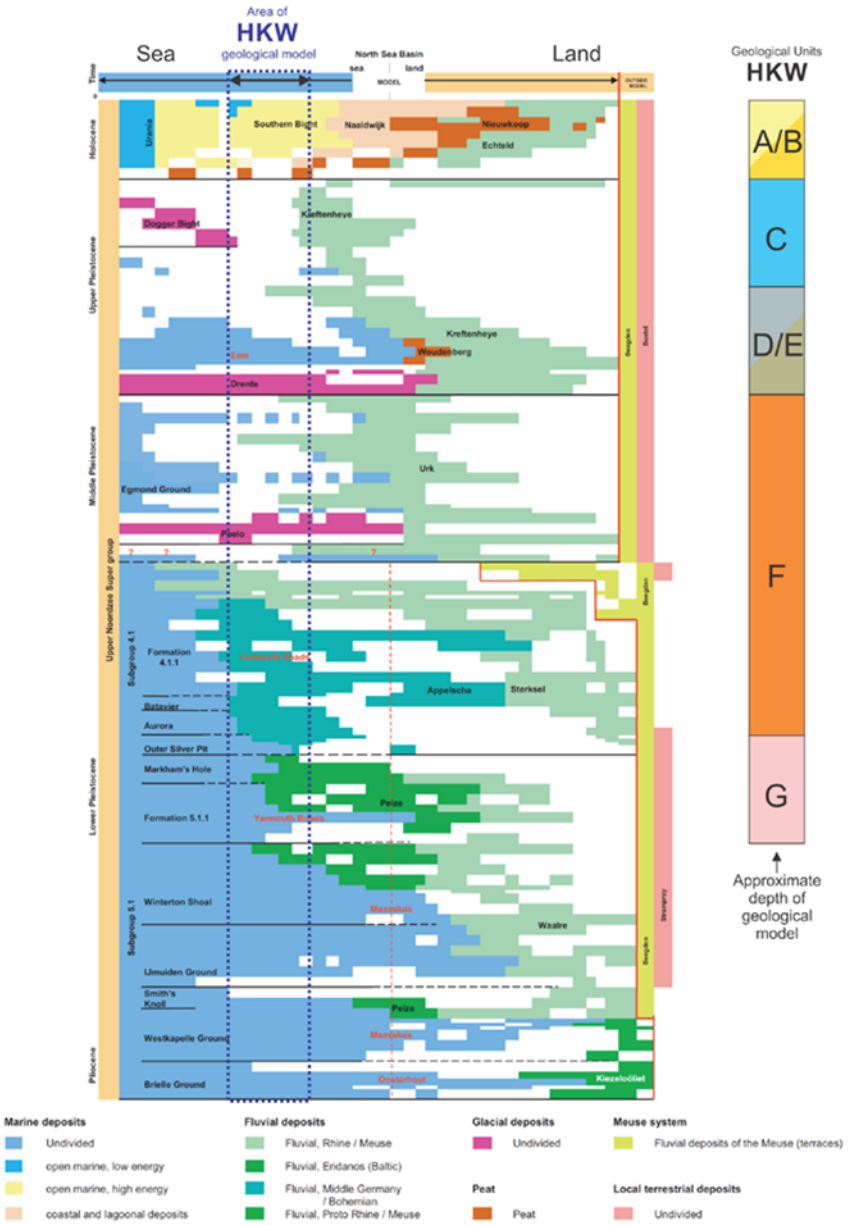

Lithostratigraphic scheme for the Netherlands and adjacent shelf (modified after Rijsdijk et al. 2005). Coloured bars show formations in space (x-axis) and in time (y-axis). The colour shows the depositional environment. The soil units identified in Hollandse Kust (west) wind farm zone (HKW) are indicated on the right.

Figure 2.4 Lithostratigraphic scheme for the Netherlands and adjacent shelf, as per geological ground model report (Fugro, 2020a). The lateral and depth-wise variability of lithostratigraphy is high.

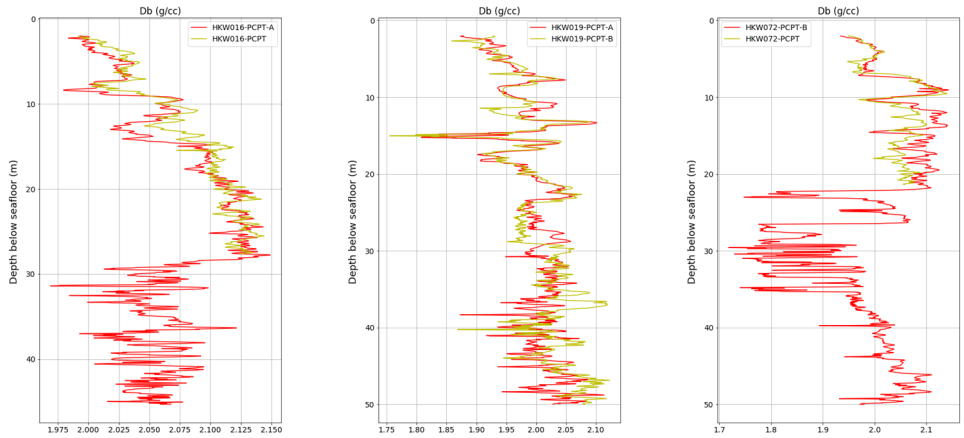

Figure 2.5 Plot of CPT q_n* curves for three different locations, each with 2 adjacent CPTs, where the yellow curve represents an initial CPT and the red curve the adjacent CPT. Already at these very close locations, a second CPT yields 10-20% different q_n* values with respect to the initial CPT, indicating high heterogeneity in the soil.

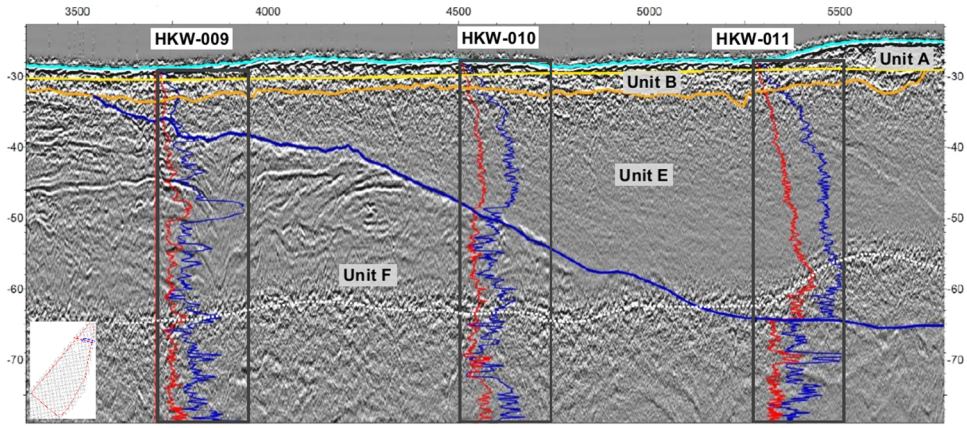

Figure 2.6 Seismic profile through the north of HKW GIA passing through three CPT locations (vertical scale in metres LAT). This profile illustrates how lateral heterogeneity occurs on small (< 1 m) scale but also on larger (~500 m) scale, making both scales challenging to predict on a CPT (from Fugro, 2020a).

Examples of the final input attribute data entering the training, testing and application of the CNN (described in next chapter) are given in Figures 2.7 to 2.9. In Figure 2.8, the differences between CPT-based geological units in 2.8A) and seismic-based geological units 2.8B) are small, in the order of 1-2 metres depth-wise. Some incidental larger differences between CPT-based units and seismic-based units exist. These are due to re-interpretations of the seismic units based on CPT data. They are recognised and compensated for prior to and during the neural network training.

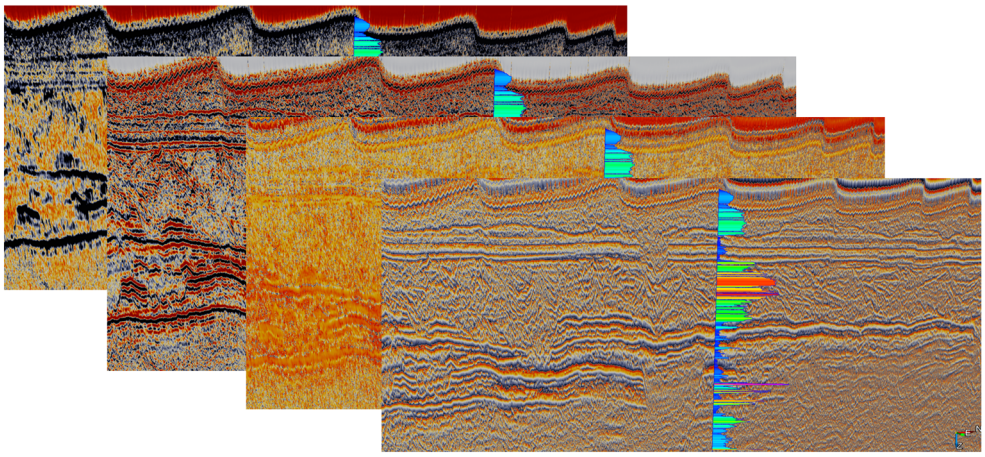

Figure 2.7 Illustration of seismic attributes that were investigated for feasibility and suitability as input to the neural network, overlaid with a CPT q_n* curve. From back to front the attributes are: seismic envelope, normal amplitude, instantaneous frequency and instantaneous phase. Not all of these attributes were used in the training of the final neural network.

A)

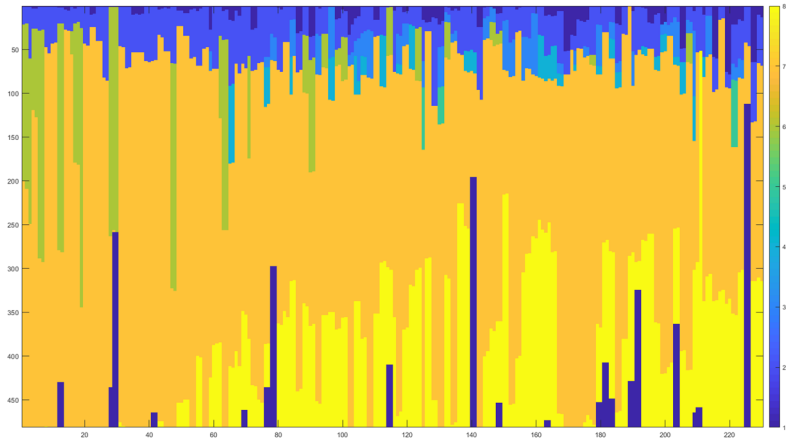

B)

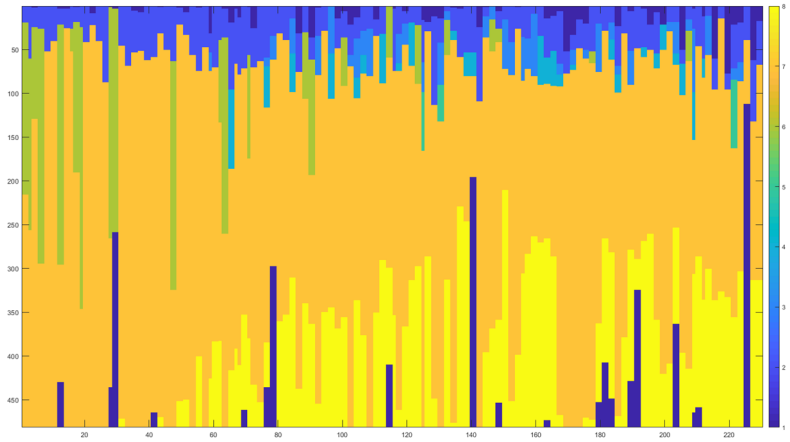

C)

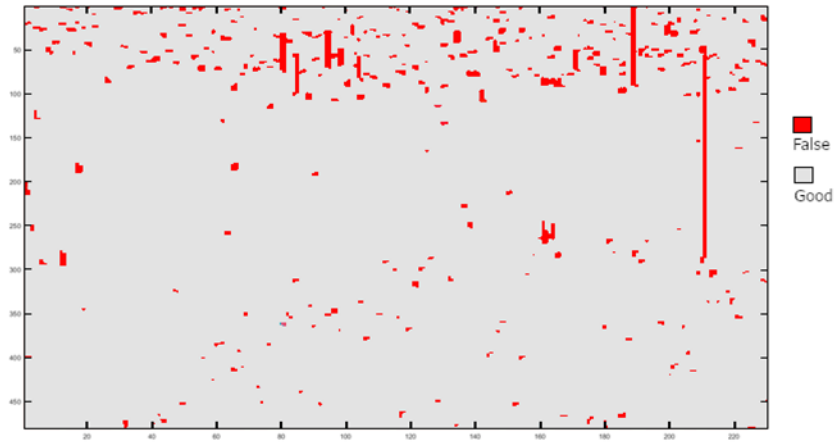

Figure 2.8 Scheme of interpreted geological Units A to G (1 to 8), plotted sequentially for all 234 seismic CDP-CPT pairs (horizontal axis). Range is 0 to 50 metres, referenced to 2 metres below seafloor (vertical axis), colour codes run from blue (1) to yellow (8). A) Units at CPT locations, as supplied, B) Units at seismic CDPs, as supplied, and C) If there is difference between A) and B), Yes = False, No = Good.

A)

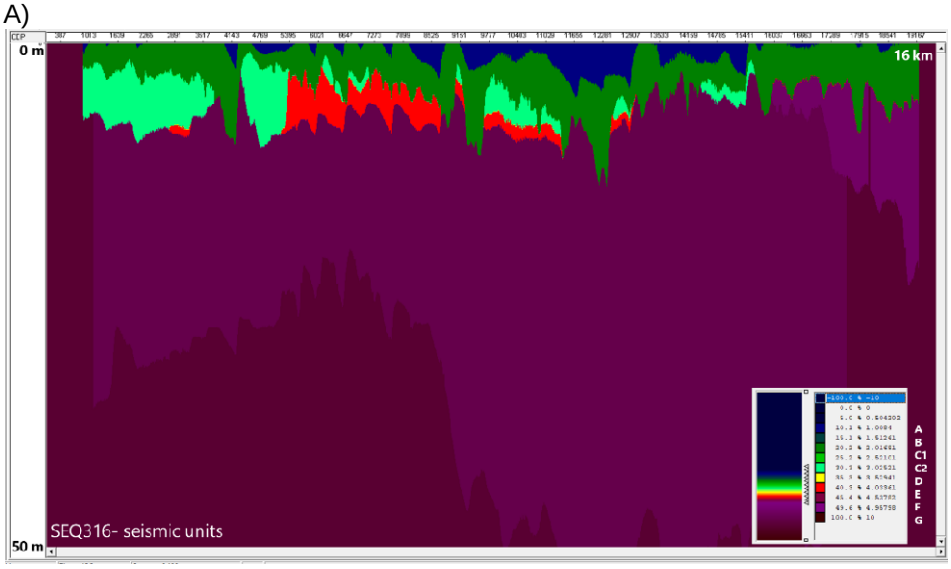
0 m
16 km
SEQ316- seismic units
50 m
A
B
C1
C2
D
E
F
G

B)

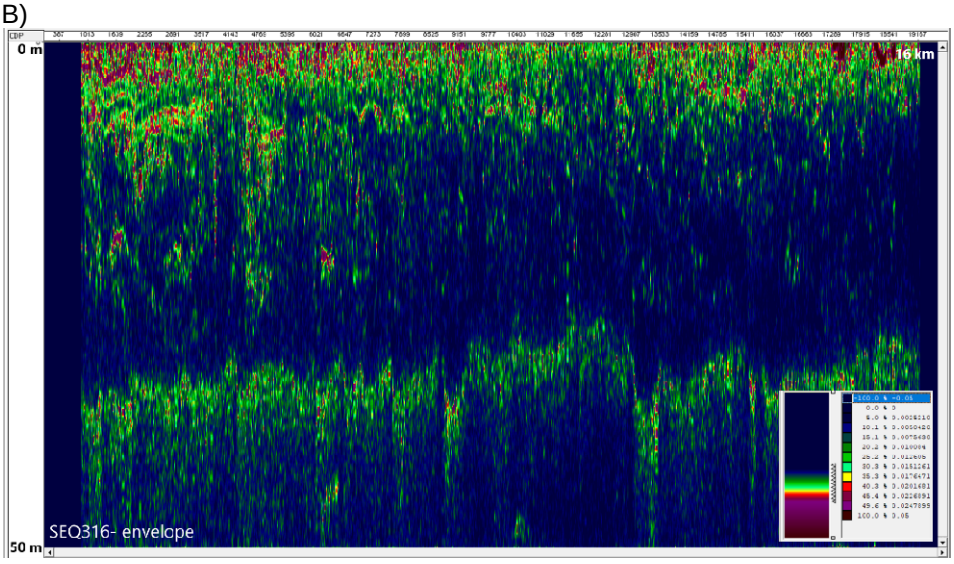
0 m
16 km
SEQ316- envelope
50 m

C)

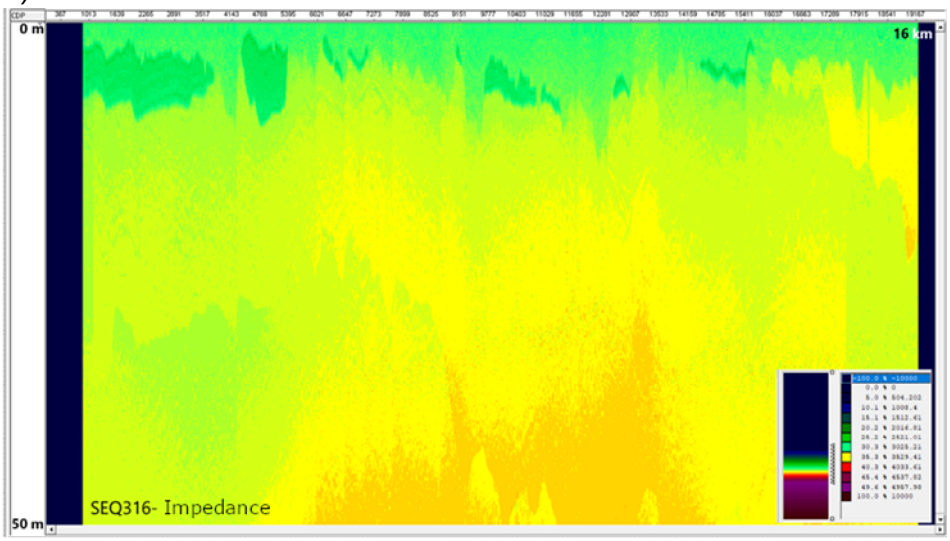
0 m
16 km
SEQ316- Impedance
50 m

D)

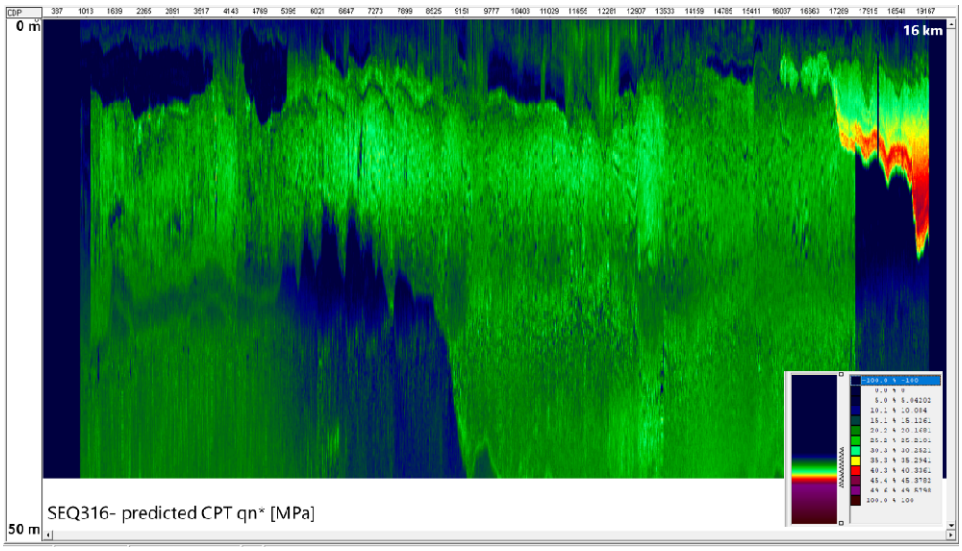

Figure 2.9 Examples of raw input and output data of the convolutional neural network for one seismic profile SEQ316. A) geological soil units, B) seismic envelope, C) seismic impedance and D) predicted CPT q_n* from the CNN with inputs A, B, C and additional seismic interval velocity and depth (not shown here). Depths are with respect to seafloor minus 2 metres. The colour scale varies per sub-plot, see inset legend for details.

2.3 Training of the CNN with supervised learning

2.3.1 General approach

The training of the CNN is performed via supervised learning. The training algorithm optimizes the parameters of the CNN to map the input attributes to the target CPT values. The overall training of the CNN comprises an actual training phase where a prediction model is learning and a testing phase where the performance of the trained model is evaluated with a testing dataset unseen during training.

Therefore, a first step is to define the training and testing dataset. To this end, we selected 21 locations to form the testing data while the remaining locations form the training data. So, the available data is split into training and testing datasets with roughly an 80%-20% split. This split is meant to secure a good amount of data for actual training as well as sufficient data for reliable testing.

The 21 testing locations are split into three groups for convenience of the analysis and for plotting purposes:

- Subgroup 1: a group of 8 locations chosen for representation of the various soil types and soil provinces (from the former defined (during phase 1) training locations)
- Subgroup 2: a group of 6 locations also chosen for their representation of the various soil types and soil provinces (from the former defined (during phase 1) reference lines)
- Subgroup 3: a group of 7 locations of which the first one is chosen because it features soil unit D. The next 6 locations are selected, randomly this time, from the remaining available locations.

2.3.2 Training

We used a 1D convolutional neural network architecture for training the CPT prediction model. The network is composed of several convolutional layers which are connected to a single output (or target) neuron with two fully connected layers. The convolutional layers correspond to successive convolution and max-pooling operations which form together the equivalent of a feature extractor. The convolution operations are performed using a number of filters with a defined length (here, 16 filters with length 3). The point values of these filters are parameters which are optimized automatically during training together with the weights of the fully-connected layers. The max-pooling operations help to achieve data reduction and to avoid over-fitting.

The input of the CNN is a 3-metres-long segment (so 30 points) over the input attributes while the output (also called target during training) is the CPT value at the top point of the same depth segment. The input segments and output value are extracted by running a 3-metres-long window with a step of 1 depth point (0.1 metres) over the attribute's profiles at a location.

To sum up, as 6 input features were selected, the shape of the inputs is 30x6 and the shape of the output is 1x1. This results (after a few pre-processing steps such as feature scaling) into the actual training dataset of 43859 input/output pairs and the actual testing dataset of 9308 pairs (also used for validation during training).

The testing dataset is in fact also used for validation during training. When used for validation, the data is not used to update the parameters of the model at each iteration. It is used to monitor the prediction performance and to control that the model is not over-fitting the training data but instead keeps a high generalization capability. Furthermore, the training is stopped when the prediction performance is not improving anymore on the validation data. Finally, the prediction model, which is selected at the end of the training phase, is the one corresponding to the best performance on the validation data.

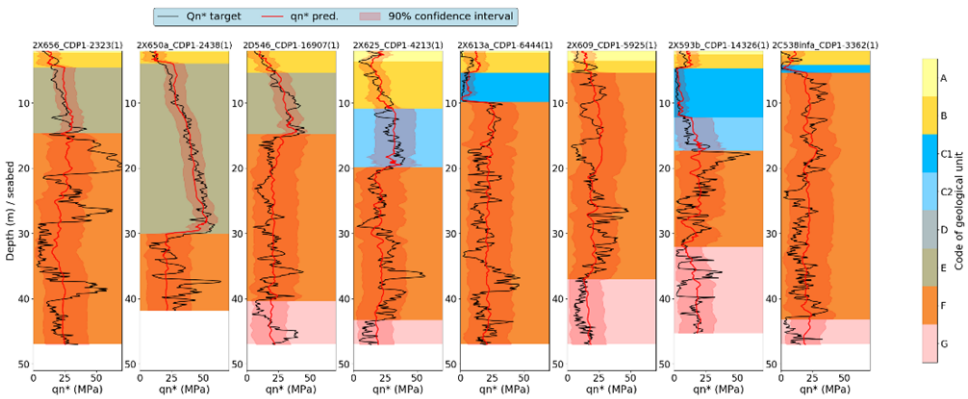

Figure 2.10 Predicted and actual CPT profiles at the testing locations from subgroup 1. The confidence interval is explained in Section 2.3.4. Depth axis is with respect to seabed, but the top of the plot coincides with seabed minus 2 m.

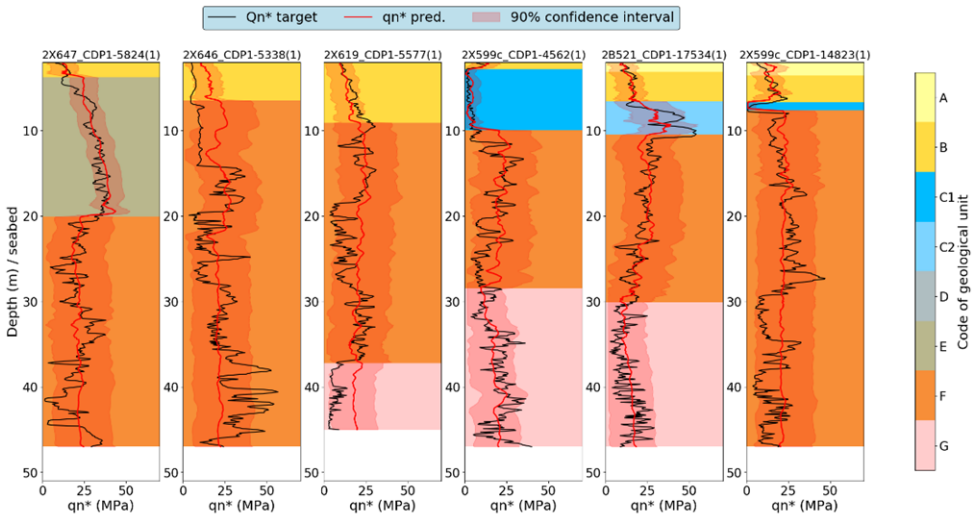

Figure 2.11 Predicted and actual CPT profiles at the testing locations from subgroup 2. The confidence interval is explained in Section 2.3.4. Depth axis is with respect to seabed, but the top of the plot coincides with seabed minus 2 m.

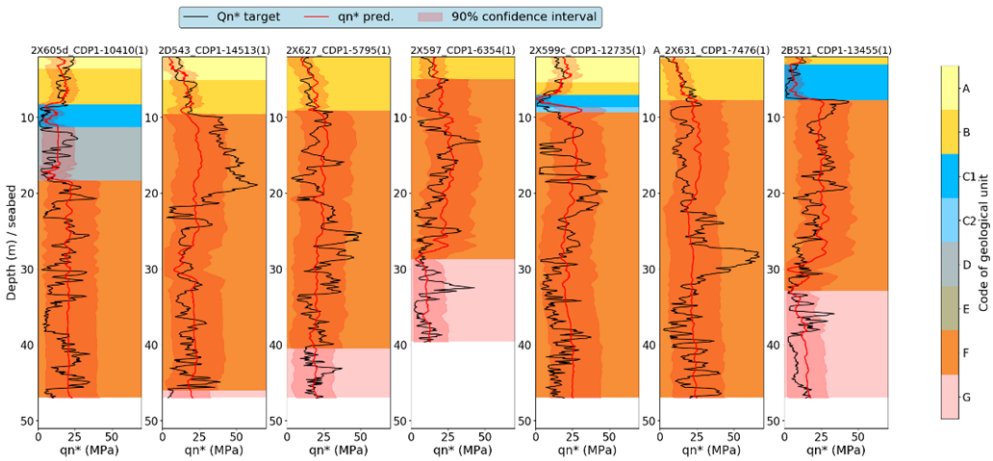

Figure 2.12 Predicted and actual CPT profiles at the testing locations from subgroup 3. The confidence interval is explained in Section 2.3.4. Depth axis is with respect to seabed, but the top of the plot coincides with seabed minus 2 m.

2.3.3 Testing

The quality of the CPT predictions is inspected by comparison with actual CPT profiles. This is done after completion of CNN training and selection of the better model according to the performance of the training set..

The error metrics that aim to quantify the overall misfit of the predictions, such as the root-mean-square error, do not provide enough detailed information about the performance of the model. Note that we did not implement any explicit pass or fail criteria for accepting or rejecting trained models, since this still remains a matter of expert judgement. For this reason, after any training phase, we control the performance not only with error metrics but also with visual inspection by plotting both the predicted and actual CPTs for comparison. Such plots are reported in Figures 2.10, 2.11 and 2.12 for the 3 subgroups of the 21 testing locations using the final trained CNN-based model. The plots visualize where (for example in which soil unit) the predictions are accurate and where they are off. Not only do we visualize the amount of misfit but we can also assess whether the trend of a CPT is captured. In turn, the plots over the testing locations provide crucial feedback and lead to possible explanations about why certain locations/depth intervals are not well predicted. This analysis also supported the decisions to train with a different set of hyper-parameters as attempt to improve the performance.

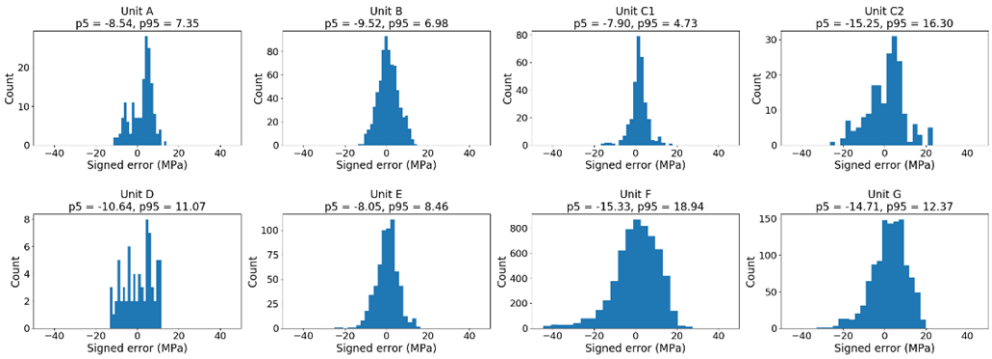

Figure 2.13 Distributions, using histograms, of the signed errors per geological unit within the 21 testing locations. The 5th and 95th percentiles are retrieved from these distributions to determine confidence intervals attached to any further prediction from the model.

2.3.4 Error analysis

With regard to indicators of prediction quality, we aimed to define confidence intervals corresponding to the predictions. For this purpose, we calculated the error distribution per soil unit since the testing plots showed a large variation of performance between different units. The error is signed and is obtained by calculating error_signed = qn*_true – qn*_pred. The resulting histograms, when using the final trained CNN, are shown in Figure 2.13. We can clearly observe that the error distribution is relatively narrow around 0 for units such as A, B, C1, E which means a good performance of the model for predicting CPT values within those units. On the contrary the distribution is wider for units C2 and G, and much wider for unit F. For these units the average trend of the modelled qn* is reasonably accurate, but here the trained model is unable to predict more detailed variations in qn*values. This means that the prediction model performs less accurately and less precisely, or thus unequally good within those units.

The width of such distributions is a fair indicator of the model performance to be expected within each unit. We leverage these test error distributions to define the confidence intervals attached to the predictions. The 5th percentile is the error value under which 5% of the error observations are made (and over which 95% of them are made) The 95th percentile is the error value under which 95% of the observations are made (and over which 5% are made). In turn, 90% of the error observations are made between the 5th and the 95th percentile. Here, we take the percentile 5th and 95th as the minimum and maximum statistical errors (let us use the notation error5 and error95,respectively) that the model would make when predicting a CPT value. These two limits vary per unit but are constant within any unit. We did explicitly not calculate the standard deviation, since this is only a representative statistical measure for normal symmetric distributions (that covers 68% of the data). In our case the error distribution per units is non-symmetric (see Figure 2.13).

The confidence interval consists in lower and upper limits attached to a CPT prediction. These limits that we refer as p5 and p95 in the output .segy and ascii files are derived for each predicted value by calculating p5 = qn*_pred + error5 and p95 = qn*_pred + error95. Together they give the value range, or confidence interval, in which the actual (but non-measured) CPT value is likely (90% probability) to fall.

2.3.5 Quality control

Quality control was required to check final predictions of cone resistance made for all seismic lines agreed with predictions made at reference locations in the training phase. This is illustrated in Figure 2.14, showing comparisons for two different CDPs for a reference line, and showing a perfect match in predictions (green and red lines). The black line represents the actual cone resistance at these positions.

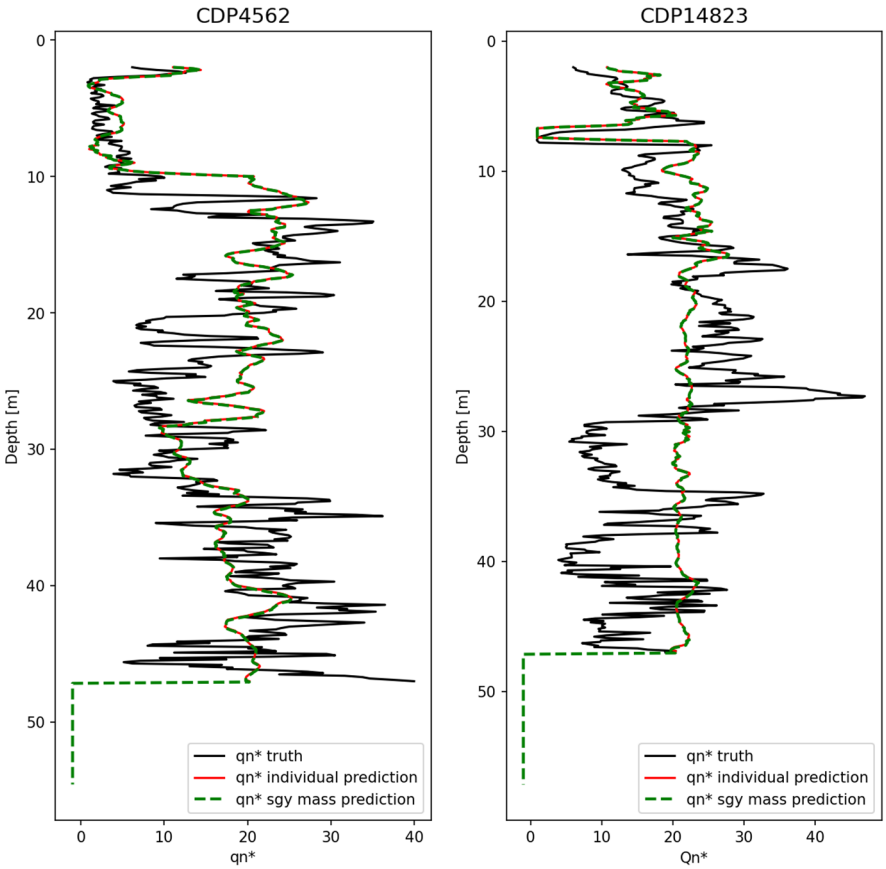

Figure 2.14 Quality control of the predictions for the individual predictions (red) and mass predictions done for all lines (green dashed) against q_n* (black) of nearest seafloor CPTs. Depths are in metres below seafloor (BSF)

2.4 Data processing and predictions

The convolutional neural network with the best overall performance was subsequently used to predict cone resistance values (q_n*) for all seismic lines of the HKW WFZ. Predictions were only done for CDPs on which actual geological units had been interpreted, since the interpreted geological units represent one of the input attributes required for the actual prediction. Typically, geological units are not interpreted outside the GIA (Fugro, 2019a).

CDP locations and samples that lack suitable input data get an output '-1' value in the output SEG-Y files (i.e. file with prediction of cone resistance, files with 5th and 95th percentile of confidence in error, and file with geological units.

Note that the data in the SEG-Ys was depth corrected, such that the associated depth was defined with respect to lowest astronomical tide (LAT). When compared against a reference depth with respect to seafloor (i.e. metres below seafloor).

While converting the reference level to LAT we accounted for the 2m interval that was initially removed from the top of the UHR MCS data and CPT data. Note that we did not add the original seismic (attribute) data of the top 2m below seabed on top of the synthetic qn* result, but instead added a 2- metre margin on top represented by '-1' values.

Note that LAT was used for all output files; i.e. predictions of cone resistance (i.e. q_n*), confidence values of the 5th and 95th percentile of the error of the predictions, as well as the geological units. A consequence of the conversion to LAT is that the SEG-Ys include the water column (in the depth range). Values in the ‘water column’ were also assigned ‘-1’ values.

The predictions are stored in SEG-Y files and visualized in the PDF figures in the digital deliverable.

3 Results

3.1 Comments on results

Predictions of cone resistance q_n* are visualized in PDF figures in the digital deliverable.

Two seismic lines were selected as reference lines that covered the key subsurface characteristics of the area of investigation (Figure 3.1). Results from these lines, *seq316* and *seq408,* are respectively shown in Figures 3.2 and 3.3 and Figures 3.4 and 3.5, which correspond to the actual graphical representation as visible in the PDFs presented in the digital PDF deliverable. Note that CDPs at the left and right parts of Figures 3.2 to 3.5 do not contain predictions and are left blank, because these are positioned outside the area of investigation. In the actual SEG-Y-file traces for these CDPs are set to -1, to differentiate them from the actual predictions for CDPs that are present inside the area of investigation.

The geological soil units (input attributes for the prediction) are shown in the top part of figures 3.2 and 3.4, respectively for lines *seq316* and *seq408*. Similarly, predictions of cone resistance are shown in the lower part of figures 3.2 and 3.4. The predictions show overall agreement with the distribution of the geological soil units along the lines. Typically for clayey channel infills, relatively low cone resistance values are predicted as is visible in Figures 3.2 and 3.4. This is in agreement with the reference CPTs on which the neural network was trained. Figures 3.3 and 3.5 show the quality indicators of the predictions, respectively for lines *seq316* and *seq408*. The top and bottom parts of these figures respectively show the 5th and 95th percentile of the confidence in the error of the prediction.

One artefact that can be observed is the relatively low values for q_n* at the position of the seafloor-multiple, which is the seismic reflection within the water column generating a second artificial arrival within the data. Although the multiple was suppressed during initial data processing, it still showed a gentle expression both in the original processed data and in the derived envelope attribute (i.e. one of the five input attributes used for the prediction). This artefact is also visible in the predictions and quality indicators, as is indicated with the arrows in figures 3.2 to 3.5. Also there are areas where multiple-artefacts overlap with actual natural features, as is indicated in Figures 3.4 and 3.5 for line *seq408*. The user should be aware of the occurrence of multiple-artefacts and be able to discriminate them from natural features when interpreting and using these predictions. Although less apparent, these multiple artefacts are also present in the ascii trace files, that were extracted from the synthetic qn* sections at every 100th CDP location. Here, multiples are present at a depth of approximately twice the water depth. When using the ascii trace files the reader should refer to the full synthetic sections to confirm the presence or absence of any artefacts from the water bottom multiple.

A 3D perspective of the CPT predictions for the two reference lines *seq316* and *seq408* including all considerations above and superposed CPT location HKW090 is presented in Figure 3.6. This gives an outlook on how the data looks and can be interpreted in 3D.

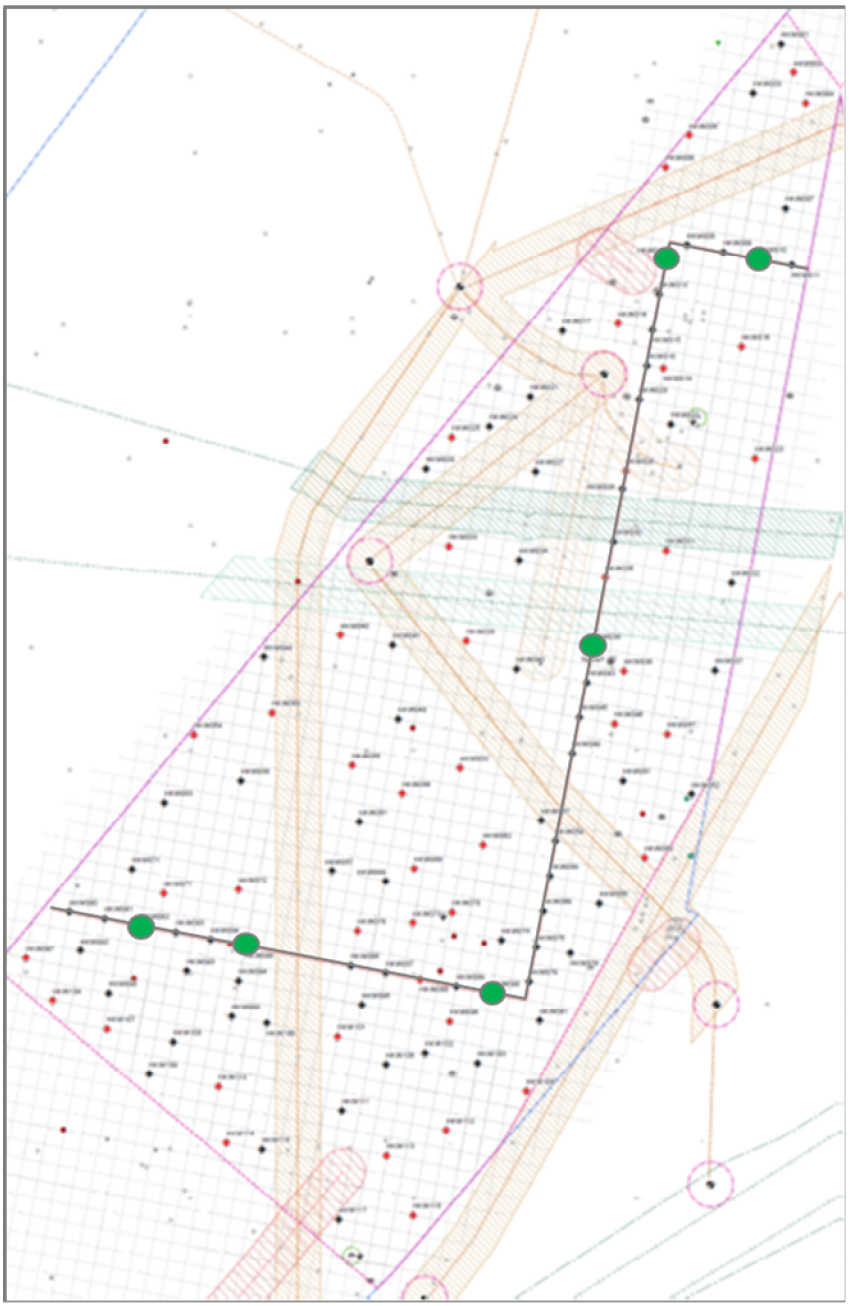

Figure 3.1 Location of GIA in the Hollandse Kust West (HKW) area. Included are the GIA polygon (blue line), all CPT locations (black and red dots), a reference line including crossing lines SEQ 316 and SEQ 408 (black line) and six reference CPT locations for initial neural network training and testing (green dots).

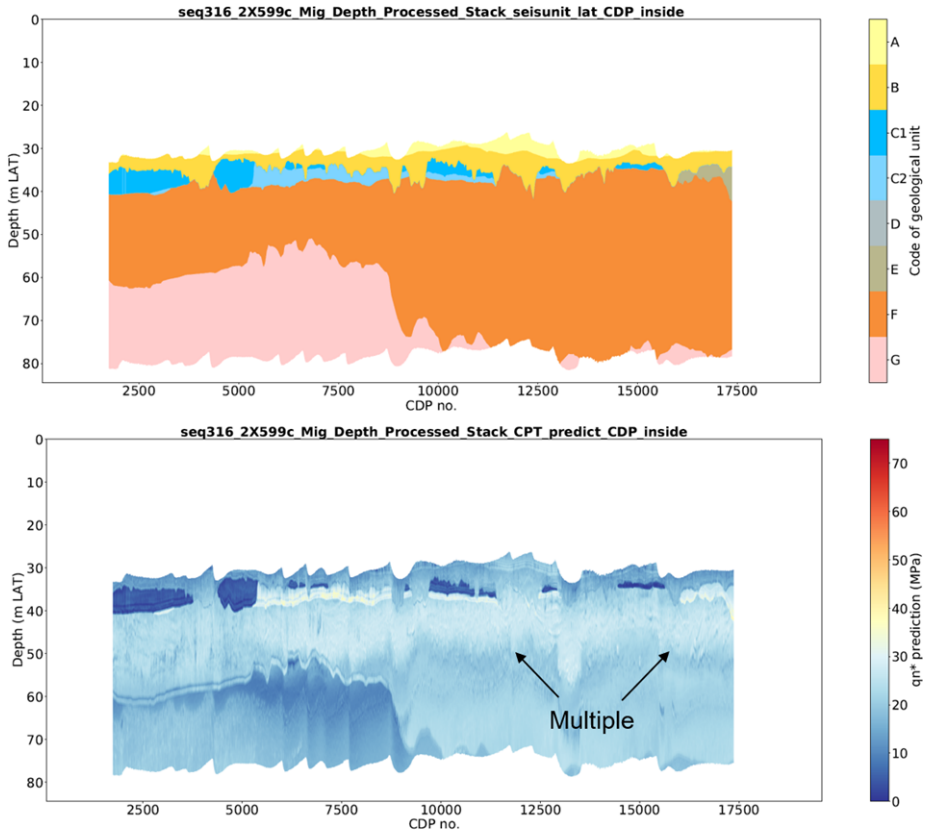

Figure 3.2 Geological units (top) and cone resistance predictions (q_n*, bottom) for line *seq316* for CDPs positioned inside the area of investigation. Depths are expressed in metres with respect to lowest astronomical tide.

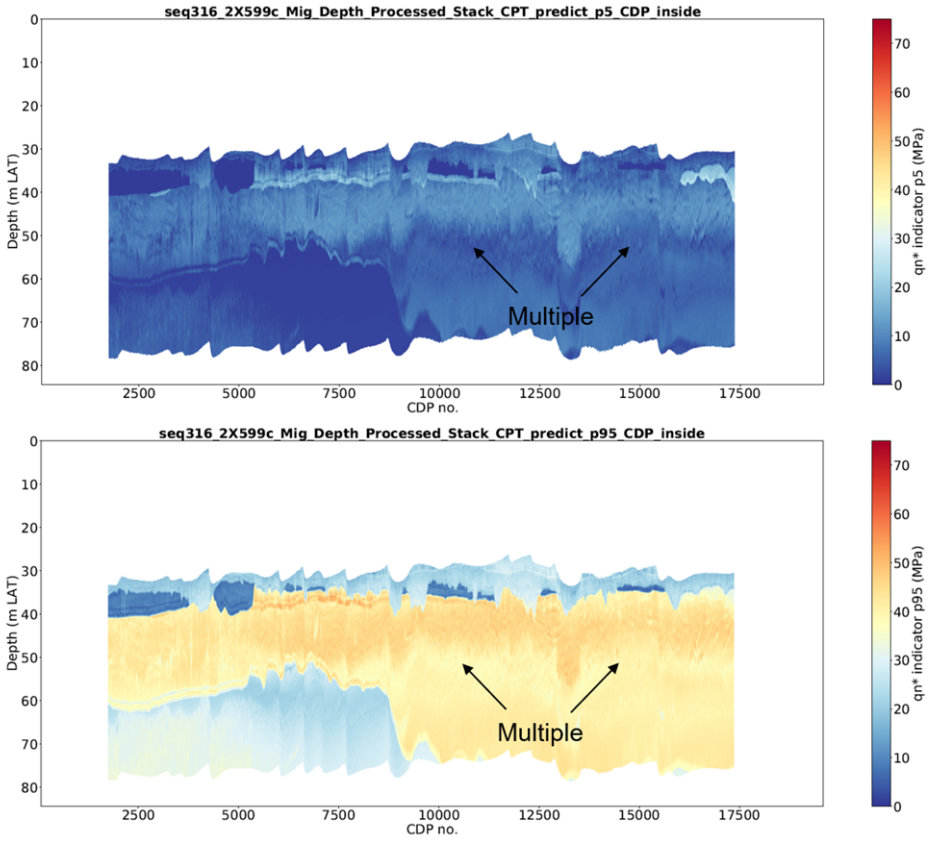

Figure 3.3 Visualization of quality indicators of q_n* prediction for line *seq316* for CDPs positioned inside the area of investigation. Top and bottom respectively show 5th and 95th percentile of confidence in error of the predictions.

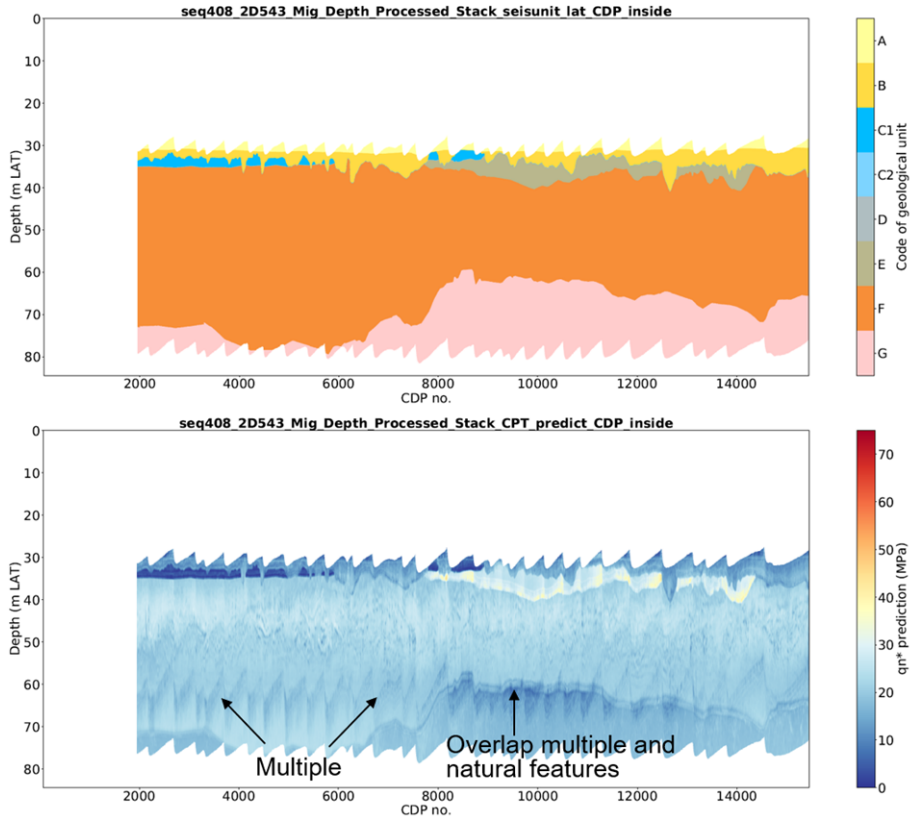

Figure 3.4 Geological units (top) and cone resistance predictions (q_n*, bottom) for line *seq408* for CDPs positioned inside the area of investigation. Depths are expressed in metres with respect to lowest astronomical tide.

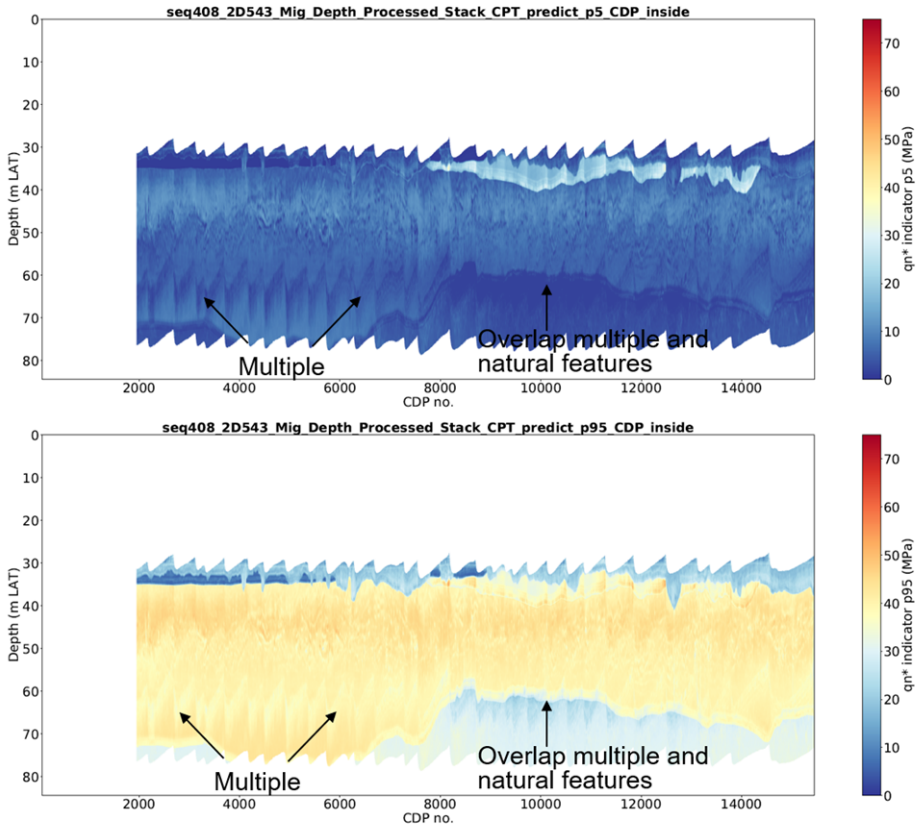

Figure 3.5 Visualization of quality indicators of q_n* prediction for line *seq408* for CDPs positioned inside the area of investigation. Top and bottom respectively show 5th and 95th percentile of confidence in error of the predictions.

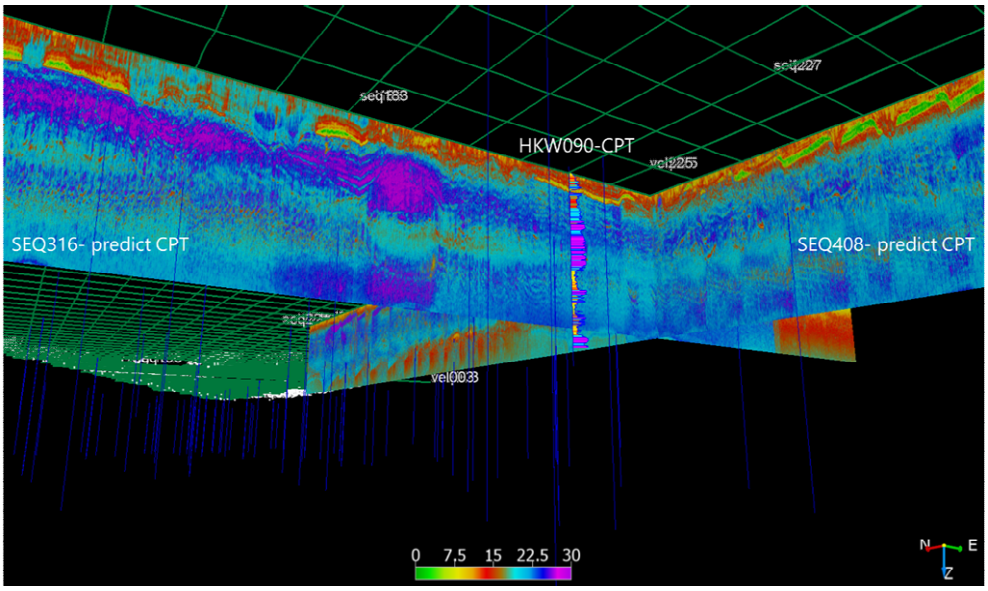

Figure 3.6 Screenshot in OpendTect of 3D intersecting lines SEQ316 and SEQ408 with overlaid CPT q_n* data at HKW090 location. The colour bar shows q_n* in MPa.

3.2 Description of PDF files and SEG-Y files

The synthetic CPT profiles made for each CDP along the 2D UHR MCS lines are presented as PDF figures. Figures for the cone resistance prediction, the two quality indicators of the predictions and the seismic units are provided for 160 seismic lines, amounting to a total 640 PDF figure files. These PDF figures are presented in the digital PDF deliverable.

In addition, 640 seismic SEG-Y files are provided for the 160 seismic lines. The SEG-Y files vary in size due to the varying number of CDPs per line. The trace header of the SEG-Y files contains various types of information, such as CDP number, coordinates of the CDP, water depth with respect to LAT and the sampling interval of 0.1 m. These SEG-Ys are provided as a separate, digital deliverable.

4 Conclusions and recommendations

In cooperation with Fugro, TNO has developed a workflow for predicting synthetic CPTs with a large element of (existing) scripting. No significant manual intervention is necessary. The input consists of the geological ground model interpretation (geological units) and seismic-based attributes.

As for the synthetic CPT prediction, we observe reasonably good CPT prediction for upper 20m below seafloor and trend-type prediction for CPT profiles below 20m including water-depth multiple. The CNN approach was checked against other Artificial Neural Networks (ANN) models and was found to be the best network.

Although most CDP locations show the typical predictions mentioned above, some soil heterogeneity is less well predicted. This especially holds for units F and G, where the model fails to predict observed maxima or minima qn* values, although extreme qn* values could be important from an engineering point of view. The trend-type prediction applies to transitional and strongly layered (<1m scale) soil, as expected. The NN model training is affected by lateral distance between CPT and nearest UHR MCS data, and the leftover discrepancy seismic and CPT interpretation of geological units.

A quality predictor is developed that applies per soil unit and considers non-gaussian parameters (median and percentiles).

The quality indicators show that the confidence in the predictions varies per seismic unit, indicating that some units have a distinctive ‘seismic signature’ that is captured in the input attributes derived from the seismic data, while other units show a less distinctive expression.

The quality indicators are a first order estimate of the confidence in the predictions, as they reflect the non-uniform distribution of CPT results over the different units. Within the CPT dataset used to train the model, some units are overrepresented, while other units are underrepresented (especially unit D). This in turn affects the reliability of the errors (truth-prediction) that are assigned to the different units to a minor extent. This is a point of consideration while using the predictions and quality indicators. Options to tackle this can be explored in future work.

5 References

Fugro, 2019. *Geophysical Results Report, Hollandse Kust (West) Wind Farm Zone Survey 2018*, Report No. P904162, Vol. 3, Revision 4 (Final). Issued 19 August 2019 to RVO, Nootdorp, Fugro.

Fugro, 2020a. *Geological Ground Model, Hollandse Kust (west) Wind Farm Zone Dutch Sector, North Sea*. Fugro Report No. P904711/06 (3), issued 12 May 2020 to RVO, Nootdorp, Fugro.

Fugro, 2020b. *Parameter Report, Hollandse Kust (west) Wind Farm Zone Dutch Sector, North Sea*. Fugro Report No. P904711/07 (3), issued 31 July 2020 to RVO, Nootdorp, Fugro.

6 Appendix

6.1 Directory structure of the data files

Figure A.1 shows the folder structure of the data files. This contains folders for the PDF figures (01_Summary Images), the SEG-Y files (02_SEG-Ys), the ascii files containing q_n* predictions (03_ASCIIs), ArcGIS shapefiles (04_GIS), and software (05_Software).

A text document, titled 'HKW_20201009_FNLM_Synthetic CPT Profiles SEG-Y Header Information_V02_F.txt', is stored within the '02_SEG-Ys' folder. This text document provides SEG-Y header information on byte locations for e.g. coordinates (X, Y) and CDPs. This basic information can be used to load the SEG-Ys in a seismic workstation / project.

The file names of the PDF figures, SEG-Y files and ascii files correspond to the line names of the original seismic lines. For each CDP number per line (every 100th) a respective ascii file is available containing information regarding the CDP number, CDP coordinates, depth (m LAT), seismic units, predicted q_n*, and the quality indicators of q_n*.

A GIS shapefile is provided that presents the locations of the selected CDP locations with reference to the provided ascii files.

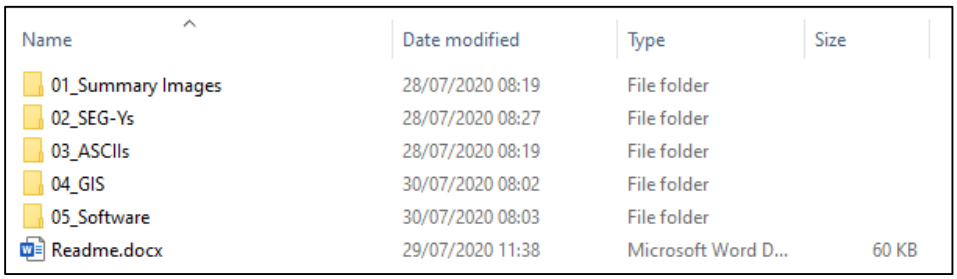

Name	Date modified	Type	Size
01_Summary Images	28/07/2020 08:19	File folder	
02_SEG-Ys	28/07/2020 08:27	File folder	
03_ASCIIs	28/07/2020 08:19	File folder	
04_GIS	30/07/2020 08:02	File folder	
05_Software	30/07/2020 08:03	File folder	
Readme.docx	29/07/2020 11:38	Microsoft Word D...	60 KB

Figure A.1. Directory structure of the data files.

6.2 How to read and use the SEG-Y files

The synthetic CPT data is stored in a mostly binary file format (SEG-Y) to save space and make examination of the data easier. This is a common format to store large quantities of (seismic) data. The SEG-Y files can be read, displayed, processed and exported by many software packages.

When unfamiliar with any of these, we recommend two free tools: SeiSee and OpendTect. The SeiSee program can read, analyse and graphically display SEG-Y files (and other file formats). The OpendTect software is an extensive and versatile package with much functionality and can do almost anything with the data, including visualising the data in 3D and loading in CPTs.

Reading SEG-Y files and visualising the seismic data with SeiSee is easy:

1) Install the SeiSee software
2) Open the SeiSee software

3) The program opens in the main display window:

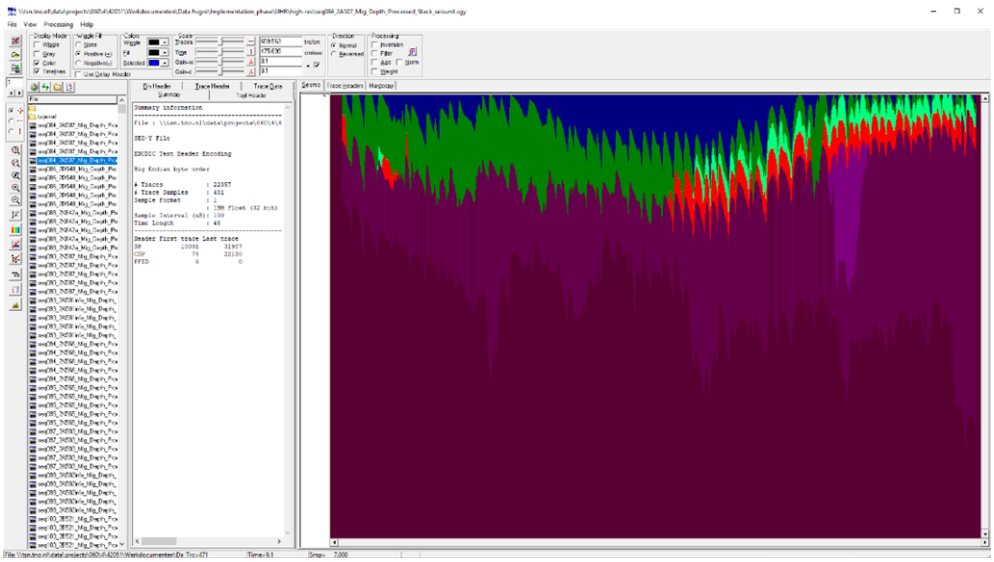

4) Select a SEG-Y file to the right and it will display

The OpendTect software has an excellent training manual that explains all steps of loading data, visualising and exporting data with examples. The training manual can be downloaded here:

https://www.dgbes.com/index.php/support

6.3 How to export traces from SEG-Y files

The programs can also write or convert a whole SEG-Y file or part of it to disk in other file formats, with the ability to select data on the basis of trace number or check header values and output a given time interval. This should suffice most needs.

In order to export traces with SeiSee:

1) Open the ‘File’ tab in the upper left and select ‘Save as’:

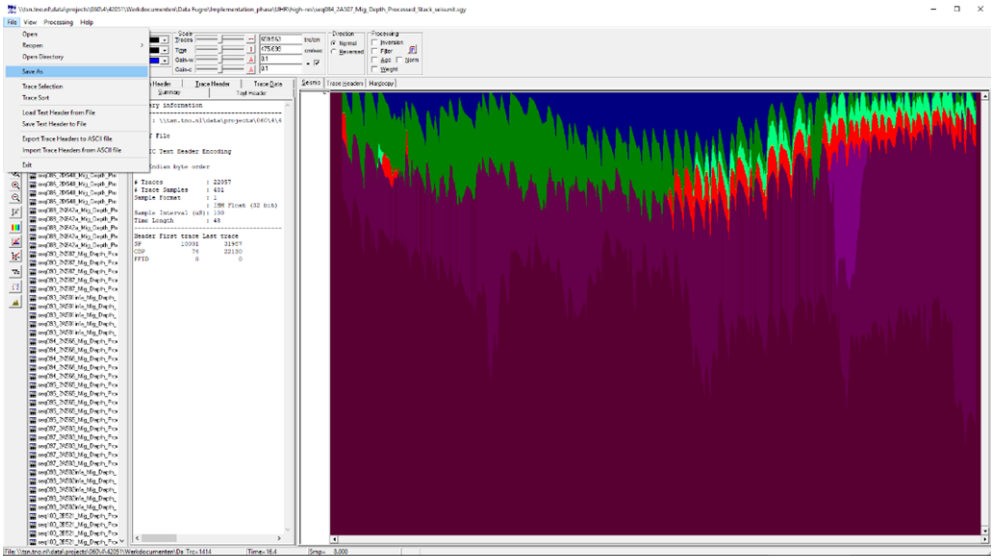

2) Click ‘Save as’ and a window will open letting you select the part of the data you wish, like a specific CDP, to export as ascii or another format:

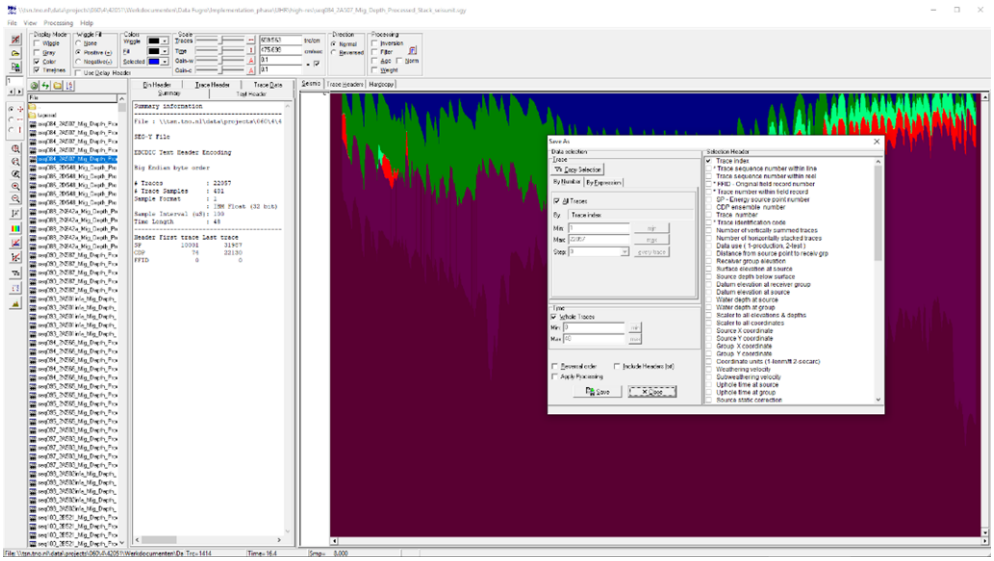

3) After selecting the proper parameters, click ‘Ok’ and the selected data will be saved in the format you have chosen.

APPENDIX C: DESCRIPTION OF METHODS AND PRACTICES

CONTENTS

	Reference
Abbreviations	FNLM/GEO/APP/080
Symbols	FNLM/GEO/APP/017
Use of Geodata and Advice	FNLM/GEO/APP/077
Cone Penetration Test	FNLM/GEO/APP/001
Cone Penetration Test Interpretation	FNLM/GEO/APP/012
Marine Reflection Seismics	FNLM/GEO/APP/016
Site Characterisation	FNLM/GEO/APP/075
Positioning Survey and Depth Measurement	FNLM/GEO/APP/029

This appendix presents method statements and terminology that are generally familiar to expert users of the information.

Abbreviations

I – General

1D	one-dimensional
2D	two-dimensional
3D	three-dimensional
API	American Petroleum Institute
ASTM	American Society for Testing and Materials
BSI	British Standards Institution
COV	coefficient of variation
FEED	front-end engineering design
GIS	geographical information system
ISO	International Organization for Standardization
SD	standard deviation

II – Geodetics

BGL	below ground level
BSF	below seafloor
CD	chart datum
CM	central meridian
DGPS	Differential Global Positioning System
CRS	coordinate reference system
ED	European Datum
ETRS	European terrestrial reference system
GNSS	Global Navigation Satellite System
GPS	Global Positioning System
GRS	Geodetic Reference System
INS	inertial navigation system
LAT	Lowest Astronomical Tide
MSL	Mean Sea Level
TM	Transverse Mercator
USBL	ultra short baseline
UTC	Coordinated Universal Time
UTM	Universal Transverse Mercator
WGS	World Geodetic System

III – Site Investigation

ABI	acoustic borehole imager
ASV	autonomous surface vehicle
AUV	autonomous underwater vehicle
BC	box core(r)
BH	borehole
BGL	borehole geophysical logging
BPT	ball penetration test
CAL	caliper tool
CDP	common depth point
CMP	common mid-point
CPT	cone penetration test
CPTU	piezocone penetration test (or PCPT)
CTD	conductivity temperature depth
FFP	free-fall penetration test
FLPC	Fugro large piston core(r)
GC	gravity core(r)
GR	natural gamma radiation
GS	grab sample(r)
HRS	high resolution seismic reflection
ID	inner diameter
LDPC	large diameter piston core(r)
LGPC	large gravity piston core(r)
MAG	magnetometer
MBES	multibeam echosounder
MBPT	miniature ball penetration test
MCS	multichannel seismic reflection
MTPT	miniature T-bar penetration test
MV	motor vessel
OD	outer diameter
PC	piston core(r)
PPDT	pore pressure dissipation test
PSSL	P and S suspension logger
RC	rotary core(r)
ROV	remotely operated vehicle
SBES	single beam echosounder
SBF	seabed frame
SBP	sub-bottom profiler, seismic reflection
SCPT	seismic cone penetration test
SCS	single channel seismic reflection
SGR	spectral gamma radiation
SIR	strong impedance reflector
SSDM	Seabed Survey Data Model
SSS	side scan sonar
STACOR®	stationary piston gravity core(r)
SV	sailing vessel
SVP	sound velocity profiler
TPT	T-bar penetration test
TWTT	two-way travel time, seismic reflection
UHRS	ultra high resolution seismic reflection
VC	vibrocore(r)
VST	vane shear test
WISON®	wireline sounding tool
WIP	wireline push sampler

IV – Site Characterisation

BP	before present
DTM	digital terrain model
Fm	geological formation
LGM	last glacial maximum
Mb	geological formation member
MDAC	methane-derived authigenic carbonate
MTD	mass transport deposit
UXO	unexploded ordnance

V – Geotechnical Analysis

ALS	accidental limit state
ASD	allowable stress design
FLS	fatigue limit state
LSD	limit state design
PFD	partial factor design
SLS	serviceability limit state
ULS	ultimate limit state
WSD	working stress design

© Fugro 2017-2020

Symbols

Symbol	Unit	Quantity
I - General		
A	m^2	Area
L	m	Length
B	m	Width
D	m	Diameter
U	-	Uncertainty of parameter value
V	m^3	Volume
W	kN	Weight
a	m/s^2	Acceleration
d	m	Depth
g	m/s^2	Acceleration due to gravity ($g = 9.81$ m/s^2)
h	m	Height or thickness
i	-	Inclination
m	kg	Mass
t	s	Time
t	a	Time, mean Julian year
v	m/s	Velocity
z	m	Penetration or depth below reference level (usually ground surface)
$\dot{\varepsilon}$	s^{-1}	Rate of strain (length)
ρ	kg/m^3	Density
π	-	Mathematical constant (= 3.14159)
e	-	Base of natural logarithm (= 2.71828)
ln	-	Natural logarithm
log	-	Logarithm base 10
II - Stress and Strain		
P_a	kPa	Atmospheric pressure
u	MPa	Pore pressure
u_o	MPa	Hydrostatic pore pressure relative to seafloor or phreatic surface
u_f	MPa	Pore pressure at failure
Δu	MPa	Change in pore pressure or excess pore pressure
σ	kPa	Total stress
σ'	kPa	Effective stress
τ	kPa	Shear stress
τ_{peak}	kPa	Peak shear stress
$\sigma_1, \sigma_2, \sigma_3$	kPa	Principal stresses
σ_h	kPa	Total horizontal stress
$\Delta\sigma_h$	kPa	Change in total horizontal stress
σ_v	kPa	Total vertical stress
$\Delta\sigma_v$	kPa	Change in total vertical stress
σ_{h0}	kPa	Total in situ horizontal stress relative to ground surface or phreatic surface
σ'_{h0}	kPa	Effective in situ horizontal stress
σ_{v0}	kPa	Total in situ vertical stress relative to ground surface or phreatic surface
σ'_{v0}	kPa	Effective in situ vertical stress (or p'_0)
σ'_h	kPa	Effective horizontal stress
σ'_v	kPa	Effective vertical stress
σ'_r	kPa	Effective radial stress
σ'_a	kPa	Effective axial stress
r_u	-	Pore pressure ratio [$= u/\sigma_{v0}$]
p'	kPa	Mean effective stress [$= (\sigma'_1 + \sigma'_2 + \sigma'_3)/3$]
q	kPa	Principal deviator stress [$= \sigma'_1 - \sigma'_3$] or [$= \sigma_1 - \sigma_3$]
q_{ref}	kPa	Reference principal deviator stress
s'	kPa	Mean effective stress in $s' - t$ space [$= (\sigma'_1 + \sigma'_3)/2$]
t	kPa	Shear stress in $s' - t$ space [$= (\sigma'_1 - \sigma'_3)/2$] or [$= (\sigma_1 - \sigma_3)/2$]
ε	-	Linear strain
$\varepsilon_1, \varepsilon_2, \varepsilon_3$	-	Principal strains
ε_v	-	Vertical strain (or volumetric strain)
ε_{vol}	-	Volumetric strain

© Fugro 1994-2020

Symbol	Unit	Quantity
γ	-	Shear strain
γ_c	-	Shear strain at maximum shear stress
ν	-	Poisson's ratio
ν_u	-	Poisson's ratio for undrained stress change
ν_d	-	Poisson's ratio for drained stress change
E	MPa	Modulus of linear deformation (Young's modulus)
E_{max}	MPa	Modulus of linear deformation at small strain
E_u	MPa	Modulus of linear deformation (Young's modulus for undrained stress change)
E_d	MPa	Modulus of linear deformation (Young's modulus for drained stress change)
G	MPa	Modulus of shear deformation (shear modulus)
G_{max}	MPa	Shear modulus at small strain
I_r	-	Rigidity index [= G/τ_{max} or G/s_u]
K	MPa	Modulus of compressibility (bulk modulus)
M	MPa	Constrained modulus [= $1/m_v$]
M_{max}	MPa	Constrained modulus at small strain
μ	-	Coefficient of friction
η	kPa.s	Coefficient of viscosity

III - Physical Characteristics of Ground

(a) Density and Unit Weights

γ	kN/m^3	Unit weight of ground (or bulk unit weight or total unit weight)
γ_d	kN/m^3	Unit weight of dry ground
γ_s	kN/m^3	Unit weight of solid particles
γ_w	kN/m^3	Unit weight of water
γ_{pf}	kN/m^3	Unit weight of pore fluid
γ_{dmin}	kN/m^3	Minimum index (dry) unit weight
γ_{dmax}	kN/m^3	Maximum index (dry) unit weight
γ'	kN/m^3	Unit weight of submerged ground (or γ_{sub})
ρ	Mg/m^3 [= t/m^3]	Density of ground (or bulk density)
ρ_d	Mg/m^3 [= t/m^3]	Density of dry ground
ρ_s	Mg/m^3 [= t/m^3]	Density of solid particles (or G_s)
ρ_w	Mg/m^3 [= t/m^3]	Density of water
D_r	-, %	Relative density [= $I_D = \gamma_{dmax}(\gamma_d - \gamma_{dmin})/\gamma_d(\gamma_{dmax} - \gamma_{dmin})$ = $(e_{max} - e)/(e_{max} - e_{min})$]
v	-	Specific volume [= $1 + e$]
e	-	Void ratio
e_0	-	Initial void ratio
$e_{\sigma'_{v0}}$	-	Void ratio at σ'_{v0} (or e_0)
e_{max}	-	Maximum index void ratio
e_{min}	-	Minimum index void ratio
G_s	-	Specific gravity of solid particles
I_D	-, %	Density index [= D_r]
R_D	-, %	Dry density ratio [= γ_d/γ_{dmax}]
n	-, %	Porosity
w	%	Water content
S_r	%	Degree of saturation
r	-, g/kg	Salinity of pore fluid [= ratio of mass of salt to mass of pore fluid]
R	g/l	Salinity of fluid [= ratio of mass of salt to volume of distilled water]
s	g/l	Salinity of fluid [= ratio of mass of salt to volume of fluid]
S	g/kg	Salinity of seawater [= ratio of mass of salt to mass of seawater]

(b) Consistency

w_L	%	Liquid limit
w_P	%	Plastic limit
I_P	%	Plasticity index [= $w_L - w_P$]
I_L	%	Liquidity index [= $(w - w_P)/(w_L - w_P)$]
I_C	%	Consistency index [= $(w_L - w)/(w_L - w_P)$]
A	-, %	Activity [= ratio of plasticity index to percentage by weight of clay-size particles]

© Fugro 1994-2020

Symbol	Unit	Quantity
(c) Particle Size		
D	mm	Particle diameter
D_n	mm	Particle diameter, where n% of the dry mass of ground has a smaller particle diameter
C_u	-	Uniformity coefficient [$= D_{60}/D_{10}$]
C_c	-	Curvature coefficient [$= (D_{30})^2/D_{10}D_{60}$]
(d) Acoustic Properties		
S_{vh}	-	S-wave propagating in the vertical direction with particle motion in the horizontal direction
S_{hh}	-	S-wave propagating in the horizontal direction with particle motion in the horizontal direction
S_{hv}	-	S-wave propagating in the horizontal direction with particle motion in the vertical direction
v_p	m/s	P-wave velocity (compression wave velocity)
v_s	m/s	S-wave velocity (shear wave velocity)
v_{s1}	m/s	S-wave velocity normalised to 100 kPa in situ vertical stress
v_{vh}	m/s	S-wave velocity, vertically (v) propagated, horizontally (h) polarised
(e) Hydraulic Properties		
k	m/s	Coefficient of permeability
k_v	m/s	Coefficient of vertical permeability
k_h	m/s	Coefficient of horizontal permeability
i	-	Hydraulic gradient
(f) Thermal and Electrical Properties		
T	K, °C	Temperature
k	W/(m·K)	Thermal conductivity
a_L	1/°C	Thermal expansion coefficient (linear)
α	m^2/s	Thermal diffusion coefficient
C	MJ/m^3K	Volumetric heat capacity
ρ	Ωm	Electrical resistivity
K	S/m	Electrical conductivity
(g) Magnetic Properties		
B	T	Magnetic flux density (or magnetic induction)
(h) Radioactive Properties		
γ	CPS	Natural gamma ray
IV - Mechanical Characteristics of Ground		
(a) Cone Penetration Test (CPT)		
q_c	MPa	Cone resistance
q_{c1}	MPa	Cone resistance normalised to 100 kPa effective in situ vertical stress
f_s	MPa	Sleeve friction
f_t	MPa	Sleeve friction corrected for pore pressures acting on the end areas of the friction sleeve
R_f	%	Ratio of sleeve friction to cone resistance
R_{ft}	%	Ratio of sleeve friction to corrected cone resistance (f_s/q_t or f_t/q_t)
u_1	MPa	Pore pressure at the face of the cone
u_2	MPa	Pore pressure at the cylindrical extension above the base of the cone or in the gap between the friction sleeve and the cone
$u_2{}^*$	MPa	Pore pressure u_2, but derived rather than measured
u_3	MPa	Pore pressure immediately above the friction sleeve or in the gap above the friction sleeve
K	-	Adjustment factor for ratio of pore pressure at u_1 to u_2 location
q_n	MPa	Net cone resistance
q_t	MPa	Corrected cone resistance (or total cone resistance)
B_q	-	Pore pressure ratio
Q_t	-	Normalized cone resistance [$= q_n/\sigma'_{v0}$]
Q_{tn}	-	Normalized cone resistance with variable stress exponent
F_r	%	Normalized friction ratio [$= f_t/q_n$]
I_c	-	Soil behaviour type index (for Q_{tn} and F_r)

© Fugro 1994-2020

Symbol	Unit	Quantity
I_{SBT}	-	Soil behaviour type index (for q_c and R_f)
N_c	-	Cone factor between q_c and s_u
N_{kt}	-	Cone factor between q_n and s_u (or N_k)
$N_{\Delta u}$	-	Pore pressure factor between $u_2 - u_0$ and s_u

(b) Standard Penetration Test (SPT)

N	Blows/0.3 m	SPT blow count
N_{60}	Blows/0.3 m	SPT blow count normalised to 60 % energy
$N_{1,60}$	Blows/0.3 m	SPT blow count normalised to 60 % energy and to 100 kPa effective in situ vertical stress

(c) Strength and Stiffness of Soil – Static

s_u	kPa	Undrained shear strength (or c_u)
s_{uC}	kPa	Undrained shear strength in laboratory triaxial compression (or c_{uC})
s_{uD}	kPa	Undrained shear strength in laboratory direct simple shear (or c_{uD})
s_{uE}	kPa	Undrained shear strength in laboratory triaxial extension (or c_{uE})
$s_{u;ref}$	kPa	Reference undrained shear strength
s_u/σ'_{v0}	-	Undrained strength ratio
κ	kPa/m	Rate of increase of undrained shear strength with depth (linear)
c'	kPa	Effective cohesion intercept
φ'	°(deg)	Effective angle of internal friction (or ϕ')
φ'_{cv}	°(deg)	Effective angle of internal friction at large strain (or ϕ'_{cv})
ψ	°(deg)	Angle of dilation (or dilatancy angle)
ε_{50}	%	External axial strain at half the maximum deviator stress (or ε_c)
ε_c	%	External axial strain at the maximum deviator stress
E_{50}	MPa	Secant Young's modulus at half the maximum deviator stress
$s_{u;r}$	kPa	Undrained shear strength of remoulded soil
$s_{u;ar}$	kPa	Undrained shear strength of aged remoulded soil
s_R	kPa	Undrained residual shear strength
S_t	-	Sensitivity [= $s_u/s_{u;r}$ or s_u/s_R]
T_x	-	Thixotropy strength ratio $[T_x(t) = s_{u;ar}(t)/s_{u;r}]$
M	-	Gradient of critical state line when projected onto a constant volume plane
A	-	Pore pressure coefficient for anisotropic pressure increment
B	-	Pore pressure coefficient for isotropic pressure increment

(d) Strength and Stiffness of Soil – Cyclic and Dynamic

N	-	Number of cycles (or cycle number)
N_f	-	Number of cycles to soil failure or final number of cycles
N_{eq}	-	Equivalent number of cycles
τ_0	kPa	Initial shear stress
τ_{av}	kPa	Average shear stress or constant shear stress (or τ_a)
τ_{cy}	kPa	Cyclic shear stress amplitude [= $(\tau_{max} - \tau_{min})/2$]
$\tau_{cy,f}$	kPa	Cyclic shear strength at a specified failure criterion [= $(\tau_{av} + \tau_{cy})_f$]
τ_{max}	kPa	Maximum shear stress
τ_{min}	kPa	Minimum shear stress
γ_{av}	%	Average shear strain (or γ_a) [= $(\gamma_{max} + \gamma_{min})/2$]
γ_{cy}	%	Cyclic shear strain amplitude [= $(\gamma_{max} - \gamma_{min})/2$]
γ_{max}	%	Maximum shear strain
γ_{min}	%	Minimum shear strain
γ_p	%	Permanent shear strain
σ'_{ac}	kPa	Effective axial consolidation stress
σ'_{rc}	kPa	Effective radial consolidation stress
σ'_{ref}	kPa	Reference effective stress
q_{cy}	kPa	Cyclic deviator stress amplitude [= $(q_{max} - q_{min})/2$]
q_{max}	kPa	Maximum deviator stress
q_{min}	kPa	Minimum deviator stress
q_{av}	kPa	Average deviator stress [= $(q_{max} + q_{min})/2$]
ε_{cy}	%	Cyclic axial strain (or cyclic vertical strain) amplitude [= $(\varepsilon_{max} - \varepsilon_{min})/2$]
ε_{max}	%	Maximum axial strain (or maximum vertical strain)
ε_{min}	%	Minimum axial strain (or minimum vertical strain)
ε_{av}	%	Average axial strain (or average vertical strain) [= $(\varepsilon_{max} + \varepsilon_{min})/2$]

© Fugro 1994-2020

Symbol	Unit	Quantity
ε_a	%	External axial strain at N_f (or external vertical strain at N_f)
E_{ext}	MPa	Young's modulus derived from loop stiffness and external axial strain
E_{loc}	MPa	Young's modulus derived from loop stiffness and local axial strain
u_a	kPa	Average pore pressure
u_{cy}	kPa	Cyclic pore pressure amplitude [$= (u_{max} - u_{min})/2$]
u_{max}	kPa	Maximum pore pressure
u_{min}	kPa	Minimum pore pressure
u_p	kPa	Permanent pore pressure
λ	-, %	Damping ratio of ground (or D)
λ_{ext}	%	Damping ratio derived from external axial strain
λ_{loc}	%	Damping ratio derived from local axial strain

(e) Strength of Rock

σ_c	MPa	Uni-axial compressive strength
$I_{s(50)}$	MPa	Point load strength index
NPR	N/mm	Needle point resistance

(f) Consolidation (One Dimensional)

σ'_{hc}	kPa	Effective horizontal consolidation stress
σ'_{vc}	kPa	Effective vertical consolidation stress
σ'_p	kPa	Effective preconsolidation stress (or effective vertical yield stress in situ)
σ^*_{ve}	kPa	Effective vertical stress on ICL at e_0
σ'_{vy}	kPa	Effective vertical yield stress in situ (or effective preconsolidation stress)
C_c	-	Compression index
C^*_c	-	Intrinsic compression index [$= e^*_{100} - e^*_{1000}$]
C_s	-	Swelling index (or re-compression)
CR	-	Primary compression ratio [$= C_c/(1 + e_0)$]
RR	-	Recompression ratio [$= C_s/(1 + e_0)$]
e_L	-	Void ratio at liquid limit w_L
e^*_{100}	-	Void ratio at σ'_v= 100 kPa during one-dimensional intrinsic compression
e^*_{1000}	-	Void ratio at σ'_v = 1000 kPa during one-dimensional intrinsic compression
C_α	-	Coefficient of secondary compression (primary compression)
$C_{\alpha s}$	-	Coefficient of secondary compression (swelling/re-compression)
c_v	m^2/s	Coefficient of consolidation
H	m	Drainage path length
ICL	-	Intrinsic compression line (Burland, 1990)
I_v	-	Void index [$= (e_0 - e^*_{100})/ C^*_c$]
m_v	m^2/MN	Coefficient of volume compressibility
M	MPa	Constrained modulus [$= 1/m_v$]
p	kPa	Vertical pressure
OCR	-	Overconsolidation ratio [$= \sigma'_p/\sigma'_{v0}$] (or yield stress ratio)
SCC	-	Sedimentation compression curve
SCL	-	Sedimentation compression line (Burland, 1990)
S_σ	-	Stress sensitivity [$= \sigma'_{vy}/\sigma^*_{ve}$]
YSR	-	Yield stress ratio [$= \sigma'_{vy}/\sigma'_{v0}$] (or overconsolidation ratio)

V - Geotechnical Design

(a) Partial Factors

γ_d	-	Factor related to model uncertainty or other circumstances
γ_f	-	Partial action factor (load factor)
γ_m	-	Partial material factor (partial safety factor)
γ_R	-	Partial resistance factor (partial safety factor)

(b) Seismicity

a_g	m/s^2	Effective peak ground acceleration (design ground acceleration)
d_g	m	Peak ground displacement
α	-	Acceleration ratio [$= a_g/g$]
τ_c	kPa	Seismic shear stress

© Fugro 1994-2020

Symbol	Unit	Quantity

(c) Compaction

ρ_{dmax}	Mg/m^3 [= t/m^3]	Maximum dry density
ρ_{max}	Mg/m^3 [= t/m^3]	Maximum density
w_{opt}	%	Optimum moisture content

(d) Earth Pressure

δ	°(deg)	Angle of interface friction (between ground and foundation)
K	-	Coefficient of lateral earth pressure
K_a	-	Coefficient of active earth pressure
K_{ac}	-	Coefficient of active earth pressure for total stress analysis
K_p	-	Coefficient of passive earth pressure
K_{pc}	-	Coefficient of passive earth pressure for total stress analysis
K_0	-	Coefficient of earth pressure at rest
K_{0nc}	-	K_0 for normally consolidated soil
K_{0oc}	-	K_0 for overconsolidated soil

(e) Foundations

A	m^2	Total foundation area
A'	m^2	Effective foundation area
B'	m	Effective width of foundation
E_s	MN/m^3	Modulus of subgrade reaction
k	MPa/m	Rate of change of modulus of subgrade reaction E_s with depth z
L'	m	Effective length of foundation
H	MN	Horizontal external force or action
V	MN	Vertical external force or action
M	MN.m	External moment
T	MN.m	External torsion moment
Q	MN	Total vertical resistance of a foundation/pile
Q_p	MN	End bearing of pile
Q_s	MN	Shaft resistance of pile
q_p	MPa	Unit end bearing
q_{lim}	MPa	Limit unit end bearing
f	kPa	Unit skin friction (or q_s)
f_{lim}	kPa	Limit unit skin friction
p	MN/m	Lateral resistance per unit length of pile
p_{lim}	MN/m	Limit lateral resistance per unit length of pile
s	m	Settlement
t	MN/m	Skin friction per unit length of pile
y	mm	Lateral pile deflection
z	mm	Axial pile displacement
α	-	Adhesion factor between ground and foundation (= f/s_u)
β	-	Adhesion factor between ground and foundation (= f/σ'_v or f/σ'_{v0})
δ	°(deg)	Angle of interface friction (between ground and foundation)
δ_{cv}	°(deg)	Constant volume or critical-state angle of interface friction (between ground and foundation)
N_c, N_q, N_γ	-	Bearing capacity factors
K_c, K_q, K_γ	-	Bearing capacity correction factors for inclined forces or actions, foundation shape and depth of embedment
i_c, i_q, i_γ	-	Bearing capacity correction factors for external force inclined from vertical shape
S_c, S_q, S_γ	-	Bearing capacity correction factors for foundation shape
d_c, d_q, d_γ	-	Bearing capacity correction factors for foundation embedment

Signs:
- A "prime" applies to effective stress.
- A "bar" above a symbol relates to average properties.
- A "dot" above a symbol denotes derivative with respect to time.
- The prefix "Δ" denotes an increment or a change.
- A “star” after a symbol denotes value corrected for pore fluid salinity.

© Fugro 1994-2020

Use of Geodata and Advice

Introduction

This document provides important information regarding the use of Fugro geodata, analyses and advice.

Site-specific acquisition of geodata can include metocean monitoring, geophysical seafloor mapping, subsurface mapping, logging of boreholes, in situ testing, laboratory testing of samples and monitoring of structures or elements of structures.

The cost of geodata acquisition, interpretation and monitoring is a small portion of the total cost of a development such as a construction project. By contrast, the costs of correcting a wrongly designed programme or mobilising alternative construction methods are often far greater than the cost of the original investigation for a site or structure.

Attention and adherence to the information presented in this document can reduce delays and cost overruns related to site-specific factors.

The focus of this document is on construction projects. This document also applies to information and advice related to asset integrity and decommissioning.

Requirements for Quality Geodata

Project quality management should follow ISO 9001 quality principles for project management and ISO 2394 for general principles on reliability for structures. Project activities usually comprise part of specific phases of a construction project. The quality plan for the entire construction project should incorporate geodata input in every phase - from the feasibility planning stages to project completion. The parties involved should do the following:

- Provide complete and accurate information necessary to plan an appropriate site investigation.
- Describe the purpose(s), type(s) and construction methods of planned structures in detail.
- Provide the time, financial, personnel and other resources necessary for the planning, execution and follow-up of a site investigation programme.
- Understand the limitations and degree of accuracy inherent in geodata.
- Understand the limitations and degree of accuracy inherent in the advice based upon site investigation data.
- During all design and construction activities, be aware of the limitations of site investigation data and analyses/ advice, and use appropriate preventative measures.
- Incorporate all geodata input in the design, planning, construction and other activities involving the site and structures. Provide the entire (set of) document(s), including digital files where applicable, to parties involved in site selection, design and construction.
- Use the site investigation data and advice for only the structures, site and activities which were described to Fugro prior to and for the purpose of planning the site investigation or the programme of analysis and advice.

Authority, Time and Resources Necessary for Site Investigations

Adequate designation of authority and accountability for site-specific aspects of construction projects is necessary. This way, an appropriate investigation can be performed, and the use of the results by project design and construction professionals can be optimised.

Figure 1 illustrates the importance of the initial project phases for gathering adequate geodata for a project. The initial phases, when site investigation requirements are defined and resources are allocated, are represented by more than 50 % of the Quality Triangle (Figure 1). Decisions and actions made during these phases have a large impact of the outcome and thus the potential of the investigation to meet project requirements.

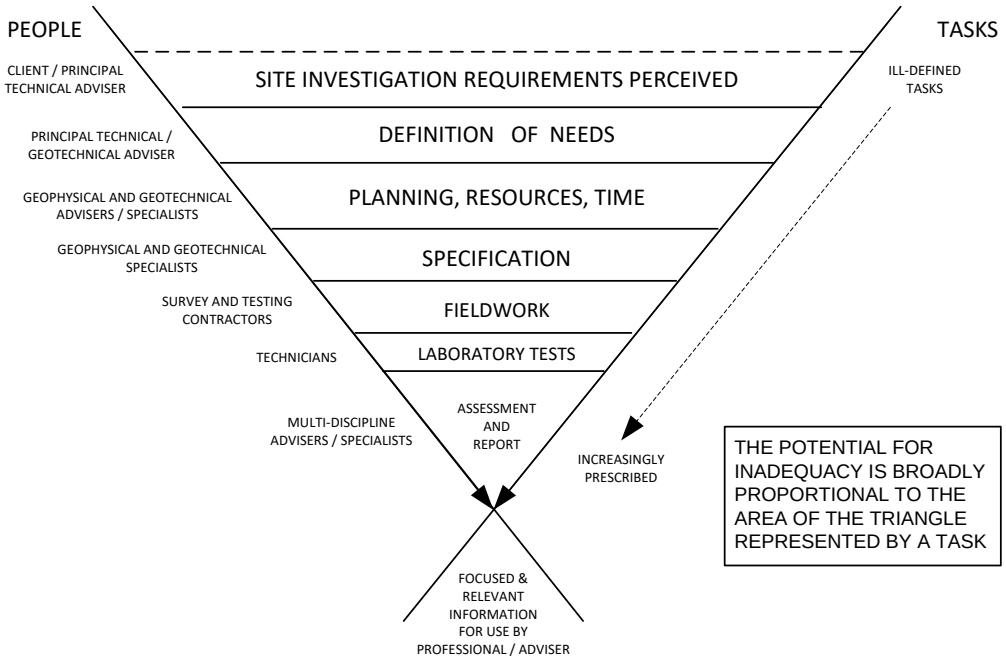

Figure 1: Quality of Site Investigation (adapted from SISG[1]).

[1] Site Investigation Steering Group SISG (1993). *Site investigation in construction 2: planning, procurement and quality management*. Thomas Telford.

© Fugro 1996-2019

Data Acquisition and Monitoring Programmes

Site-specific investigations, such as geophysical and geotechnical investigations, are operations of discovery. Investigation should proceed in logical stages. Planning should allow operational adjustments deemed necessary by newly available information. This observational approach permits the development of a sound engineering strategy and reduces the risk of discovering unexpected (geo)hazards during or after construction.

Data Types and Limitations

1. Reliability of Supplied Information

Analysis and advice can involve the use of information and physical material that is publicly available or supplied by the client. Examples are geodetic data, geological maps, geophysical records, earthquake data, earlier geotechnical logs and soil samples. Fugro endeavours to identify potential anomalies but does not independently verify the accuracy or completeness of public or client-supplied information unless indicated otherwise. This information, therefore, can limit the accuracy of the geodata, analyses and advice.

2. Complexity of Ground Conditions

There are hazards associated with the ground. An adequate understanding of these hazards can help to minimize risks to a project and the site. The ground is a vital element of all structures which rest on or in the ground. Information about ground behaviour is necessary to achieve a safe and economical structure. Often less is known about the ground than for any other element of a structure.

3. Site Investigation - Spatial Coverage Limitations

Geophysical investigations typically provide information about ground conditions along survey track lines. Geotechnical investigations collect data at specific test locations. Interpretation of ground conditions away from survey track lines and test locations is a matter of extrapolation and judgement based on geological and geotechnical knowledge, as well as on experience. Nevertheless, actual conditions in untested areas may differ from predictions. For example, the interface between ground materials may be far more gradual or abrupt than indicated by the geodata. It is not realistic to expect a site investigation to reveal or anticipate every detail of ground conditions. Nevertheless, an investigation can reduce the residual risk associated with unforeseen conditions to a tolerable level. If ground problems do arise, it is important to have relevant expertise available to help reduce and mitigate safety and financial risks.

4. Role of Judgement and Opinion In Analysis and Advice

Analysis and advice that involve geodata are less exact than most other design disciplines. Extensive judgement and opinion are often required. Therefore, geodata, analyses and advice may contain definitive statements that identify where the responsibility of Fugro begins and ends. These are not exculpatory clauses designed to transfer liabilities to another party, but they are statements that can help all parties involved to recognise their individual responsibilities and take appropriate actions.

Complete Information should be Available to all Parties Involved

To prevent costly construction problems, construction contractors should have access to the best available information. They should have access to the complete original (set of) documents including digital files where applicable, to prevent or minimize any misinterpretation of site conditions and advice. To prevent errors or omissions that could lead to misinterpretation, geophysical sections, geotechnical logs and illustrations should not be redrawn, and users of geodata and advice should confer with the authors when applying the geodata and/or advice.

Information is Project-Specific

Fugro's investigative programmes, analyses and advice are designed and conducted specifically for the client described project and conditions. Thus the geodata, analyses and advice present information for a unique construction project. Project-specific factors for a structure include but are not limited to:

- location
- size and configuration of structure
- type and purpose or use of structure
- other facilities or structures in the area.

Any factor that changes subsequent to the preparation of the geodata, analyses and advice may affect its applicability. A specialised review of the impact of changes would be necessary. Fugro is not responsible for conditions which develop after change of any factor in site investigation programming, development or structure.

For purposes or parties other than the original project or client, the geodata, analyses and advice may not be adequate and should not be used.

Changes in Site Conditions Affect the Accuracy/Suitability of the Data

Ground is complex and can be changed by natural phenomena such as earthquakes, floods, seabed scour and groundwater fluctuations. Construction operations at or near the site can also change ground conditions. The geodata, analyses and advice consider conditions at the time of investigation. Construction decisions should consider any changes in site conditions, regulatory provisions, technology or economic conditions subsequent to the investigation. In general, two years after the date of geodata, analyses and advice, the information may be considered inaccurate or unreliable. A specialist should be consulted regarding the adequacy of the geodata, analyses and advice for use after any passage of time.

© Fugro 1996-2019

Cone Penetration Test

Introduction

The cone penetration test (CPT) involves the measurement of the resistance of ground to steady and continuous penetration of a cone penetrometer equipped with internal sensors. The measurements comprise penetration depth, cone resistance, sleeve friction and, optionally, pore pressure and inclination from vertical. These measurements permit interpretation of ground conditions.

CPT apparatus and procedures adopted by Fugro are in general accordance ISSMGE (1999), ASTM (2020), ISO (2012) and ISO (2014). BS 5930 (BSI, 2015) refer to ISSMGE (1999). General agreement also applies to Eurocode 7 (CEN, 2007).

Fugro offers CPT systems operated from (1) ground surface and seafloor (non-drilling deployment mode) and (2) downhole in a borehole (drilling deployment mode).

CPT Apparatus

General

CPT apparatus includes various parts as described below:

- Thrust machine: apparatus providing thrust to the push rods so that the recommended rate of penetration (20 mm/s) is controlled;
- Reaction equipment: reaction for the thrust machine;
- Push rod: thick-walled cylindrical tube used for advancing the penetrometer to the required test depth. Push rods may also consist of drill pipe;
- Friction-cone penetrometer (CPT): cylindrical terminal body mounted on the lower end of the push rods, including a cone, a friction sleeve and internal sensing devices for the measurement of cone resistance, sleeve friction and, optionally, inclination;
- Piezocone penetrometer (CPTU or PCPT): cylindrical terminal body mounted on the lower end of the push rods, including a cone, a friction sleeve, a filter and internal sensing devices for the measurement of cone resistance, sleeve friction, pressure and, optionally, inclination;
- Measuring system: apparatus and software, including sensors, data transmission apparatus, recording apparatus and data processing apparatus.

Deployment from ground surface or seafloor

Specific additional apparatus for CPT deployment from ground surface and seafloor can include:

- Push rod casing: guide for the part of the push rods protruding above the soil, and for the push rod length exposed in water or soil, to prevent buckling when the required penetration pressure increases beyond the safe limit for the exposed upstanding length of push rods;
- Friction reducer: ring or special projections fixed on the outside of the push rods, with an outside diameter larger than the base of the cone, to reduce soil friction acting on the push rods.

Downhole Borehole Deployment

Downhole CPT systems latch into a bottom hole assembly at the lower end of a drill pipe. System options are:

1. Operation of a downhole thrust machine by applying mud pressure in the borehole;
2. Remote control of a downhole thrust machine by hydraulic pressure transmitted through an umbilical cable connected to a surface-based pump unit, together with;
3. Application of thrust to drill rods where CPT apparatus and a short push rod are latched in the bottom hole assembly; the thrust machine is at ground surface or seafloor.

Data recording can be surface-based and/or downhole.

Downhole CPTs require drilling apparatus for advancing the borehole. The maximum CPT stroke is generally 1.5 m or 3 m.

Cone Penetrometer

Typical features of Fugro penetrometers (Figure 1) include:

- Cone base areas of 500 mm^2, 1000 mm^2 or 1500 mm^2; other sizes are also in use, e.g. 3300 mm^2;
- Cone and friction sleeve sensors placed in series, i.e. subtraction-type penetrometers;
- Pore pressure measurements either at the face of the cone (u_1) or at the cylindrical extension of the cone (u_2). Multiple-sensor penetrometers (u_1, u_2 and u_3) are also available. The u_3 location is immediately above the friction sleeve;
- Inclinometer;
- Storage of signals from the penetrometer in digital form for subsequent computer-based processing and presentation.

Procedure

Figure 2 summarises the test procedure. The procedure includes several stages. The stage of Additional Measurements is optional.

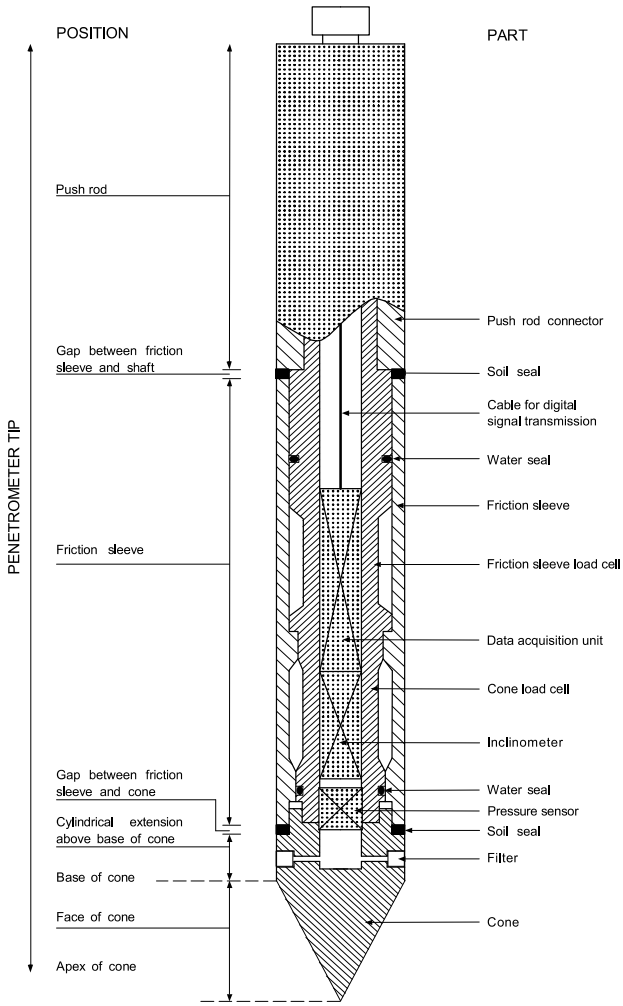

Figure 1: Piezocone Penetrometer

© Fugro 1995-2020

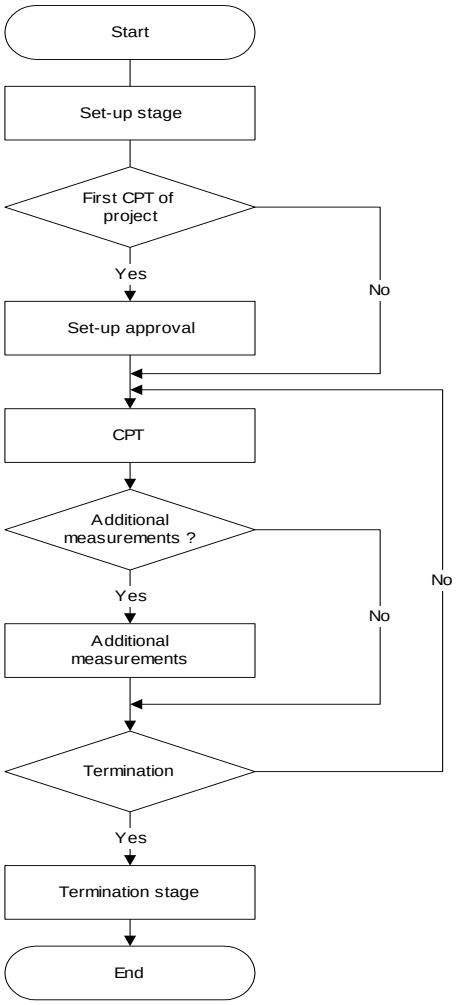

Figure 2: Flow chart

The set-up stage is at discretion of the equipment operator, particularly considering suitability of expected ground type(s), accessibility, risk of damage to equipment and safety of persons.

Set-up requires a reasonably flat, accessible, ground surface with a slope of 5° or less. Most onshore thrust machines have levelling facilities allowing a vertical start of penetration. Seabed frames used for offshore CPT activities have no levelling facilities, i.e. start of penetration may not be vertical.

For over-water (marine/ offshore activities), additional accessibility considerations include:

- Minimum water depth for the selected pontoon, jack-up or vessel and the selected test equipment;
- Maximum water depth for the selected pontoon, jack-up or vessel;
- Maximum depth below water (sea) level of selected test equipment;
- Metocean conditions, particularly wind, waves, currents.

The set-up stage typically includes selection of equipment and procedures according to a required accuracy class or application class, type of cone penetrometer and data processing/ submission. Table 1 presents ISSMGE accuracy classes and Tables 2 and 3 summarise ISO application classes. The allowable minimum accuracy of a measured parameter is the larger value of the two quoted. A percentage value applies to the measured value and not to the measuring range. The concept of application classes considers intended soil conditions for selection of an application class. For example, Application Class 1 of ISO (2014) can be selected for "very soft to soft soil deposits", which is approximately equivalent to $q_c < 0.5$ to $q_c < 1$ MPa. In other words, Application Class 1 should not apply to "mixed bedded soil profiles with weak to strong layers".

The accuracy values apply to ground surface or seafloor as reference. They are uncoupled from uncertainty of spatial position below ground surface or seafloor.

The set-up stage or the termination stage includes the location survey, i.e. the determination of the coordinates and the ground surface elevation (or the water depth).

The set-up stage and the termination stage for a downhole CPT include lowering of the CPT apparatus into the borehole and lifting respectively. Most projects require multiple downhole tests in a single borehole.

Table 1: Accuracy Classes (ISSMGE, 1999)

Accuracy Class	Parameter	Allowable Minimum Accuracy	Maximum Length between Measurements
1	Cone resistance Sleeve friction Pore pressure, Inclination Penetration depth	50 kPa or 3 % 10 kPa or 10 % 5 kPa or 2 % 2° 0.1 m or 1 %	20 mm
2	Cone resistance Sleeve friction Pore pressure Inclination Penetration depth	200 kPa or 3 % 25 kPa or 15 % 25 kPa or 3 % 2° 0.2 m or 2 %	20 mm
3	Cone resistance Sleeve friction Pore pressure Inclination Penetration depth	400 kPa or 5 % 50 kPa or 15 % 50 kPa or 5 % 5° 0.2 m or 2 %	50 mm
4	Cone resistance Sleeve friction Penetration length	500 kPa or 5 % 50 kPa or 20 % 0.1 m or 1 %	50 mm

Table 2: Application Classes (ISO, 2012)

Application Class	Parameter	Allowable Minimum Accuracy	Maximum Length between Measurements
1	Cone resistance Sleeve friction Pore pressure, Inclination Penetration length	35 kPa or 5 % 5 kPa or 10 % 10 kPa or 2 % 2° 0.1 m or 1 %	20 mm
2	Cone resistance Sleeve friction Pore pressure, Inclination Penetration length	100 kPa or 5 % 15 kPa or 15 % 10 kPa or 3 % 2° 0.1 m or 1 %	20 mm
3	Cone resistance Sleeve friction Pore pressure, Inclination Penetration length	200 kPa or 5 % 25 kPa or 15 % 50 kPa or 5 % 5° 0.2 m or 2 %	50 mm
4	Cone resistance Sleeve friction Penetration length	500 kPa or 5 % 50 kPa or 20 % 0.2 m or 2 %	50 mm

© Fugro 1995-2020

Table 3: Application Classes (ISO, 2014)

Application Class	Parameter	Allowable Minimum Accuracy
1	Cone resistance	35 kPa or 5 %
	Sleeve friction	5 kPa or 10 %
	Pore pressure	25 kPa or 5 %
2	Cone resistance	100 kPa or 5 %
	Sleeve friction	15 kPa or 15 %
	Pore pressure	50 kPa or 5 %
3	Cone Resistance	200 kPa or 5 %
	Sleeve friction	25 kPa or 15 %
	Pore pressure	100 kPa or 5 %

For piezocone testing, the set-up stage also includes the following steps:

- Office-based or site-based: de-airing of the filter in glycerine by application of 24-hour vacuum and storage in a glycerine-filled container;
- On-site: glycerine filling of hollow space in the cone penetrometer and subsequent mounting of the filter;
- On-site: application of a flexible membrane around the filter to prevent loss of saturating fluid prior to the start of a test.

Land-based tests may include specific measures to help retention of filter saturation during penetration of partially saturated zones. Relaxation of requirements typically applies to offshore tests where water pressures will force entrapped air into solution.

Criteria for test termination are as follows, unless specifically agreed otherwise:

- As instructed by client;
- Reaching target penetration;
- Reaching maximum capacity of the thrust machine, reaction equipment, push rods and/or measuring sensors;
- Sudden increase in penetrometer inclination;
- Risk of damage to apparatus or safety of persons, at discretion of equipment operator or as determined by software algorithms;

whichever occurs first and as applicable. Note that ASTM and ISO standards provide no specific requirements for maximum penetrometer inclination from vertical. A value of 15° is commonly considered.

Special apparatus and procedures may apply to:

- Specific additional measurements (for example shear wave velocity);
- Specific applications (for example offshore tests and measurements for application/accuracy Classes 1 and 2).

Results

CPT Parameters

Presentation of results from cone penetration tests typically includes:

- CPT parameters q_c, f_s and R_f versus depth below ground surface or versus elevation;
- Additional CPTU parameters u_1 or u_2 and, optionally, q_t, q_n, B_q, Q_t, Q_{tn}, F_r and I_c for tests with pore pressure measurements;
- Optionally, inclination i for tests with inclination measurements;
- Standard graphical format and optional ASCII and AGS formats.

Most standards specify scales for graphical presentation as follows:

- Axis for penetration depth z: 1 scale unit = 1 m;
- Axis for cone resistance q_c, corrected cone resistance q_t and net cone resistance q_n: 1 scale unit = 2 MPa or 0.5 MPa;
- Axis for sleeve friction f_s: 1 scale unit = 50 kPa;
- Axis for friction ratio R_f: 1 scale unit = 2 %;
- Axis for pore pressure u: 1 scale unit = 0.2 MPa or 0.02 MPa;
- Axis for pore pressure ratio B_q: 1 scale unit = 0.5.

Graphical presentation aims for these scale units and scale ratios, where suitable and practicable.

The reference level of a test is (1) the ground surface for onshore tests, (2) the seafloor for nearshore and offshore tests. Historically, the bottom of the borehole was used as the reference level of downhole tests. Data processing presumes a hydrostatic pore pressure profile relative to seafloor, unless specifically indicated otherwise. The definition of CPT parameters is as follows:

z = penetration depth relative to ground surface or seafloor, corrected for inclination from vertical (i) where a test includes inclination measurements, as follows:

$$z = \int_0^l \cos\, i \cdot \mathrm{d}l$$

where:

z = penetration depth for the conical base of the cone penetrometer
l = recorded penetration length
i = recorded inclination from vertical

q_c = cone resistance relative to the reference level of the test.

f_s = sleeve friction relative to the reference level of the test. A calculated depth correction applies so that the presented sleeve friction corresponds with the cone depth.

f_t = corrected sleeve friction relative to the reference level of the test. Sleeve friction is corrected for pore pressures acting on the end areas of the friction sleeve

$$f_t = f_s - \frac{(u_2 * A_{sb} - u_3 * A_{st})}{A_s}$$

or simplified to:

$$f_t = f_s - u_2 \frac{(A_{sb} - A_{st})}{A_s} \quad \text{or}$$

$$f_t = f_s - (u_2 * a_{fs})$$

where:

A_{sb} = cross sectional area in the gap between the friction sleeve and the cone
A_{st} = cross sectional area in the gap above the friction sleeve
A_s = surface area of the friction sleeve
a_{fs} = net area ratio of the friction sleeve $(A_{sb} - A_{st})/A_s$

R_f = ratio of sleeve friction to cone resistance (f_s/ q_c). This calculated ratio is for the cone depth.

R_{ft} = corrected friction ratio (f_s/ q_t). The ratio f_t/q_t applies if f_t is known.

I_{SBT} = non-normalized soil behaviour type index (Robertson, 2010)

© Fugro 1995-2020

$$I_{SBT} = [(3.47 - \log(q_c/P_a))^2 + (\log R_f + 1.22)^2]^{0.5}$$

where:

P_a = atmospheric pressure

u_1 = pore pressure at the face of the cone, relative to the reference level of the test.

u_2 = pore pressure at the cylindrical extension above the base of the cone or in the gap between the friction sleeve and the cone, relative to the reference level of the test.

u_3 = pore pressure immediately above the friction sleeve or in the gap above the friction sleeve, relative to the reference level of the test.

q_t = corrected cone resistance (also called total cone resistance). This includes corrections for hydrostatic and transient pore pressures, and cone construction. The corrected cone resistance is relative to ground surface or seafloor:

$q_t = q_c + (1\text{-}a)u_2$ or

$q_t = q_c + (1\text{-}a)[K(u_1 - u_0) + u_0]$

Historically, equations for downhole tests were:

$q_t = q_c + (1\text{-}a)u_2 + u_{0i}$ or

$q_t = q_c + (1\text{-}a)[K(u_1 + u_{0i} - u_0) + u_0] + a * u_{0i}$

where:

a = net area ratio of the cross-sectional steel area at the gap between cone and friction sleeve to the cone base area. This ratio is penetrometer-type dependent. The a-factor indicates the effect of pore pressure on unequal cross-sectional areas of the cone.

u_0 = hydrostatic pore pressure at the cone, relative to the phreatic surface or the seafloor. This is a calculated value.

u_{0i} = hydrostatic pore pressure at the bottom of the borehole, relative to seafloor. This is a calculated value.

K = adjustment factor for the ratio of pore pressure at the cylindrical extension above the base of the cone to pore pressure on the cone face $K = (u_2 - u_0)/(u_1 - u_0)$

The term $u_2 - u_0$ refers to excess pore pressure (with respect to hydrostatic pore pressure). Common symbols for excess pore pressure are du_2 or Δu_2. Similarly, du_1 or Δu_1 can represent the term $u_1 - u_0$.

The K-factor is only of interest for processing of CPTU results with pore pressure measurement at the cone face (u_1). The factor depends on soil characteristics such as fabric, overconsolidation ratio, compressibility and crushability. The K-factor (Peuchen et al., 2010) can be estimated from:

$$K = 0.91\mathrm{e}^{-0.09Q_t^{0.47}}\left(\frac{1}{1+F_r(0.17+0.061(Q_t-21.6)^{1/3})} - \mathrm{e}^{-2F_r}\right)$$

q_n = $q_t - \sigma_{vo}$ = net cone resistance. This includes corrections for hydrostatic and transient pore pressures, in situ stress, and cone construction. The symbol for q_n may also be q_{net}.

where:

σ_{vo} = total in situ vertical stress at the cone base, relative to ground surface or seafloor. This is a calculated value.

Q_t = q_n/σ'_{v0} = normalized cone resistance

where:

σ'_{v0} = effective in situ vertical stress at the cone base, relative to ground surface or seafloor. This is a calculated value.

Q_{tn} = normalized cone resistance with variable stress exponent n, where:

$Q_{tn} = [(q_t - \sigma_{v0})/P_a](P_a/\sigma'_{v0})^n$

$n = 0.381\,(I_c) + 0.05\,(\sigma'_{vo}/P_a) - 0.15$ and $n \leq 1$

(Zhang et al., 2002)

I_c = soil behaviour type index (Robertson and Wride,1998)

$I_c = [(3.47 - \log Q_{tn})^2 + (\log F_r + 1.22)^2]^{0.5}$

F_r = f_t/q_n = normalized friction ratio.

B_q = pore pressure ratio $B_q = (u_2 - u_0)/q_n$ or

$B_q = K(u_1 - u_0)/q_n$

Presented values for u_2, q_t, q_n and B_q may be denoted by u_2^*, q_t^*, q_n^*, B_q^*, Q_t^* and F_r^* *if* u_2 is derived rather than measured, for example if derived by applying a K-factor.

Pore pressure u_2 at the cylindrical extension is commonly assumed equal to u_{2g} in the gap. The assumption $u_2 = u_{2g}$ is probably reasonable for deepwater CPTs and associated high values of ambient pressure that promote saturated conditions in the gap. A similar comment applies to u_3. Note that CPTU saturation procedures apply to the pore pressure measuring system only. These procedures exclude the gaps below and above the friction sleeve.

Some deployment systems allow monitoring of CPT parameters in reverse mode, i.e. upon retraction of the cone penetrometer. This optional feature presents additional information that can improve interpretation of ground behaviour, for example strength sensitivity of fine-grained soil.

Accuracy Classes and Application Classes

Cone penetration test standards can follow a "prescriptive" approach, whereby specific detailed measures provided a "deemed to comply" practice. ASTM (2020) is an example of this approach. ISSMGE (1999) and ISO (2012, 2014) specify "performance" criteria for cone penetration test measurements. The ISO standard on metrological confirmation (ISO, 2003) provides the general framework for assessment of performance compliance.

The following comments apply:

- Accuracy is the "closeness of a measurement to the true value of the quantity being measured". It is the accuracy as a whole that is ultimately important not the individual parts. Precision is the "closeness of each set of measurements to each other". The resolution of a measuring system is the "minimum size of the change in the value of a quantity that it can detect". It will influence the accuracy and precision of a measurement.

© Fugro 1995-2020

- Accuracy Class 3 and Application Class 3 typically represents industry practice. They are approximately equivalent to the more implicit requirements of ASTM International. Class 3 applies, unless specifically agreed otherwise.

So-called "zero drift" of a measured parameter is an approximate performance indicator for the measuring system (Peuchen and Terwindt, 2014). Zero drift is the absolute difference of the zero readings, reference readings or zero reference reading of a measuring system between the start and completion of the cone penetration test. The reference readings can be taken at (1) atmospheric pressure at ground surface or above water level or (2) under hydrostatic water pressure close to seafloor. The zero drift of the measured parameters can be compared with the allowable minimum accuracy according to the selected application class, per test. This comparison considers the maximum range of values of q_c, f_s and, where applicable, u_1 or u_2 for calculation of the percentage box values (Tables 1, 2 or 3).

Differences in interpretation about compliance with the ISSMGE and ISO box values for accuracy became apparent after publication of ISO 22476-1:2012 and, subsequently, publication of ISO 19901-8:2014. Unfortunately, the interpretational challenges emerged from contractual disputes, unnecessary re-work and CPT results assigned higher confidence than actual (Peuchen and Parasie, 2019).

Peuchen and Terwindt (2014, 2015) provide guidance on uncertainty estimation for cone penetration test results. The calculation model for uncertainty estimates for q_c, f_s and u considers the following uncertainty contributions, where applicable: (1) force and pressure sensors, (2) geometry of the cone penetrometer, (3) effects from ambient and transient temperature, (4) non-axial force on cone penetrometer (bending moment), (5) ambient fluid pressure in soil and (6) zero offsets for q_c, f_s and u relative to seafloor.

Accuracy considerations for strongly layered soils should allow for heat flux phenomena. Heat flux gives an apparent shift in cone resistance (Post and Nebbeling, 1995). For example, friction in dense sand causes a cone to heat by about 1°C/MPa cone resistance. Resulting heat flux decreases cone resistance by an apparent shift in the order of 100 kPa to 200 kPa for a penetrating probe going from dense sand into clay. This is a temporary decrease lasting about 5 minutes. Ambient temperature compensation systems cannot avoid heat flux effects. Penetration interruption can serve as mitigation measure.

Pore Pressures

A CPTU pore pressure measuring system is intended for use in water-saturated uncemented fine-grained soil. Pore pressure measurements (u) are commonly assumed to represent pore water pressures. This assumption is reasonable for soils saturated under in situ stress conditions and remaining saturated during penetration of the cone penetrometer.

Pore pressure results obtained for ground conditions such as partially saturated soils, very dense sands and cemented soils may not be representative and/or repeatable. For example, stiffness differences between the steel components of the cone penetrometer and the piezocone filter can affect results for very dense sands.

Loss of saturation of the pore pressure measuring system can occur during a test (Lunne et al., 1997; Peuchen and Terwindt, 2014). Loss of saturation usually causes a sluggish pore pressure response during penetration of ground below the zone causing desaturation of the pore pressure measuring system. Reasons for loss of saturation include:

- penetration of partially saturated ground, for example ground containing significant amounts of gas;
- reduction of pore pressure to below in situ pore pressure, causing gas in solution to become free gas;
- measurement of negative pore pressures such that cavitation occurs; for example, this is not uncommon for a piezocone filter located at the cylindrical extension above the base of the cone (u_2 location), at the time of penetration of dense sand or overconsolidated clay layers.

Re-saturation of a pore pressure measurement system can take place upon further penetration into soil. Particularly, re-saturation may take place in saturated low-permeability soils (clays) that are normally consolidated or lightly overconsolidated and where the gap can become saturated by adequate supply of water and/or water pressure.

Measured pore pressures affected by desaturation of the pore pressure measurement system may not be representative of soil behaviour. Consequently, derived parameters that use pore pressure may also not be representative.

Shallow Penetration

Shallow penetration will affect CPT measurements. Values of q_c, f_s and u for initial penetration of a cone penetrometer below ground surface, seafloor or bottom of a borehole will differ from a fully embedded cone penetrometer. As a general guide, initial penetration effects can be expected for a distance of about 8 times the diameter of the cone penetrometer for q_c, u_1 and u_2, and for a distance of about 15 times the diameter of the cone penetrometer for f_s. Initial penetration effects can be deeper for downhole borehole deployment. This is because of (1) complex ground stress conditions immediately below the required borehole and (2) borehole-induced ground disturbance that cannot be avoided.

Use of reaction equipment will affect stress conditions for shallow penetration. Particularly, offshore conditions may include extremely soft ground at seafloor. Soil disturbance, pore pressure build-up and consolidation of near-surface soft soil may take place.

Penetration Rate

CPT standards typically provide limits of ± 5 mm/s for a nominal penetration rate of 20 mm/s. Considerations include:

- A typical thrust machine provides a push speed with an uncertainty within ± 5 mm/s under favourable conditions. Under adverse conditions, penetration rates may be outside these limits, for example with strongly varying thrust and towards the thrust limit of a thrust machine;
- The penetration rate is not necessarily equal to the push speed because of inevitable vertical movements of the thrust machine and length variation and bending of the push-rod string.

Penetration Interruption

A penetration interruption may be unavoidable, for example to add a push rod or to perform a pore pressure dissipation test. This will affect test results.

Consolidation of low-permeability soil around a cone tip is of particular interest. A stationary cone penetrometer can apply local stresses that approach failure conditions, i.e. about 9 times the undrained shear strength or about 2 times the in situ mean

© Fugro 1995-2020

effective stress. Pore pressure re-distribution and dissipation occur, resulting in a local increase in undrained shear strength and hence cone (bearing) resistance. A doubling of cone resistance may not be unreasonable for 100 % consolidation. Supplementary considerations include:

- Small downward movement of a penetrometer (order of millimetres) during a test can contribute to maintaining local stresses approaching failure conditions;
- Soil consolidation around a cone penetrometer may lead to soil/penetrometer adhesion that is sufficient to give an increase in "cone" diameter. Resumption of penetration will lead to loss of adhered soil, usually within an equivalent distance of a few times the cone diameter;
- A low B_q value may imply partially drained penetration conditions. It is likely that any steady-state penetration conditions will not apply instantaneously upon resumption of penetration;
- Measuring sensors in a probe generate heat, but this is probably not significant for any stationary measurement. Fugro's strain-gauge load sensors are compensated for ambient temperature fluctuations.

Depth Measurement for Offshore Conditions

Offshore definition of the seafloor (ground surface) is difficult for extremely soft ground at seafloor (Peuchen et al., 2005). Penetration of the reaction equipment into a near-fluid zone of the seabed may take place unnoticed. Such settlement affects the start of penetration depth z. Also, settlement may continue at the time of testing.

Downhole CPT systems rely on depth control applicable to borehole drilling. Depth control according to Z2 of Table 4 is typically feasible for drilling systems deployed from a fixed platform, for example a jack-up. This value excludes uncertainty associated with determination of seafloor level. Drilling control from floating equipment, for example a geotechnical survey vessel, may be subject to the additional influence of waves and tides. Z2 is typically feasible for favourable conditions. Z3 or Z4 may apply for adverse conditions.

Table 4: Depth Accuracy Classes according to ISO (2014)

Depth Accuracy Class	Maximum Data Point Depth Uncertainty [m]
Z1	0.1
Z2	0.5
Z3	1.0
Z4	2.0
Z5	> 2.0

Zero-Correction for Offshore Conditions

Water pressures generate significant values of cone resistance and pore pressure. The standardised practice is to correct these reference readings to zero at seafloor. CPT systems for non-drilling mode and for seafloor drilling mode allow zero-correction to hydrostatic conditions prior to the start of a test, typically with a zero-correction uncertainty approaching the resolution of the CPT system. Downhole borehole CPT systems latch into the lower end of a drill pipe. The pressure conditions in the drill pipe may not be in full equilibrium with the surrounding ground water pressure and zero-correction will be subject to increased uncertainty, i.e. uncertainty for pore pressure in the order of 100 kPa for deepwater tests (Peuchen, 2000). This uncertainty depends on factors such as the free-flow and viscosity of drill fluid between the drill bit and the seafloor. The uncertainty typically decreases with decreasing depth of the drill bit below sea level and below seafloor. Uncertainty for the zero-correction of cone resistance is approximately equivalent, but by a factor representing the net area ratio effect.

Deepwater Tests

A deepwater environment presents some favourable conditions for cone penetration tests, notably temperature. Ambient temperature conditions are practically constant and the measuring system has ample time to adjust to these temperatures. In addition, transient heat flow phenomena in a cone penetrometer are usually not applicable. This is because a cone penetrometer accumulates negligible (frictional) heat when penetrating the generally prevalent soils of very soft consistency.

Deepwater (piezocone) pore pressure measurements are essentially similar to shallow-water measurements, with the exception of an increased measuring range for pore pressure leading to some reduction in sensor accuracy. Saturation of a pore pressure measuring system is excellent for a deepwater environment, as the high pressures will force any gas bubbles into solution.

Currently available evidence indicates that a high-quality subtraction-type cone penetrometer is adequate for very soft soil characterisation to a water depth of 3000 metres and probably beyond.

Additional Measurements

Friction-cone and piezocone penetrometers allow specific additional measurements, such as friction set-up tests, pore pressure dissipation tests and measurements of ground water pressure. These additional measurements require a penetration interruption or may be feasible at the end of a test. It is also common to add other in situ test devices to a cone penetrometer. Table 5 presents the more common types.

Table 5: Probes for additional In Situ Tests

Type of Probe	Properties	Units
Electrical Conductivity Penetrometer (ECPT)	Electrical conductivity, K	S/m
Temperature Cone Penetrometer (TCPT)	Temperature, T, and thermal conductivity, k	K, W/(m·K)
Seismic Cone Penetrometer (SCPT)	S-wave velocity, v_s, and P-wave velocity, v_p	m/s
Cone Pressuremeter (CPMT)	Shear stress-strain-time response, σ, ε, t	MPa, -, s
Natural Gamma Penetrometer (GCPT)	Natural gamma ray, γ	CPS
Cone Magnetometer (CMMT)	Magnetic flux density B, magnetic field horizontal angle θ and vertical angle ϕ	µT, °, °
Hydraulic Profiling Tool (HPT)	Permeability, k	m/s

S	=	Siemens	s	=	second
m	=	metre	Pa	=	Pascal
K	=	Kelvin (or °C)	CPS	=	counts per second
W	=	Watt	T	=	Tesla

© Fugro 1995-2020

References

ASTM International (2020). *Standard test method for electronic friction cone and piezocone penetration testing of soils (*ASTM D5778-20). https://www.astm.org/Standards/D5778.htm.

BSI (2015). *Code of practice for ground investigations* (BS 5930:2015). https://shop.bsigroup.com/ProductDetail?pid=000000000030268443.

European Committee for Standardization (2010). *Eurocode 7 - geotechnical design – part 2: ground investigation and testing* (EN 1997-2:2007+ AC:2010) https://standards.cen.eu/dyn/www/f?p=204:110:0::::FSP_PROJECT,FSP_ORG_ID:23735,6231&cs=14A2DCCA6BF367BFBD54D9FC0822BE0ED

International Organization for Standardization (2003). *Measurement management systems - requirements for measurement processes and measuring equipment* (ISO 10012:2003) https://www.iso.org/standard/26033.html

International Organization for Standardization (2012). *Geotechnical investigation and testing – Field testing – Part 1: Electrical cone and piezocone penetration test* (ISO 22476-1:2012). https://www.iso.org/standard/57728.html

International Organization for Standardization (2014). *Petroleum and natural gas industries – specific requirements for offshore structures – part 8: marine soil investigations* (ISO 19901-8:2014). https://www.iso.org/standard/61145.html

International Society for Soil Mechanics and Geotechnical Engineering (1999). International reference test procedure for the cone penetration test (CPT) and the cone penetration test with pore pressure (CPTU): Report of the ISSMGE technical committee 16 on ground property characterisation from in-situ testing. In F.B.J. Barends et al. (eds.) *Geotechnical engineering for transportation infrastructure: proceedings of the twelfth European conference on soil mechanics and geotechnical engineering, Amsterdam, Netherlands, 7-10 June 1999, Vol. 3* (pp. 2195-2222). Balkema.

Lunne, T., Robertson, P.K. & Powell, J.J.M. (1997). *Cone penetration testing in geotechnical practice*. Blackie Academic & Professional.

Peuchen, J. (2000). Deepwater cone penetration tests. In *32nd Annual Offshore Technology Conference, 2000: OTC Paper 12094* https://doi.org/10.4043/12094-MS

Peuchen, J., Adrichem, J. & Hefer, P.A. (2005). Practice notes on push-in penetrometers for offshore geotechnical investigation. In S. Gourvenec and M. Cassidy (Eds.) *Frontiers in offshore geotechnics ISFOG 2005: proceedings of the first international symposium on frontiers in offshore geotechnics, University of Western Australia, Perth, 19-21 September 2005.* (pp. 973-979). Taylor & Francis.

Peuchen, J., VandenBerghe, J.F. & Coulais, C. (2010), Estimation of u_1/u_2 conversion factor for piezocone. In *CPT'10: 2nd International symposium on cone penetration testing, Huntington Beach, California: conference proceedings*.

Peuchen, J. & Terwindt, J. (2014). Introduction to CPT accuracy. In *3rd International symposium on cone penetration testing CPT14 : May 12-14 (2014) - Las Vegas, Nevada*.

Peuchen, J. & Terwindt, J. (2015). Measurement uncertainty of offshore cone penetration tests. In V. Meyer (ed.) *Frontiers in offshore geotechnics III: proceedings of the third international symposium on frontiers in offshore geotechnics (ISFOG 2015), Oslo, Norway, 10-12 June 2015.* (pp. 1209-1214) CRC Press..

Peuchen, J. & Parasie, N. (2019). Challenges for CPT accuracy classes. *Proceedings of the XVII ECSMGE-2019: geotechnical engineering foundation of the future.* IGS publishing https://www.ecsmge-2019.com/uploads/2/1/7/9/21790806/0049-ecsmge-2019_peuchen.pdf

Post, M.L. & Nebbeling, H. (1995). Uncertainties in cone penetration testing. In *International Symposium on Cone Penetration Testing CPT'95, Linköping, Sweden, October 4-5, 1995, Vol. 2* (SGF Report, No. 3:95) (pp. 73-78). Swedish Geotechnical Society.

Robertson, P.K. & Wride (Fear), C.E. (1998). Evaluating cyclic liquefaction potential using the cone penetration test. *Canadian Geotechnical Journal*, *35*(3), 442-459. https://doi.org/10.1139/t98-017

Robertson, P.K. (2010). Soil behaviour type from the CPT: an update. In *2nd International symposium on cone penetration testing, Huntington Beach, CA, Vol. 2.* (pp. 575-583*)*

Zhang, G., Robertson, P.K. & Brachman, R.W.I. (2002). Estimating liquefaction induced ground settlements from CPT for level ground. *Canadian Geotechnical Journal*, *39*(5) 1168-1180. https://doi.org/10.1139/t02-047

© Fugro 1995-2020

Cone Penetration Test Interpretation

Scope

This document presents a summary of interpretation methods for cone penetration test (CPT) results. The project-specific selection of methods depends on the agreed project requirements. Some of the methods suit computer-based interpretation of CPT data records.

Parameter Interpretation

Interpretation of cone penetration test results helps provide parameters for geotechnical models. Conventional models are typically based on plasticity theory for ultimate limit states, and on elasticity theory and consolidation theory for serviceability limit states. Features of these geotechnical models are:

- analysis of either drained (sand model) behaviour or undrained (clay model) behaviour for plasticity models
- analysis for the ultimate limit state differs from that for the serviceability limit state.

CPT interpretation methods are mostly based on empirical correlations with limited theoretical backing. Data integration with other, complementary investigation techniques (such as geological analysis, borehole/sample logging and laboratory testing) can improve confidence levels.

The interpretation techniques discussed below are subject to limitations such as:

- CPT measurements, including measurement uncertainty (Peuchen & Terwindt, 2014 & 2015) and effects resulting from deployment method, initial embedment of a cone penetrometer, penetration interruption and inevitable loss of saturation of a pore pressure measuring system.
- Most interpretation methods apply a transformation model to "conventional" sands (drained soil behaviour) and clays (undrained soil behaviour). Conventional methods may not be appropriate for silts, sand/clay/gravel mixtures, varved or layered soils, gassy soils, underconsolidated soils, peats, carbonate soils, cemented soils and residual soils. These non-conventional soils warrant a more specific approach.
- Drained or undrained behaviour for the geotechnical analysis at hand may or may not coincide with respectively drained or undrained behaviour during fixed-rate penetration testing. This interpretation difficulty remains largely unresolved at this time.
- CPT interpretation techniques can be indirect, i.e. requiring estimates of various other parameters. This is consistent with an integrated geotechnical investigation approach. Inevitably, this approach also includes some redundancy of data.
- Empirical correlations can rely on data pairing, for example pairing of CPT net cone resistance at a point in space with laboratory undrained shear strength applicable to another, nearby spatial position. Data pairing uncertainty can be limited by applying judgement.
- Empirical correlations can use reference parameters such as the undrained shear strength determined from a laboratory single-stage isotropically consolidated undrained triaxial compression test on an undisturbed specimen obtained by means of push sampling techniques (e.g. Van der Wal et al., 2010). The reference parameter may not be appropriate for the selected geotechnical model, and adjustment may be necessary. Also, adjustment for test conditions may be necessary, for example in situ temperature versus laboratory temperature.
- The cone penetration test offers limited direct information on serviceability limit states (deformation), as the penetration process imposes large strains in the surrounding soil. In comparison to ultimate limit states, better complementary data will usually be required.
- The interpretations typically apply to conditions as encountered at the time of the geotechnical investigation. Geological, environmental and construction/operational factors may alter as-found conditions.

Penetration Behaviour

Soil behaviour during cone penetration testing shows large displacements in the immediate vicinity of the penetrometer, and small elastic displacements further away from the penetrometer. Density/structure, stiffness and in situ stress conditions significantly affect the measured parameters.

The measured cone resistance (q_c) includes hydrostatic water pressures as well as induced pore pressures resulting from stresses and strains related to the penetration process. The induced pore pressures are usually negligible for clean sand because the ratio of effective stress to pore pressure is high. This ratio can be low for penetration into normally consolidated and slightly overconsolidated clays. Knowledge of pore pressures around the penetrometer can thus be important. CPT parameters that take account of pore pressure effects include corrected cone resistance (q_t), net cone resistance (q_n) and pore pressure ratio (B_q). These parameters can be calculated if piezocone penetration test (PCPT or CPTU) data are available. The influence of pore pressures on sleeve friction f_s is relatively small. It is common to ignore this influence. Calculation of friction ratio R_f (defined as f_s/q_c) includes no allowance for pore pressure effects.

The penetration rate with respect to soil permeability determines whether soil behaviour is primarily undrained, drained or partially drained. Partial drainage may also be denoted as partial consolidation. In general, soil behaviour during cone penetration testing is:

- Drained in clean sand, i.e. no measurable pore pressures because of (1) soil displacements and (2) soil volume change depending on dilative/contractive soil behaviour;
- Undrained in clay, i.e. no significant soil volume change immediately around the cone penetrometer and pore pressure change depending on dilative/contractive soil behaviour;
- Partially drained in soils with intermediate permeability, such as sandy silt, i.e. potential for (1) some soil volume change depending on dilative/contractive soil behaviour and (2) potential for pore pressure change depending on dilative/ contractive soil behaviour;

Results of a pore pressure dissipation test can provide indications for partial drainage conditions. Particularly, partial drainage conditions should be considered when t_{50} is less than about 100 s (DeJong and Randolph, 2012). The term t_{50} represents the time for 50 % dissipation of excess pore pressure at the u_2 location of a cone penetrometer.

© Fugro 1996-2020

CPT parameters can be influenced by the presence of thin (< 0.2 m thick) layers in a ground profile. Boulanger and DeJong (2018) proposed a method that provides estimates of corrected q_c and f_s values based on an inverse filtering procedure that accounts for thin layer and transitional effects during cone penetration.

The following sections mostly consider interpretation of drained soil behaviour (sand) and undrained soil behaviour (clay).

Soil Behaviour Identification

Identification of soil stratigraphy in terms of general soil behaviour (and to a lesser degree soil type) is a more important feature of CPT than other investigation techniques.

Figures 1 and 2 show soil behaviour identification according to procedures given by Robertson (2009), representing an update of Robertson (1990) by exchange of Q_t with Q_{tn}. The procedures consider a normalised soil behaviour classification that provides general guidance on likely soil type (silty sand for example) and a preliminary indication of parameters such as angle of internal friction φ', overconsolidation ratio (OCR) and clay sensitivity (S_t). Classification is possible for $1 \leq Q_{tn} \leq 1000$, $0.1 \leq F_r \leq 10$ and $-0.2 \leq B_q \leq 1.4$. The procedures require piezocone test data:

$$Q_{tn} = [(q_t - \sigma_{v0})/P_a](P_a/\sigma'_{v0})^n \qquad Q_t = \frac{q_t - \sigma_{vo}}{\sigma'_{vo}}$$

$$F_r \text{ or } nR_f = \frac{f_s}{q_t - \sigma_{vo}} 100\% \qquad B_q = \frac{u - u_0}{q_t - \sigma_{vo}}$$

where:

B_q = pore pressure ratio
F_r = normalised friction ratio
Q_{tn} = normalised cone resistance with variable stress exponent
Q_t = normalised cone resistance
q_t = corrected cone resistance
σ_{vo} = total in situ vertical stress
σ'_{vo} = effective in situ vertical stress
P_a = atmospheric pressure
n = stress exponent
f_s = measured sleeve friction
u = measured pore pressure
u_0 = theoretical hydrostatic pore pressure.

The stress exponent n is according to Zhang et al. (2002):

$$n = 0.381\,(I_c) + 0.05\,(\sigma'_{vo} / P_a) - 0.15$$

where $n \leq 1$.

Robertson and Wride (1998) defined soil behaviour type index I_c (Figure 2) as follows:

$$I_c = [(3.47 - \log Q_{tn})^2 + (\log F_r + 1.22)^2]^{0.5}$$

Soils with $I_c < 2.05$ are generally cohesionless, coarse grained, where cone penetration is generally drained and soils with $I_c > 2.60$ are generally cohesive, fine grained, where cone penetration is generally undrained (Robertson & Wride, 1998). Cone penetration in soils with $2.05 < I_c < 2.60$ is often partially drained.

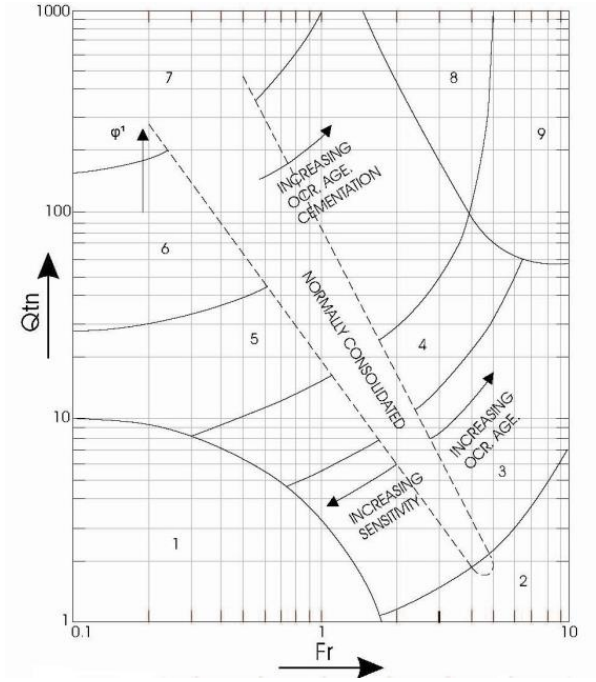

Figure 1: Classification chart Robertson (2009)

1. Sensitive, fine grained
2. Organic soils - peats
3. Clays- clay to silty clay
4. Silt mixtures – clayey silt to silty clay
5. Sand mixtures – silty sand to sandy silt
6. Sands – clean sand to silty sand
7. Gravelly sand to sand
8. Very stiff sand to clayey sand*
9. Very stiff, fine grained*

(*) Heavily overconsolidated or cemented

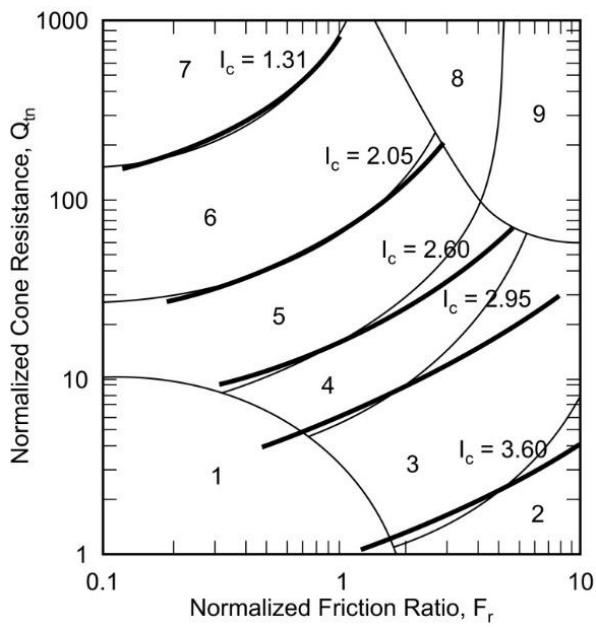

Figure 2: Soil behaviour type index I_c superimposed on Robertson (2009) classification chart

© Fugro 1996-2020

Figure 3 presents a classification chart for friction cone data according to Robertson (2010). This procedure requires no pore pressure input. A non-normalised soil behaviour type index, I_{SBT} applies:

$$I_{SBT} = [(3.47 - \log(q_c/P_a))^2 + (\log R_f + 1.22)^2]^{0.5}$$

I_{SBT} is similar to I_c. Values for I_{SBT} and I_c are typically comparable for effective in situ vertical stress between 50 kPa and 150 kPa.

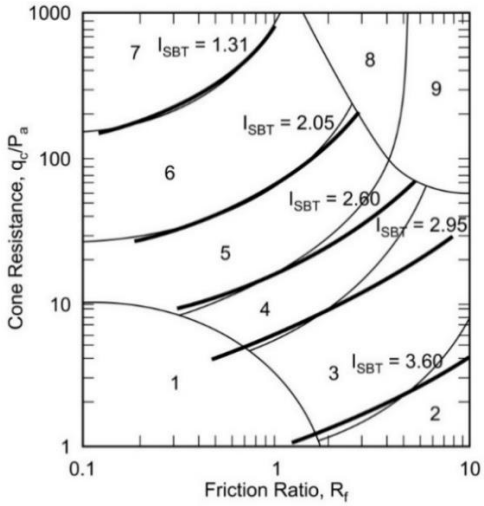

Figure 3: Robertson (2010) classification chart including I_{SBT}

Figure 4 presents a classification chart focusing on contractive and dilative soil behaviour, according to Robertson (2016a). The equations for the contractive-dilative boundary (CD) and modified soil behaviour type index (I_B) are as follows:

$$CD = (Q_{tn} - 11)(1 + 0.06F_r)^{17} \text{ and}$$

$$I_B = 100(Q_{tn} + 10)/(70 + Q_{tn}F_r)$$

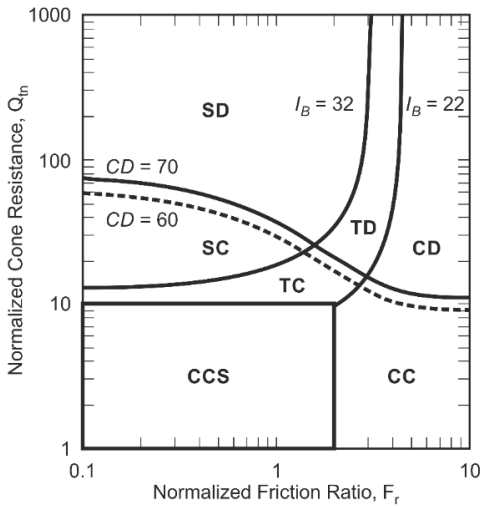

Figure 4: Classification chart according to Robertson (2016a)

CCS Clay-like – Contractive - Sensitive
CC Clay-like – Contractive
CD Clay-like – Dilative
TC Transitional – Contractive
TC Transitional – Dilative
SC Sand-like Contractive
SD Sand-like Dilative

Suggested values of CD are $CD = 60$ (low value) and $CD = 70$ (high value). Suggested values for I_B are $I_B = 32$, representing a low value for sand-like soil behaviour types and $I_B = 22$ representing a high value for clay-like soil behaviour types. The region between $I_B = 32$ and $I_B = 22$ represents soils typically showing transitional or intermediate soil behaviour types.

Sand Model

Unit Weight – Sand

Unit weight of uncemented (silica) sand, silt and clay soils may be derived according to Mayne et al. (2010):

$$\gamma = 1.95\gamma_w \left(\frac{\sigma'_{vo}}{P_a}\right)^{0.06} \left(\frac{f_t}{P_a}\right)^{0.06}$$

where total unit weight γ and unit weight of water γ_w are in kN/m^3 and effective in situ vertical stress σ'_{vo} is in kPa. The symbol f_t refers to sleeve friction corrected for pore pressures acting on the end areas of the friction sleeve, with units in kPa. Atmospheric pressure P_a is in kPa.

Unit weight may also be derived according to Lengkeek et al. (2018):

$$\gamma = \gamma_{ref} - \beta \cdot (\log(q_{t,ref}/q_t))/(\log(R_{f,ref}/R_f))$$

where γ_{ref} is a reference unit weight at which q_t is constant regardless of friction ratio R_f, β is a factor for unit weight contouring, $q_{t,ref}$ is a reference for total cone resistance q_t at which γ is constant regardless of R_f, and $R_{f,ref}$ is a reference friction ratio. The default values are: $\gamma_{ref} = 19$ kN/m^3, $\beta = 4.12$, $q_{t,ref} = 5$ MPa, and $R_{f,ref} = 30$ %. The correlation allows development of project-specific estimation of unit weight.

Shear Wave Velocity – Sand

If no in situ measurements of shear wave velocities (v_s) are available, then empirical correlation with CPT parameters may be considered. Hegazy and Mayne (2006) published a statistical correlation derived from 73 sites worldwide representing a range of soil types including sands, clays, soil mixtures and mine tailings (Figure 6). The correlation considers a normalized cone resistance (q_{c1N_hm}) and a soil behaviour type index (I_{c_hm}) as follows:

$$v_s = 0.0831 q_{c1N_hm} (\sigma'_{vo}/P_a)^{0.25} e^{(1.786 I_{c_hm})}$$

(Hegazy & Mayne, 2006)

where shear wave velocity v_s is in m/s and q_{c1N_hm} and I_{c_hm} are dimensionless. Calculations for q_{c1N_hm} and I_{c_hm} require iteration, and consider cone resistance q_c or corrected cone resistance q_t, sleeve friction f_s, total in situ vertical stress σ_{vo}, effective in situ vertical stress σ'_{vo} and atmospheric pressure P_a.

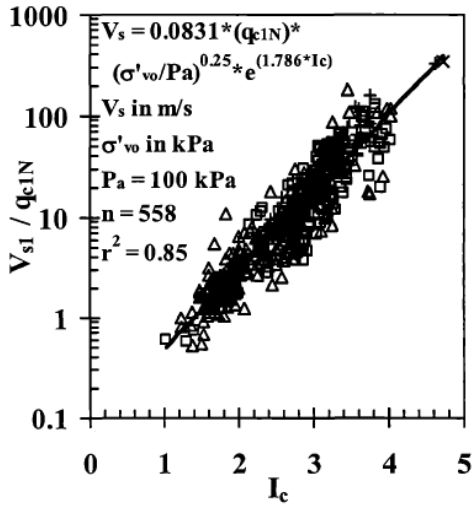

Figure 6: v_s – q_c correlation according to Hegazy and Mayne (2006)

© Fugro 1996-2020

Robertson and Cabal (2015) present a v_s correlation incorporating net cone resistance q_n ($= q_t - \sigma_{vo}$) and soil behaviour type index (I_c) as defined by Robertson and Wride (1998):

$$v_s = [\alpha_{vs}(q_t - \sigma_{vo})/P_a]^{0.5} \text{ where } \alpha_{vs} = 10^{(0.55\, I_c + 1.68)}$$

(Robertson & Cabal, 2015)

where shear wave velocity v_s is in m/s and corrected cone resistance q_t, total in situ vertical stress σ_{vo} and atmospheric pressure P_a are in kPa. The method can be applied to a wide range of soil behaviour types, notably uncemented Holocene to Pleistocene age soils. Older deposits could have a higher shear wave velocity. Exceptions are Zones 1, 8 and 9 of Robertson (1990 and 2009).

Baldi et al. (1989) derived a correlation between shear wave velocity v_s and cone resistance q_c for uncemented silica sands. This correlation is based on data from CPT, cross-hole and Seismic Cone Penetration Tests (SCPT) performed in quaternary deposits of the predominantly silica Po river sand and Gioia Tauro sand with gravel.

$$v_s = 277 q_c^{\,0.13} \sigma'_{vo}{}^{\,0.27} \qquad \text{(Baldi et al., 1989)}$$

where shear wave velocity v_s is in m/s and cone resistance q_c and effective in situ vertical stress σ'_{vo} are in MPa.

Shear wave velocity may be normalised according to Robertson and Cabal (2015):

$$v_{s1} = v_s \cdot (P_a/\sigma'_{vo})^{0.25} \qquad \text{(Robertson \& Cabal, 2015)}$$

In Situ Stress Conditions - Sand

A knowledge of in situ stress conditions is required for estimation of parameters such as relative density D_r and angle of internal friction of a sand deposit φ'. The effective in situ vertical stress σ'_{vo} may be calculated with a reasonable degree of accuracy but the effective in situ horizontal stress $\sigma'_{ho} = K_0 \cdot \sigma'_{vo}$ is generally unknown. Usually, it is necessary to consider a range of conditions for K_0 (coefficient of earth pressure at rest). The range can consider overconsolidation as inferred from a geological assessment, preconsolidation pressures of intermediate clay layers and/or theoretical limits of K_0.

Geological factors concerning overconsolidation include ice loading, soil loading and groundwater fluctuations (influence from desiccation). Possible subdivisions for these factors are mechanical, suction, cyclic and ageing consolidation.

The following approach can be applied for direct estimation of K_0 based on Agaiby and Mayne (2019):

$$K_0 = 0.45\sqrt{(OCR)}$$

using: $OCR = \frac{\sigma'_p}{\sigma'_{v0}}$ $\quad \sigma'_p = 0.33 \cdot q_n^{m'}$ $\quad m' = 1 - \frac{0.28}{1+\left(\frac{I_c}{2.65}\right)^{25}}$

where OCR is overconsolidation ratio, σ'_p is effective preconsolidation stress, σ'_{v0} is effective in situ vertical stress, q_n is net cone resistance in kPa and I_c is soil behaviour type index.

The $K_0 - OCR$ relationship represents a schematisation of $K_0 = (1 - sin\varphi') \cdot OCR^{sin\varphi'}$ proposed by Mayne and Kulhawy (1982). Mayne and Kulhawy (1982) investigated mechanical overconsolidation of reconstituted laboratory specimens for over 170 different soils. For many soil types (e.g. Mayne, 2020), it can be shown that the $K_0 = 0.45\sqrt{(OCR)}$ equation provides similar statistics to the Mayne and Kulhawy correlation using φ' (effective angle of internal friction):

$$K_0 = (1 - sin\varphi') \cdot OCR^{sin\varphi'}$$

Figure 5 presents an approximate CPT-based correlation for K_0 according to Robertson (2016b). K_0 limits are typically set to 0.5 and 2. Linear interpolation is applied for the region between $K_0 = 0.5$ and $K_0 = 2$.

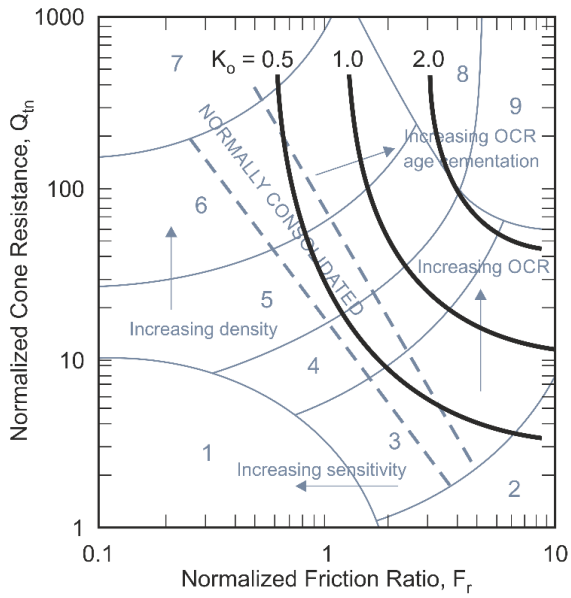

Figure 5: K_0 correlation according to Robertson (2016b)

No laboratory study can fully capture in situ behaviour. Particularly, K_0 may be underestimated if effects such as ageing and cyclic loading are relevant.

In general, in situ K_0 values are limited to the range $K_0 = 0.5$ to $K_0 = 1.5$. For many situations, K_0 values are believed to be relatively low at greater depths (say $K_0 < 1$ for depths exceeding 50 m). Jamiolkowski et al. (2003) recommend using a limiting value $K_0 = 1$ in practice, for limit states where low values of soil resistance and soil stiffness are critical.

Relative Density - Sand

The relative density concept applies to sands with a percentage fines of less than about 15 %.

Relative density is defined as $D_r = (e_{max} - e)/(e_{max} - e_{min})$, where e_{max} is maximum index void ratio, e represents in situ void ratio and e_{min} is minimum index void ratio. Maximum and minimum index void ratios are defined by laboratory testing. Relative density can exceed 100 %, because in situ void ratio can be lower than laboratory values for minimum index void ratio.

CPT-based correlations are commonly used for estimation of in situ relative density. These correlations rely on database results of CPTs carried out in sand samples reconstituted in laboratory calibration chamber tests. Use of such correlations implies dependence on, for example:

- soil type of database versus soil type in situ;
- reference laboratory test method for determination of index void ratios, particularly sensitivity to minimum index void ratio;
- range of stress levels and K_0 values for calibration testing;
- results applicable to reconstituted sand samples, sample preparation method and soil stress history simplifications.

Jamiolkowski et al. (2003) proposed the following relationship between q_c and D_r for normally and overconsolidated silica (dry) sands:

© Fugro 1996-2020

$$D_{r(dry)} = \frac{1}{2.96} \ln \left[\frac{\frac{q_c}{P_a}}{24.94 \left(\frac{\sigma'_{vo} \left(\frac{1+2K_o}{3} \right)}{P_a} \right)^{0.46}} \right]$$

and for saturated sands:

$$D_{r(sat)} = \left(\frac{-1.87 + 2.32 \ln \frac{q_c}{(P_a * \sigma'_{vo})^{0.5}}}{100} + 1 \right) \frac{D_r(dry)}{100}$$

where relative density D_r is a fraction. The correlation for saturated sands results in relative densities that can be up to about 10% higher compared to the correlation for dry sands.

Kulhawy and Mayne (1990) proposed:

$$D_r^2 = Q_{tn*}/Q_f \qquad \text{where: } Q_{tn*} = \left(\frac{q_t}{P_a}\right) / \left(\frac{\sigma'_{v0}}{P_a}\right)^{0.5}$$

and q_t is corrected cone resistance, P_a is atmospheric pressure, σ'_{v0} is effective in situ vertical stress. Kulhawy and Mayne (1990) suggested using $Q_f = 280$ for highly compressible normally consolidated sands and $Q_f = 450$ for highly compressible overconsolidated sands (overconsolidation ratio of > 8) based on their dataset. Robertson and Cabal (2015) suggested $Q_f = 350$ for clean, uncemented, medium compressible quartz sands of about 1000 years old. Values for Q_f can be closer to 300 for fine sands and closer to 400 for coarse sands. Furthermore, Q_f increases with age and increases significantly when age exceeds 10 000 years.

Determination of laboratory minimum and maximum index void ratios forms the basis for the relative density concept (loose, dense sand, etc.). No internationally agreed procedure is available. It is understood that Jamiolkowski et al. (2003) used results from one of the ASTM vibratory table methods for determination of minimum index void ratio. It is not clear which specific ASTM method was used, i.e. a vibratory table method requiring oven-dried soil or wet soil.

Calibration chamber test results apply to a limited range of stress conditions; typically:

50 kPa	<	σ'_{vo}	<	400 kPa
0.4	<	K_0	<	1.5

Sample preparation for laboratory chamber tests is usually by means of dry pluviation. Soil stress history application is by mechanical overconsolidation.

Effective Angle of Internal Friction - Sand

The effective shear strength parameter φ' is not a true constant. It depends on factors such as density, stress level, shearing mode and mineralogy. There is evidence that overconsolidation ratio, method of deposition and in situ stress anisotropy is less important.

Correlation of angle of internal friction φ' to cone resistance q_c may be done at various levels of sophistication. Simple procedures rely on a conservative assessment of soil behaviour classification. A more sophisticated empirical correlation consists of:

a. Estimation of in situ stress conditions σ'_{vo} and σ'_{ho}
b. Estimation of relative density D_r
c. Empirical correlation of angle of internal friction φ' with D_r, σ'_{vo} and σ'_{ho}.

Estimation of stress conditions and relative density has been discussed above.

The empirical procedure proposed by Bolton (1986 and 1987) is used for estimation of φ'. This correlation applies to clean sands and considers peak secant angle of internal friction in Isotropically Consolidated Drained triaxial compression (CID) of reconstituted sand. This procedure requires estimation of the dilatancy index and the critical state angle of internal friction.

Kulhawy and Mayne (1990) determined an equation based upon 20 data sets obtained from calibration chamber tests. This equation is almost identical to the empirical formula determined earlier by Trofimenkov (1974) which was based on mechanical cone data. Mayne (2007) validated the use of total cone resistance q_t instead of cone resistance q_c used in the equation from Kulhawy and Mayne (1990).

$$\varphi' = 17.6 + 11.0 \log \left(\left(\frac{q_t}{P_a}\right) / \left(\frac{\sigma'_{vo}}{P_a}\right)^{0.5} \right) \qquad \text{(Mayne, 2007)}$$

Undrained Shear Strength - Sand

Undrained shear strength of cohesionless soil can be important for assessment of cyclic mobility and liquefaction potential. Geotechnical procedures other than the conventional limit state models are employed.

Constrained Modulus - Sand

Kulhawy and Mayne (1990) derived two formulas for the determination of the constrained modulus for both normally consolidated and overconsolidated sands by indicating that the modulus is a function of relative density. The determination of relative density can be done with, for example, the methods indicated above.

$$M = q_c * 10^{1.09 - 0.0075 D_r}$$

(normally consolidated sands, Kulhawy & Mayne, 1990)

$$M = q_c * 10^{1.78 - 0.0122 D_r}$$

(overconsolidated sands, Kulhawy & Mayne, 1990)

where D_r is in %, and q_c and M in kPa respectively.

Young's Modulus - Sand

A common guideline is an empirical correlation given by Baldi et al. (1989). The correlation is for silica-based sand and considers cone resistance q_c, in situ stress conditions and secant Young's modulus for drained stress change E'. The ratio of E'/q_c typically ranges from about 3 to 5 for recently deposited normally consolidated sands up to about $E'/q_c = 6$ to $E'/q_c = 25$ for overconsolidated sands. The correlation has been inferred from laboratory conditions; including CPTs in a calibration chamber and conventional triaxial compression tests on reconstituted sand samples. It takes account of the degree of deformation and overconsolidation. In this regard, it is noted that secant deformation moduli are strongly dependent on strain level: the elastic modulus increases with decreasing strain to an upper limit at about 10^{-4} % strain.

Shear Modulus at Small Strain - Sand

For estimation of initial (small strain) or dynamic shear moduli, ratios of G_{max}/q_c of between about 4 and 20 can be considered, in accordance with Baldi et al. (1989). The basis for this correlation is similar to that of secant Young's modulus, except that laboratory resonant column tests serve as reference instead of triaxial compression tests. Results of limited in situ seismic cross-hole and downhole tests provide an approximate check of this correlation.

© Fugro 1996-2020

Interpretation of low-strain shear modulus can also be estimated from a correlation proposed by Rix and Stokoe (1991) in which data from calibration test measurements is compared to the correlation obtained between G_{max} and q_c by Baldi et al. (1989).

$$G_{max} = 1634(q_c)^{0.25}(\sigma'_{vo})^{0.375}$$

(Rix & Stokoe, 1991)

where G_{max}, q_c and σ'_{vo} are in kPa.

CLAY MODEL

Unit Weight – Clay

Empirical correlation between unit weight of clay and CPT parameters is as described in "Unit Weight – Sand" above.

Shear Wave Velocity – Clay

Hegazy and Mayne (2006) and Roberson and Cabal (2015) present empirical correlations between shear wave velocity and CPT parameters for a wide range of soils including clays, as described in "Shear Wave Velocity v_s – Sand" above. The Hegazy and Mayne correlation is sensitive to use of q_c or q_t. It should be used with caution for soils showing undrained or partially drained CPT response.

Mayne and Rix (1995) derived a correlation between shear wave velocity v_s and cone resistance q_c for intact and fissured clays. A database from Mayne and Rix (1993) was used including 31 different clay sites.

$$v_s = 1.75{q_c}^{0.627}$$ (Mayne & Rix, 1995)

where shear wave velocity v_s is in m/s and cone resistance q_c is in kPa.

In Situ Stress Conditions - Clay

Similar to sand, a knowledge of in situ stress conditions is generally necessary for estimation of other parameters such as consistency (soft, stiff, etc.) of a clay deposit and compressibility.

Calculation of the effective in situ vertical stress σ'_{vo} is reasonably accurate. A more approximate estimate applies to the effective in situ horizontal stress σ'_{ho}, or K_0 as $\sigma'_{ho} = K_0 \cdot \sigma'_{vo}$.

Direct correlations for interpretation of the coefficient of earth pressure at rest K_0 are the same as described for the Sand Model.

For normally consolidated clays and silts, K_{0nc} may be correlated with angle of internal friction, in accordance with Jaky (1944), or more simply, in accordance with Mayne and Kulhawy (1982):

$$K_0 = (1 - sin\varphi') \cdot OCR^{sin\varphi'}$$

where OCR is overconsolidation ratio and φ' is effective angle of internal friction. For many types of clay (e.g. Agaiby and Mayne, 2020), this equation can be approximated by $K_0 = 0.45\sqrt{(OCR)}$.

The plasticity index together with OCR may also be used for preliminary estimates of K_{0oc} as indicated by Brooker and Ireland (1965).

Overconsolidation Ratio - Clay

Overconsolidation ratio is defined as $OCR = \sigma'_p/\sigma'_{vo}$ where σ'_p is the effective preconsolidation stress considered to correspond with the maximum vertical effective stress to which the soil has been subjected in the past, and σ'_{vo} is the current effective in situ vertical stress. The effective preconsolidation stress approximates a stress level where relatively small strains are separated from relatively large strains occurring on the virgin compression stress range. The reference OCR is usually based on laboratory oedometer tests carried out on undisturbed samples. It may thus be influenced by factors such as sample disturbance, strain rate effects and interpretation procedure.

The following approach can be applied (Agaiby and Mayne, 2019):

$$OCR = \frac{\sigma'_p}{\sigma'_{v0}} \qquad \sigma'_p = 0.33 \cdot q_n^{m'} \qquad m' = 1 - \frac{0.28}{1+\left(\frac{I_c}{2.65}\right)^{2.5}}$$

where OCR is overconsolidation ratio, σ'_p is effective preconsolidation stress, σ'_{v0} is effective in situ vertical stress, q_n is net cone resistance in kPa and I_c is soil behaviour type index.

Chen and Mayne (1996) presented the following correlation for 205 clay sites around the world:

$$OCR = 0.317 \cdot Q_t$$

Overconsolidation ratio may also be inferred indirectly from a geological assessment and from undrained strength ratios. Geological factors concerning overconsolidation have been discussed under "in situ stress conditions - sand". An empirical procedure for estimation of OCR based on undrained strength ratio s_u/σ'_{vo} is given by Wroth (1984). The procedure uses the strength rebound parameter Λ. Guidance for selection of Λ and normally consolidated undrained strength ratio is given by Mayne (1988). Historically, much use has also been made of the Skempton (1957) relationship between normally consolidated undrained strength ratio and plasticity index I_P. This equation is useful for preliminary estimates, considering that I_P probably relates to φ' in some complex manner.

Undrained Shear Strength - Clay

No single undrained shear strength exists. The in situ undrained shear strength s_u depends on factors such as mode of failure, stress history, anisotropy, strain rate and temperature.

Various theoretical and empirical procedures are available to correlate q_c with s_u. Theoretical approaches use bearing capacity, cavity expansion or steady penetration solutions, all of which require several simplifying assumptions. Empirical approaches are more common in engineering practice because of difficulties in realistic soil modelling. An empirical correlation for soft to stiff, intact and relatively homogeneous clays is given by Battaglio et al. (1986) as follows:

$$s_u = (q_c - \sigma_{vo})/N_c$$

where s_u, σ_{vo} and q_c are in kPa. N_c is an empirical factor that typically ranges between 10 and 25. The higher N_c factors typically apply to clays with a relatively low plasticity index and/or apply to heavily overconsolidated clays. Lower N_c factors are generally appropriate for normally consolidated and slightly overconsolidated clays. The reference undrained shear strength is that determined from in situ vane test results. The term σ_{vo} (total in situ vertical stress) becomes insignificant for stiff clays at shallow depth so that the equation reduces to $s_u = q_c/N_c$.

For specific design situations, a different s_u reference strength should be used. For example, offshore axial pile capacity predictions in accordance with API (2011) recommend s_u to be based on undrained triaxial compression tests, which are likely to yield lower s_u values than in situ vane tests. A site-specific or regional approach should generally be preferred.

If piezocone test data are available, then improved correlations are feasible because of the pore pressure information. Empirical correlations of piezocone test results with laboratory undrained shear strengths are commonly expressed, as follows:

$$s_u = q_n/N_{kt}$$

© Fugro 1996-2020

N_{kt} ranges typically between 8 and 30 with the higher N_{kt} factors applying to heavily overconsolidated clays.

Mayne and Peuchen (2018) account for N_{kt} variation according to B_q:

$$N_{kt} = 10.5 - 4.6 \cdot ln\,(B_q + 0.1)$$

where $B_q > -0.1$. The equation is based on 407 paired CPT and laboratory test results, particularly anisotropically consolidated triaxial compressive strength. Factoring of N_{kt} can be applied by multiplying the calculated N_{kt} factor by, for example, 0.85 and 1.2.

Mayne et al. (2015) recommend a mean $N_{kt} = 12$ with a standard deviation of 2.8 for correlation with laboratory anisotropically consolidated triaxial compressive strength. The recommendations are based on a study of 51 onshore and offshore clays and apply to normally consolidated to slightly overconsolidated clays with q_n values of typically less than 8 MPa. Slightly higher N_{kt} values can be expected for average laboratory undrained shear strength, defined as the average of laboratory triaxial compression, simple shear and triaxial extension.

Clay Sensitivity

The sensitivity of a clay (S_t) is the ratio of undisturbed undrained shear strength to remoulded undrained shear strength. Sensitivity may be assessed from the CPT friction ratio R_f, in accordance with Schmertmann (1978):

$$S_t = N_s/R_f$$

where N_s is a correlation factor typically ranging between 5 and 10. The correlation is expected to be inaccurate for sensitive clays where uncertainty in very low values for sleeve friction may dominate results.

The reference S_t value is often taken to be that determined from undisturbed and remoulded laboratory unconsolidated undrained triaxial tests. This reference S_t value may differ from that determined from other tests, for example laboratory miniature vane tests. This is partly related to the definition of sensitivity. For vane tests, several measurements of undrained shear strength are possible:

- Intact (I) = undisturbed undrained shear strength as measured on an intact/undisturbed specimen.
- Intact-Residual (I-R) = measured post peak during initial shearing of the intact specimen.
- Intact-Vane Remoulded (I-VR) = measured after multiple-quick rotations of the vane after completion of the intact test.
- Hand Remoulded (HR) = steady state (post-peak if exists) resistance of hand remoulded test specimen.
- Hand Remoulded – Vane Remoulded (HR-VR) = steady state resistance of hand remoulded specimen measured after applying multiple-quick vane rotations.

Skempton and Northey (1952) present a correlation of sensitivity and laboratory liquidity index I_L. This correlation may allow a check on CPT-based interpretation of sensitivity.

Effective Shear Strength Parameters - Clay

Measurement of pore water pressures during penetration testing has led to development of interpretation procedures for estimation of effective stress parameters of cohesive soils. Background information may be found in Sandven (1990). Currently available procedures are evaluated to be "experimental" and are yet not commonly adopted.

In general, CPT interpretation of effective shear strength parameters for clay and silt relies on soil behaviour-type classification.

It is noted that significant silt and sand fractions in a clay deposit will increase φ', while a significant clay fraction in silt will decrease φ'.

Masood and Mitchell (1993) provide an equation for the determination of φ' by combining sleeve friction with the Rankine earth-pressure theory. The equation is based on the following assumptions:

- Unit adhesion between soil and sleeve is negligible.
- Friction angle between soil and sleeve = $\varphi'/3$.
- Lateral earth pressure coefficient during penetration is equal to the Rankine coefficient of lateral earth pressure under passive conditions.

$$\frac{f_s}{\sigma'_{vo}} = \tan^2(45° + \frac{\varphi'}{2})\tan(\frac{\varphi'}{3})$$

(Masood & Mitchell, 1993)

Mayne (2001) proposed an approximation of the Masood and Mitchell equation, as follows:

$$\varphi' = 30.8\left[\log(\frac{f_s}{\sigma'_{vo}}) + 1.26\right]$$ (Mayne, 2001)

Mayne (2001) also proposed the following approximation of friction angle φ' based on pore pressure ratio B_q and the cone resistance number N_m (Senneset, Sandven and Janbu, 1989):

$$\varphi' = 29.5{B_q}^{0.121}(0.256 + 0.336B_q + \log N_m)$$

(Mayne, 2001)

where

$$N_m = \frac{q_t - \sigma_{vo}}{\sigma'_{vo} + a}$$

where the cone resistance number N_m is dimensionless, total cone resistance q_t, total in situ vertical stress σ_{vo} and effective in situ vertical stress σ'_{vo} are in kPa.

Senneset et al. (1989) use the attraction value a as a function of soil type. In general, the attraction value ranges from 5 to > 50 for both sands and clays and may be estimated directly from CPT results. The correlation is valid if the angle of plastification β is zero. In general, a plastification angle of zero applies to medium sands and silts, sensitive clays and highly compressible clays.

Constrained Modulus - Clay

Mitchell and Gardner (1976) present an approximate correlation of cone resistance with constrained modulus M (or coefficient of volume compressibility m_v, where $M = 1/m_v$). Typical ratios of M/q_c range between 1 and 8 for silts and clays. Refinements include q_c ranges and soil type (silt, clay, low plasticity, high plasticity, etc.). The correlation relies on the results of conventional laboratory oedometer tests carried out on undisturbed clay and silt samples.

Kulhawy and Mayne (1990) correlated constrained modulus M with net cone resistance data. This relationship is based on data from 12 (clay) test sites, with constrained moduli up to 60 MPa. The published standard deviation is 6.7 MPa.

$$M = 8.25\ q_n$$ (Kulhawy & Mayne, 1990)

Young's Modulus – Clay

Young's modulus E_u can be derived as follows:

a. Estimation of undrained shear strength s_u from CPT data, as outlined above.

© Fugro 1996-2020

b. Estimation of secant Young's moduli for undrained stress change in general accordance with correlations based on s_u, as presented by Ladd et al. (1977).

Laboratory undrained triaxial tests carried out on undisturbed clay specimen form the basis for the E_u versus s_u correlations. Typical E_u/s_u ratios at a shear stress ratio of 0.3 range between about 300 and 900 for normally consolidated clays and $E_u/s_u = 100$ to $E_u/s_u = 300$ for heavily overconsolidated clay. Higher E_u/s_u ratios would apply to lower shear stress ratios, and vice versa.

Shear Modulus at Small Strain - Clay

Mayne and Rix (1993) determined a relationship between G_{max} and q_c by studying 481 data sets from 31 sites all over the world. G_{max} ranged between about 0.7 MPa and 800 MPa.

$$G_{max} = 2.78\ {q_c}^{1.335} \qquad \text{(Mayne \& Rix, 1993)}$$

where G_{max} and q_c are in kPa.

References

Agaiby, S.S. & Mayne, P.W. (2019). CPT evaluation of yield stress in soils. *Journal of Geotechnical & Geoenvironmental Engineering* 145(12): doi.org/10.1061/(ASCE)GT.1943-5606.0002164

American Petroleum Institute [API] (2014). *Planning, designing and constructing fixed offshore platforms - working stress design.* (API RP 2A-WSD, 22nd Edition) https://www.apiwebstore.org/publications/item.cgi?b9e32dec-268b-404d-988e-5cda65c27757

Baldi, G., Bellotti, R., Ghionna, V.N., Jamiolkowski, M., & Lo Presti, D.C.F. (1989). Modulus of sands from CPTs and DMTs. In *Proceedings of the 12th international conference on soil mechanics and foundation engineering*, *Rio de Janeiro, 13–18 August 1989* (pp. 165–170). Balkema.

Battaglio, M., Bruzzi, D., Jamiolkowski, M., & Lancellotta, R. (1986). Interpretation of CPTs and CPTUs, part 1: Undrained penetration of saturated clays. In *Field instrumentation and in-situ measurements: Proceedings of the fourth international geotechnical seminar*, *25–27 November 1986, Mandarin Hotel, Singapore* (pp. 129–143). Nanyang Technological Institute.

Bolton, M.D. (1986). The strength and dilatancy of sands. *Géotechnique*, *36*(1), 65–78. http://www-civ.eng.cam.ac.uk/geotech_new/people/bolton/mdb_pub/14_Geotechnique_No36_Is1_65_78.pdf

Bolton, M.D. (1987). Author's reply to discussion of the strength and dilatancy of sands. *Géotechnique*, 37(2) 225-226 https://doi.org/10.1680/geot.1987.37.2.219

Boulanger, R.W. & DeJong, J.T. (2018). Inverse filtering procedure to correct cone penetration data for thin-layer and transition effects. In M.A. Hicks, F. Pisanò & L.J. Peuchen, L.J. (eds.) *Cone Penetration Testing 2018: Proceedings of the 4th International Symposium on Cone Penetration Testing (CPT18): Delft, The Netherlands, 21-22 June 2018* (pp. 25-44). CRC Press

Brooker, E.W. & Ireland, H.O., 1965. Earth pressures at rest related to stress history. *Canadian Geotechnical Journal*, *2*(1), 1–15. https://doi.org/10.1139/t65-001

Chen, B.SY., & Mayne, P.W. (1996). Statistical relationships between piezocone measurements and stress history of clays. *Canadian Geotechnical Journal*, *33*(3), 488–498. doi.org/10.1139/t96-070

DeJong, J.T. & Randolph, M.F. (2012). Influence of partial consolidation during cone penetration on estimated soil behavior type and pore pressure dissipation measurements. *Journal of Geotechnical and Geoenvironmental Engineering*, 138(7) 777-788: doi.org/10.1061/(ASCE)GT.1943-5606.0000646

Hegazy, Y.A., & Mayne P.W. (2006, June). *A global statistical correlation between shear wave velocity and cone penetration data [*conference presentation]. GeoShanghai International Conference, Shanghai, China. ASCE. https://doi.org/10.1061/40861(193)31

Jaky, J. (1944). The coefficient of earth pressure at rest. *Magyar Mérnök és Epitész Egylet Közlönye,* 78(22) 355-358. (in Hungarian).

Jamiolkowski, M., Lo Presti, D.C.F., & Manassero, M. (2003). Evaluation of relative density and shear strength of sands from CPT and DMT. In J.T. Germaine, T.C. Sheahan & R.V. Whitman (Eds.), *Soil behavior and soft ground construction* (pp. 201–238). American Society for Civil Engineers. https://doi.org/10.1061/9780784406595

Kulhawy, F.H., & Mayne, P.W. (1990). *Manual on estimating soil properties for foundation design.* (Report EL-6800). Electric Power Research Institute.

Ladd, C.C., Foott, R., Ishihara, K., Schlosser, F. & Poulos, H.G. (1977). Stress-deformation and strength characteristics. In *Proceedings of the ninth international conference on soil mechanics and foundation engineering, 1977, Tokyo* (volume 2) (pp. 421-494). Japanese Society of Soil Mechanics and Foundation Engineering

Lengkeek, H.J., De Greef, J. & Joosten, S. (2018). CPT based unit weight estimation extended to soft organic soils and peat. In M.A. Hicks, F. Pisanò & L.J. Peuchen, L.J. (eds.) *Cone Penetration Testing 2018: Proceedings of the 4th International Symposium on Cone Penetration Testing (CPT18): Delft, The Netherlands, 21-22 June 2018* (pp. 389-394). CRC Press

Masood, T. & Mitchell, J.K. (1993). Estimation of in situ lateral stresses in soils by cone-penetration test. *Journal of Geotechnical Engineering, 119*(10) 1624-1639: doi.org/10.1061/(ASCE)0733-9410(1993)119:10(1624)

Mayne, P.W. (1988). Determining OCR in clays from laboratory strength. *Journal of Geotechnical Engineering, 114*(1) 76-92: doi.org/10.1061/(ASCE)0733-9410(1988)114:1(76)

Mayne, P.W. (2001). *Geotechnical site characterization using cone, piezocone, SCPTu, and VST*. Georgia Institute of Technology.

Mayne, P.W. (2020). The 26th Széchy Lecture: Use of in-situ geotechnical tests for foundation systems. *Proceedings of the Széchy Károly Emlékkonferencia*, published by the Hungarian Geotechnical Society, Budapest: 12-73

Mayne, P.W. (2007). In-situ test calibrations for evaluating soil parameters. In T.S. Tan, K.K. Phoon, D.W. Hight & S. Leroueil (eds.) Characterisation and *Engineering Properties of Natural Soils* (Volume 3) (pp. 1601-1652). Taylor & Francis.

Mayne, P.W., & Kulhawy, F.H. (1982). K_0-OCR relationships in soil. *Journal of the Geotechnical Engineering Division*, *108*(6), 851–872.

Mayne, P.W. & Rix, G.J. (1993). G_{max}-qc relationships for clays. *Geotechnical Testing Journal, 16*(1) 54-60 https://doi.org/10.1520/GTJ10267J

Mayne, P.W., & Rix, G.J. (1995). Correlations between shear wave velocity and cone tip resistance in natural clays. *Soils and*

© Fugro 1996-2020

Foundations, *35*(2), 107–110. https://doi.org/10.3208/sandf1972.35.2_107

Mayne, P.W., Peuchen, J. & Bouwmeester, D. (2010). Soil unit weight estimation from CPTs. In CPT'10: 2nd International symposium on cone penetration testing, Huntington Beach, California: conference proceedings.

Mayne, P.W., Peuchen, L.J. & Baltoukas, D.B. (2015). Piezocone evaluation of undrained strength in soft to firm offshore clays. In V. Meyer (ed.) *Frontiers in Offshore Geotechnics III: proceedings of the Third International Symposium on Frontiers in Offshore Geotechnics (ISFOG 2015), Oslo, Norway, 10-12 June 2015.* (pp. 1091-1096) CRC Press.

Mayne, P.W. & Peuchen, L.J. (2018). Evaluation of CPTU N_{kt} cone factor for undrained strength of clays. In M.A. Hicks, F. Pisanò & L.J. Peuchen, L.J. (eds.) *Cone Penetration Testing 2018: Proceedings of the 4th International Symposium on Cone Penetration Testing (CPT18): Delft, The Netherlands, 21-22 June 2018*. (pp. 423-429) CRC Press.

Mitchell, J.K. & Gardner, W.S. (1976). In situ measurement of volume change characteristics. In Proceedings of the conference on in situ measurement of soil properties, June 1-4, 1975, Raleigh, North Carolina: Specialty Conference of the Geotechnical Engineering Division, ASCE, II (pp. 279-345). American Society of Civil Engineers.

Peuchen, J. & Terwindt, J. (2014). Introduction to CPT accuracy. In 3rd International symposium on cone penetration testing CPT14 : May 12-14 (2014) - Las Vegas, Nevada.

Peuchen, J. & Terwindt, J. (2015). Measurement uncertainty of offshore cone penetration tests. In V. Meyer (ed.) Frontiers in offshore geotechnics III: proceedings of the third international symposium on frontiers in offshore geotechnics (ISFOG 2015), Oslo, Norway, 10-12 June 2015. (pp. 1209-1214) CRC Press.

Rix, G.J., & Stokoe, K.H. (1991). Correlation of initial tangent nodulus and cone penetration resistance. In A.-B. Huang (Ed.), Proceedings of the 1st international symposium on calibration chamber testing, ISOCCT1 (pp. 351–362). Elsevier.

Robertson, P.K. (1990). Soil classification using the cone penetration test. Canadian Geotechnical Journal, 27(1), 151–158. https://doi.org/10.1139/t90-014

Robertson, P.K. (2009). Performance based earthquake design using the CPT. In T. Kokusho, Y. Tsukamoto, & M. Yoshimine (Eds.), Performance-based design in earthquake geotechnical engineering: From case history to practice (pp. 3–20). CRC Press.

Robertson, P.K. (2010). Soil behaviour type from the CPT: an update. In 2nd International symposium on cone penetration testing, Huntington Beach, CA, Vol. 2. (pp. 575-583)

Robertson, P.K. (2016a). Cone penetration test (CPT)-based soil behaviour type (SBT) classification system — an update. *Canadian Geotechnical Journal, 53*(12) 1910-1927 https://doi.org/10.1139/cgj-2016-0044

Robertson, P.K. (2016b). Estimating K0 in sandy soils using the CPT. In B.M. Lehane, H.E. Acosta-Martinez & R.B. Kelly (eds.) Geotechnical and geophysical site characterization 5: proceedings of the fifth international conference on geotechnical and geophysical site characterization (ISSMGE TC-102 - ISC'5), Gold Coast, Queensland, Australia, 5-9 September 2016 (pp. 515-518). Australian Geomechanics Society

Robertson, P.K. & Cabal, K.L. (2015) *Guide to cone penetration testing for geotechnical engineering*. (6th ed.) Gregg Drilling & Testing.

Robertson, P.K. & Wride (Fear), C.E. (1998). Evaluating cyclic liquefaction potential using the cone penetration test. *Canadian Geotechnical Journal*, *35*(3), 442-459. https://doi.org/10.1139/t98-017

Robertson, P.K., Woeller, D.J. & Finn, W.D.L. (1992). Seismic cone penetration test for evaluating liquefaction potential under cyclic loading. *Canadian Geotechnical Journal, 29*(4) 686-695 https://doi.org/10.1139/t92-075

Sandven, R. (1990). *Strength and deformation properties of fine grained soils obtained from piezocone tests* [Thesis]. Norwegian Institute of Technology, Department of Civil Engineering

Schmertmann, J.H. (1978). *Guidelines for cone penetration test: Performance and design* (Report no. FHWA-TS-78-209). Federal Highway Administration, US Department of Transportation.

Senneset, K., Sandven, R., & Janbu, N. (1989). The evaluation of soil parameters from piezocone tests. *Transportation Research Record*, *1235*, 24–37. http://onlinepubs.trb.org/Onlinepubs/trr/1989/1235/1235-003.pdf

Skempton, A.W. (1957). Discussion on Airport Paper No. 35: The planning and design of the new Hong Kong Airport. *Proceedings of the Institution of Civil Engineers, 7*(2) 306.

Skempton, A.W., & Northey, R.D. (1952). The sensitivity of clays. *Géotechnique*, *3*(1), 30–53. https://doi.org/10.1680/geot.1952.3.1.30

Trofimenkov, J.G. (1974). Penetration testing in USSR: state-of-the-art report. in *Proceedings of the European symposium on penetration testing ESOPT, Stockholm, June 5-7, 1974, 1* (pp. 147-154). National Swedish Building Research.

Van der Wal, T., Goedemoed, S. & Peuchen, J. (2010). Bias reduction on CPT-based correlations. In *CPT'10: 2nd international symposium on cone penetration testing, Huntington Beach, CA: conference proceedings*.

Wroth, C.P. (1984). The interpretation of in situ soil tests. *Géotechnique*, *34*(4), 449–489. https://doi.org/10.1680/geot.1984.34.4.449 https://www.icevirtuallibrary.com/doi/pdf/10.1680/geot.1984.34.4.449

Zhang, G., Robertson, P.K. & Brachman, R.W.I. (2002). Estimating liquefaction induced ground settlements from CPT for level ground. *Canadian Geotechnical Journal*, *39*(5) 1168-1180. https://doi.org/10.1139/t02-047

.

© Fugro 1996-2020

Marine Reflection Seismics

Introduction

Marine geophysical investigation by seismic reflection methods provides a continuous acoustic record of the seafloor and seabed (ground below seafloor). The acquired data are typically interpreted for site characterisation, particularly mapping of stratigraphic, geomorphological, structural and geohazard features of the seabed.

This document covers 2D high resolution (HR), ultra-high resolution (UHR) and ultra-ultra-high resolution (UUHR) seismic and sub-bottom profiler (SBP) seismic reflection methods.

- HR seismic: method that acquires data containing frequencies between 75 Hz and 300 Hz; expected vertical resolution range: 1 m to 7 m;
- UHR seismic: method that acquires data containing frequencies between 250 Hz and 800 Hz; expected vertical resolution range: 0.5 m to 2 m;
- UUHR seismic: method that acquires data containing frequencies between 750 Hz and 2000 Hz; expected vertical resolution range: 0.2 m to 1 m;
- SBP: method that acquires data containing frequencies between 1000 Hz and 15000 Hz; expected vertical resolution range: < 0.5 m.

These methods are commonly required to provide input for design, installation, operation and decommission of offshore structures (ISO, 2015; ISO, 2019)

Apparatus and procedures adopted by Fugro are in general accordance with ISO/DIS 19901-10:2018 (ISO, 2018) and ISSMGE (2005). The scope of marine geophysical investigation is according to agreed project specifications.

A marine geophysical investigation is commonly followed by marine soil investigation (ISO, 2014).

Apparatus

Overview

Reflection seismic survey spreads comprise the following components:

- Survey platform;
- Source to produce a discrete and repeatable acoustic pulse;
- Receiver (array) to receive the reflected signals;
- Posititioning equipment;
- Recording/display unit(s).

Survey Platforms

Examples of survey platforms are:

- Geophysical survey (surface) vessel;
- Autonomous surface vessel (ASV);
- Remotely operated vehicle (ROV);
- Autonomous underwater vehicle (AUV).

Selection of a survey platform depends on factors such as scope of investigation, water depth and seafloor terrain (including gradients).

Sources

Acoustic sources are commonly classified on the basis of power levels and operation frequency. In general, higher power levels result in lower frequencies and imply greater penetration in the seabed but with less resolution. Acoustic sources include:

- Pinger: a low energy device with an array of acoustic transducers that convert an electric pulse into an acoustic pulse within the frequency range of 3 kHz to 7 kHz;
- Chirp: type of pinger that emits a frequency-modulated pulse over a specified range of frequencies;
- Boomer: source powered by a rapid high-voltage discharge of capacitor banks through a spark gap. Combinations of energy supply and energy discharge units give available power levels ranging from 100 Joules to more than 1 000 Joules with a frequency range of 50 Hz to a few kHz;
- Sparker: a seismic source that operates by producing an electric discharge in water. The heat generated by the discharge vaporises the water at the electrode tips, creating an effect equivalent to a small explosion of bubbles, which oscillate and collapse after a few milliseconds. Sparker sources are generally limited to an energy range of 200 Joules to 10 000 Joules, though there is generally little advantage to be gained in increasing the energy level beyond 3 000 Joules;
- Airgun: source which injects a bubble of highly compressed air into the water.

In some systems, a source is combined with a receiver in a single unit (transducer), e.g. a pinger system mounted in the hull of a survey platform.

In many cases, a source is towed behind a geophysical survey vessel, either at the sea surface or at some depth below the sea surface.

Receivers

Receivers convert the transmitted acoustic energy (i.e. seabed reflections) into electric signals. Receivers include:

- Hydrophones;
- Geophones;
- Accelerometers.

Receiver configurations can comprise a single receiver (single channel), multiple receivers (ocean bottom nodes/ cables) or a group of receivers (array; multichannel). A group of receivers is incorporated in a flexible streamer, which is towed by the survey platform, either at the sea surface or at some depth below the sea surface.

Positioning Equipment

Positioning equipment typically includes multiple GNSS systems, mounted on the survey platform and in some cases on the source and receiver systems. For example, a streamer may be fitted with a tail buoy that includes a GNNS positioning system.

AUV and ROV survey platforms include subsea positioning systems.

Recording/ Display Units

A control unit is an integrated source trigger and recorder unit, which records the electrical signals from the receivers. The control unit may allow initial processing to the recorded data including:

- Overall and time varied gain (TVG);
- Swell filters;
- trace stacking;
- band-pass filters.

Signals are displayed in real-time and recorded digitally.

© Fugro 1994-2020

Procedure

Overview

The procedure for marine reflection seismics generally includes activities ranging from survey design to integrated geosciences. The agreed project specifications can cover some or all of the steps in the procedure.

Survey Design and Selection of Apparatus

Survey design depends on the required level of seabed detail. Particularly, it includes selection of apparatus and layout of survey track lines.

One or more seismic reflection methods can be selected, for example a combination of SBP and UHR methods. This selection phase takes account of factors such as:

- Feasible combinations of required resolution and penetration depth into the seabed;
- Inherent limitations, e.g. detailed imaging of the upper 0.5 m below seafloor (Peuchen and Westgate, 2018); this depth interval can be important for design of sub-sea templates, surface-laid pipelines and cables.

Survey platform, source and receiver (single or multiple) configurations are then selected. In general, such selection depends on expected wave heights, (tidal) currents, water depths, seabed conditions and sustainability considerations.

Where applicable, the tow depths of a source and of a receiver array (streamer) can be selected to minimise metocean effects (e.g. swell) on data quality of the recorded signals.

The survey line plan (i.e. survey design) typically considers:

- Required spatial detail of the ground model as function of survey track line spacing, e.g. lateral delineation of soil provinces, ground units and geological features;
- Detection of isolated seabed features, smaller than the distance between survey track lines (e.g. isolated boulders, shallow gas pockets, anthropogenic debris below seafloor etc.);
- Survey line orientations, taking into account seafloor morphological features that may impair adequate transmittal of seismic waves (e.g. survey track lines perpendicular to steep slopes to reduce unwanted noise in seismic data);
- Sustainability considerations including use of energy (e.g. reduction of negative effects on marine life).

Equipment Deployment

Equipment can be deployed (1) as integral part of the survey platform, (2) launched and towed behind a surface vessel and (3) by detached operations (e.g. for ocean bottom nodes).

For AUV and ASV operations, the survey line plan is uploaded in an internal navigation computer of these survey platforms. Following deployment, these systems autonomously acquire data along a programmed line plan, using a suite of acoustic sensors to avoid obstacles and maintain a specified speed and (in case of AUV) a near-constant elevation above seafloor.

For ROV operations, a ROV operator controls the survey platform from a vessel or from an onshore remote operations centre.

Equipment deployment can include a verification and testing programme for key components of the apparatus, for example by data acquisition along a line within the site. This line can be surveyed several times to adjust acquisition parameters (e.g. operating frequency and/or energy levels, equipment tow depth) for local conditions to optimise trade-off between resolution and depth of penetration.

Data Processing

SBP data can be processed either in real-time or separately as a post-acquisition exercise. Basic processing steps include:

- Adding detailed geodetic positions to the acquired seismic traces;
- Applying a correction for tidal effects during data acquisition.

Additional processing typically applies to HR, UHR and UUHR seismic reflection data. Processing steps will vary according to agreed project specifications and site-specific conditions. The focus of the processing is typically on maintaining the relative amplitude relationships and preserving the high frequency content for the depth zone(s) of interest.

Processing techniques include (ISO, 2018):

- Gain recovery/amplitude manipulation;
- Velocity analysis;
- Mute;
- Normal moveout (NMO) correction and common mid-point (CMP) stack;
- Designature techniques;
- Demultiple techniques;
- Deconvolution before stack (DBS);
- Pre-stack time migration (PSTM);
- Post-stack coherent noise attenuation;
- Zero-phase conversion;
- Time varying filter (TVF);
- Time-depth conversion.

Assessment of Data Quality

For surface vessels, the quality of the data can depend on sea state, e.g. wave height during data acquisition. An example would be 'tugging' of a towing cable caused by large waves, having a detrimental effect on data quality.

Data acquisition in shallow coastal water may be impaired by surface breaking waves (i.e. surf zone). Acquisition in such areas is challenging and may require an exceptionally calm sea state.

Shallow gas in the seabed can make it impossible for seismic reflection methods to obtain adequate resolution at and below the upper surface of shallow gas. The presence of even a small amount of gas in the seabed causes substantial soil can drastically increase the attenuation of the acoustic signal, causing (acoustic) blanking.

Information from the data interpretation phase and the integrated geosciences phase can support assessment of data quality.

Data Interpretation

The data interpretation phase can make use of specialist interpretation software, allowing interrogation of seismic records or lines. Seismic reflectors, that correspond to geological and/or geotechnical ground units can be mapped as horizons. Furthermore, data interpretation allows mapping and assessment of potential geohazards, for example:

- Cemented coarse soil layers;
- Shallow gas;
- Buried channels (i.e. spatial variation in soil conditions).

Reflectors mapped in the time domain (e.g. two-way travel time as depth scale) can be converted to depth using an estimate for seismic velocity. Velocity estimates can be obtained from general

© Fugro 1994-2020

knowledge of the seabed, nearby marine geophysical investigation, a (seismic) velocity model and, preferably, by correlation (ground truthing) with site-specific geotechnical data (e.g. cone penetration test data showing distinct changes in cone resistance at soil unit boundaries) and data derived from borehole geophysical logging. Ground truthing increases reliability of data interpretation.

Integrated Geosciences

Integration of seismic reflection data with other methods of investigation can be done at different levels:

- Stratigraphic Zonation: integration focussing on achieving stratigraphic alignment between seismic profiles obtained by non-intrusive techniques and stratigraphic interpretation from results of intrusive ground investigation;
- Geotechnical Zonation: integration providing a vertical and horizontal zonation and includes mapping of 'soil provinces', with each soil province having a representative vertical soil profile and distinct seismic character;
- Geotechnical Zonation and Analysis – integration as per Geotechnical Zonation, additionally including engineering assessments for specific project requirements.

Results

Reporting Scope and Format

The results of a marine reflection seismics typically include documentation of data acquisition, data processing steps and interpretive features (e.g. seismic data character of the seabed and illustrative data examples). In addition, the following can be provided, depending on agreed project specifications:

- Track charts presenting positions of the survey track lines;
- Shallow structure maps, presenting depth to top or base of interpreted ground units;
- Isopach maps, presenting thickness range of interpreted ground units;
- Geological features maps, presenting positions of e.g. interpreted buried channels, shallow gas anomalies, etc.
- Cross sections;
- GIS data base;
- Digital, seismic interpretation project (e.g. Kingdom Suite project, Petrel project);
- Voxel ground model for GIS-type visualisation.

Reflection Amplitude

Reflection amplitude (high, medium, low) is the deviation of a seismic wave from the zero-crossing along a trace. It provides a measure of relative reflection strength and can provide an indication of lithological contrast (seismic velocity - density of ground), ground layer spacing, possible pore fluid/gas content etc.

In general, high amplitude events correlate to strong vertical variation of contrasting lithologies (e.g. sand / clay), while low amplitude indicates more comparable lithologies on both sides of an interface (e.g. sand / silty sand).

High amplitudes typically occur at seafloor, where there is a large contrast in density (unit weight) and velocity between seawater and seabed. A boundary between soil and rock is generally also associated with high amplitude reflectors. High amplitude reflections can also be associated with soil including (free, undissolved) gas, due to the low velocities for gassy soil.

A reversed (polarity) amplitude – as in ''polarity reversal'' is an amplitude feature characterised by reversal of the seismic reflection polarity along a horizontal interface, when followed from trace to trace. This may be due to a change in fluid/gas contents of pore space. Reversed polarity is commonly associated with gas in soil.

Seismic Frequency

Seismic frequency (high, medium, low) is commonly associated with resolution of seismic data. Resolution is the ability to distinguish two seabed features from one another (e.g. top and base of a ground layer and interbedding).

The vertical resolution (limit of separability) can be taken as ¼ of the seismic wavelength (λ). The wavelength in turn can be calculated from seismic velocity v, i.e. $\lambda = v/F$ where F is seismic frequency.

Seismic frequency decreases with increasing depth, as high frequencies in a seismic signal are more quickly attenuated. Conversely, seismic velocity generally increases with depth. As a result, vertical resolution of seismic data is depth dependent (Brown, 2004).

In general, high frequency seismic data imply reduced signal penetration below seafloor, but with greater overall vertical resolution.

Reflection Configuration

Reflection configuration can be described as parallel or sub-parallel, divergent, wavy, hummocky, chaotic, transparent etc.

Reflection configuration is related to the geometry/ pattern of ground layering/ bedding pattern resulting from specific depositional processes, original palaeotopography and post-depositional processes. For example, a high energy depositional environment (e.g. fluvial environment, debris flows) generally results in a more chaotic seismic response.

Reflection Continuity

Reflection continuity (continuous, discontinuous, truncation of reflectors) describes continuity of ground layers. It is directly related to sedimentation processes and post-sedimentation processes (e.g. erosion) and hence, to geological setting.

In general, the less energetic the environment, the more continuous the seismic response. Continuity also indicates greater lateral extent of certain depositional conditions, while discontinuities may suggest rapid changes in energy levels during deposition and/or effects of post-depositional erosion.

For example, flood plain deposits are generally associated with a low energy environment that may be laterally continuous. The reflections associated with a flood plain are generally continuous (parallel bedded reflectors). The reflections associated with a (meandering) stream or fluvial channel are localised and of low lateral continuity.

Multiple Reflections

'Multiples' are commonly associated with seismic datasets. Multiple reflections are reflections generated by acoustic waves travelling several times (reverberation) between two strong interfaces (e.g. seafloor and a boundary between rock / soil layers) before they arrive at the receiver. Multiple reflections can be strong and can interfere with reflections of geological interfaces, whereby the latter are obscured in the depth interval where the multiples appear.

For example, an acoustic wave traveling from its source may be reflected off the seafloor, the sea surface and the seafloor again before arriving at the receiver (seafloor multiples). The "ray-path"

© Fugro 1994-2020

of this multiple is approximately twice that of a normal source-seafloor-receiver ray-path.

If two strong subsurface reflectors are present, acoustic signals may ''bounce'' several times between them, before the wave-front can be recorded at the receiver (peg-leg multiples).

Seismic Artefacts

Seismic artefacts may be caused by lateral variation of seabed conditions, including buried boulders and steeply dipping ground strata. Examples are:

- Pull-up effects below seafloor sand waves, where seismic reflectors can appear at slightly higher elevations than where sand waves are not present. This is due to small seismic velocity variations and steep-sided slopes of the sand waves;
- Acoustic transparency and signal attenuation below crests of sand waves and enhanced amplitude reflections or signal tuning at the troughs of the sand waves. These feature can mask seismic signal;
- Pull-down effects as indicator for the presence of free gas in the seabed. Gassy soils have lower seismic velocity and hence acoustic waves travel slower than in fluid-saturated soils, causing seismic reflectors to (locally) occur lower than in non-gassy soils;
- Hyperbole-shaped reflections (i.e. diffraction hyperbolae) originating from "point sources" in the seabed. Typical point sources are buried boulders, pipelines and cables.

Bibliography

Brown, A. (2004). *Interpretation of three-dimensional seismic data*. (6th ed.) American Association of Petroleum Geologists (AAPG); Society of Exploration Geophysicists (AAPG Memoir ; 42)(SEG Investigations in Geophysics ; No. 9)

International Organization for Standardization (2019). *Petroleum and natural gas industries – general requirements for offshore structures* (ISO 19900-2019). https://www.iso.org/standard/69761.html

International Organization for Standardization (2018). *Petroleum and Natural gas industries - specific requirements for offshore structures – part 10: marine geophysical investigations* (ISO 19901- 10:2018). https://www.iso.org/standard/77017.html.

International Organization for Standardization (2015). *General principles on reliability for structures* (ISO 2394:2015). https://www.iso.org/standard/58036.html

International Organization for Standardization (2014). *Petroleum and natural gas industries – specific requirements for offshore structures – part 8: marine soil investigations* (ISO 19901-8:2014). https://www.iso.org/standard/61145.html

International Society for Soil Mechanics and Geotechnical Engineering, Technical Committee 1 (2005). *Geotechnical & geophysical investigations for offshore and nearshore developments*. International Society for Soil Mechanics and Geotechnical Engineering (ISSMGE)

Peuchen, L.J. and Westgate, Z.J. (2018). Defining geotechnical parameters for surface-laid subsea pipe-soil interaction. In M.A. Hicks, F. Pisanò & L.J. Peuchen, L.J. (eds.) *Cone Penetration Testing 2018: Proceedings of the 4th International Symposium on Cone Penetration Testing (CPT18): Delft, The Netherlands, 21-22 June 2018*. (pp. 519-524) CRC Press.

© Fugro 1994-2020

Site Characterisation

Introduction

Site characterisation may be defined as a fit-for-purpose model of a site. For the context of this document, site is defined as a geographical part of the earth at a particular time or period, that:

- Incorporates the surface of the earth and ground below this surface;
- Can include water and air above the ground surface;
- Can include man-made objects and structures in or connected to the ground.

Ground is defined as soil and rock, including made ground, pore fluid and pore gas.

A fit-for-purpose site model is fundamental to managing ground risks and optimizing opportunities. The model is a prediction and a reduction of reality and can be used to:

- Provide sound information with which to define and assess the suitability of a site for proposed facilities;
- Detect and assess the possible effects of geohazards and changes in seabed conditions with time;
- Choose parameter values for verification of limit states and to assess the feasibility of building/installing, operating, and/or decommissioning a structure.

The model has interpretive limits that typically depend on:

- Structure characteristics and project phase such as conceptual design, installation and structure re-assessment;
- Data selected and available at the time of study:
  - Stratigraphic schematisation, e.g. partial data coverage or detection limits of deployed investigation tools and an interface between strata being more gradual than indicated;
  - Level of detail and accuracy in interpretation of geotechnical parameter values, which can be affected by test data, sample size, quality, and coverage;
- Public-domain information such as geological understanding;
- Data visualisation algorithms, e.g. for data contouring.

Other terms used in practice for (parts of) site characterisation include integrated study, integrated geosciences, desk study, and seabed characterisation.

Site characterisation can also refer to the activities required to create the model of the site (e.g. Evans, 2010; Peuchen, 2012). Ideally, site characterisation benefits from integration of multidisciplinary data (e.g. geotechnical and geophysical data integration).

This document focuses on marine projects. Site characterisation is an integral part of offshore structure design and operation according to reliability principles covered by standards and codes of practice; for instance API (2014a, 2014b and 2015), ASTM (2018), DNV GL (2017), RenewableUK (2013), CEN (2009 and 2015); ISO (2014, 2016a, 2016b, 2017, 2019a and 2019b).

Table 1 shows levels of integration that can be considered.

The terms seabed and seafloor are according to ISO (2016a):

- Seabed comprises materials below the sea in which a structure is founded, whether of soils such as sand, silt or clay, cemented materials or, of rock
- Seafloor is defined as the interface between the sea and the seabed.

This document also uses the geological term 'sediments' as synonym of uncemented soil.

Table 1: Levels of Integration for Marine Site Characterisation

Integration Level	Integration Type	Description
1	Bundled Information	Each data acquisition activity is interpreted and reported separately. No specific effort is made to consider and reconcile potential conflicts between information sources.
2	Stratigraphic Integration	This level of integration specifically focusses on achieving stratigraphic alignment between (1) sub-surface/sub-bottom profiles obtained by non-intrusive geophysical techniques (e.g. seismostratigraphy) and (2) stratigraphic interpretation from results of ground investigation obtained at specific locations (e.g. geotechnical soil unitisation). The stratigraphic alignment considers vertical zonation of a site.
3	Geotechnical Zonation	This level of integration provides a vertical and horizontal geotechnical zoning of a site. The horizontal zonation comprises a delineation and mapping of 'soil provinces'. Each soil province has a representative vertical soil profile and envelopes of ground characterisation such as shear strength, relative density, friction angle, unit weight, etc. The 'horizontal and vertical zoning' facilitates selection of engineering criteria (e.g. geotechnical parameter values/ranges) for analysis of trenchability, anchor holding capacity, foundation bearing resistance, etc.
4	Geotechnical Zonation and Analysis	This level of integration not only provides geotechnical zonation but also incorporates engineering assessments for specific project requirements such as bearing resistance, trenching resistance, anchor holding capacity, upheaval buckling resistance, scour potential etc. These requirements are usually specific to the type of facility, construction method and project phase.

© Fugro 2014-2020

Procedure

Figure 1 summarises the general procedure. Decisions on scope and adequacy are project-specific and depend on input such as project specifications, management of site risk, sustainability considerations and schedule constraints.

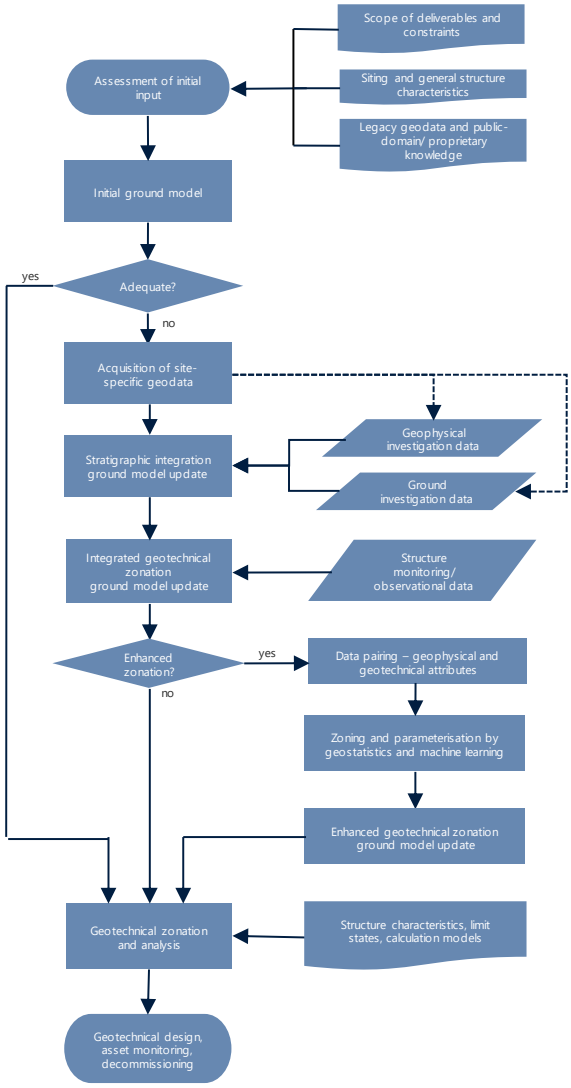

Figure 1: General procedure

Figure 1 includes terms of Table 1. The procedure item "enhanced zonation" is relatively novel to industry and ISO (2019b) recommends appropriate caution.

Visualisation of Ground Model

Diagrams, still images, video and 3-D visualisation can communicate and convey site characterisation to experts, users of the model, and the public at large.

For Integration Levels 2, 3 and 4 (Table 1), a common approach for data management and imaging is combining a GIS (geographical information system) with one or more separate software packages. SubsurfaceViewer software for 3-D voxel visualisation, IHS Markit® Kingdom software for geophysical data and GeODin® software for geotechnical data are examples of such software packages for nearshore and offshore projects.

Site Hazards

Types of Hazards, Risk and Mitigation

Site hazards may be grouped into:

- Natural geohazards;
- Man-made hazards.

Natural geohazards are commonly referred to as geohazards or geological hazards. They are about past geological processes and events that have shaped the seafloor and seabed. Some of these processes may still be active today. The resulting seafloor topography, and geological and geotechnical conditions within the seabed can be hazardous when installing offshore structures including infrastructure (e.g. Clayton and Power, 2002; IOGP, 2009, 2017; API, 2014a).

Man-made hazards include shipwrecks, fallen objects, seafloor debris and unexploded ordnance. Within the context of this document, man-made hazards exclude accidental events such as vessel impact, sabotage, well drilling problems, and fishing activities.

In relation to offshore activities, geohazards can be defined as local and/or regional site conditions and ground conditions having a potential of developing into a condition (e.g. irregular seafloor topography) or process (e.g. currents, submarine slides) that could cause loss of life or damage to health, environments and/or assets. The event-triggering sources can be ongoing geological processes or human induced changes (IOGP, 2009). Figure 2 presents a schematic overview of offshore geohazards.

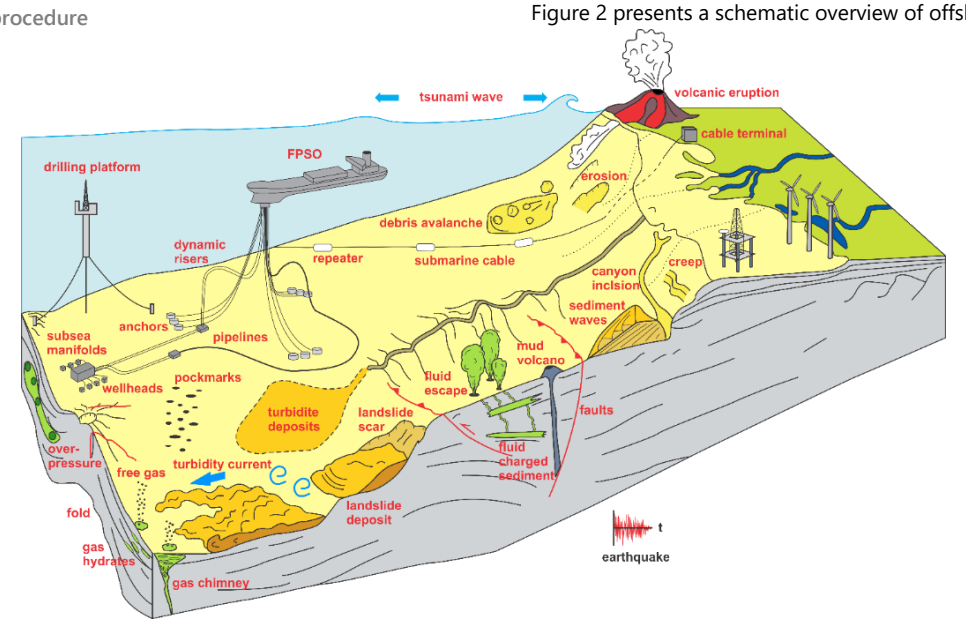

Figure 2: Offshore natural geohazards (modified after Campbell et al., 1986)

© Fugro 2014-2020

The damage potential of site hazards can range from, for example, local effects on pipelines and subsea structures to complete loss of all installations in a license areas and third party losses (IOGP, 2009).

The table below presents an overview of potential impacts and/or consequence associated with natural geohazards (and man-made hazards) occurring offshore.

Table 2: Potential Impact/Consequence Associated with Site Hazards

Impact/Consequence	Natural Geohazards and Man-made Hazards															
	Irregular Seafloor Topography	Seafloor Bedforms	Seafloor Outcrops and Hard Seafloor	Soil Liquefaction	Shallow Gas and Gassy Soils	Gas Hydrates	Gas and Fluid Seepage	Diapirs (e.g. Mud /Salt) and Mud Volcanoes	Earthquakes	Faults	Tsunamis	Slope Failure	Submarine Mass Movement	Wind, Waves and Currents	Seafloor Scour and Sediment Mobility	Man-Made Hazards
Uneven support (foundation instability)		x				x				x	x				x	
Loss of support (structural stresses)				x			x		x		x	x	x			
Spanning (pipeline and flowlines)	x	x	x							x						
Increased foundation settlements, reduced access				x	x											
Burial/embedment leading to additional loading and reduced access		x		x									x		x	
Reduced soil strength and bearing resistance				x	x		x									
Lateral loading of structure leading to overstressing of foundation/structure components									x		x	x	x	x		x
Structure displacement and structural damage				x					x	x	x	x	x			x
Increased potential for soil liquefaction					x	x	x		x		x			x		
Increased potential for shallow soil instability and submarine sliding					x	x	x	x	x		x			x	x	
Foundation and structure installation difficulties	x	x	x		x	x	x									x
Steel abrasion, gouging and denting; excessive wear of trenching equipment			x													
Gas and fluid migration (excess pore pressures)					x	x	x	x		x	x			x		
Corrosion of steel structures, pipelines, flowlines					x		x	x								
Well (borehole) instability					x	x	x			x						
Mud losses (well/borehole drilling)										x						
Damage to casing string and pile foundations										x						
Presence of environmentally protected chemosynthetic communities					x		x	x								
Explosions leading to changed site conditions																x

© Fugro 2014-2020

Site hazards can generally not be treated on a statistical basis applying solely historical data. The nature of a hazard is often site and time dependent. In addition, natural geohazards are often interrelated. This may be due to a common trigger mechanism (e.g. earthquake, slope failure), or that one geohazard occurrence or process forms a trigger for other geohazards.

For instance:

- Earthquakes will induce dynamic actions on a structure and may induce elevated pore pressures leading to increased susceptibility to soil liquefaction;
- Slope failures and their deposits may result in irregular seafloor topography;
- Mud and salt diapirs are commonly associated with radial fault patterns, and continuous diapirism may result in (shallow) slope failures.

Table 3 highlights some relations between natural geohazards.

Table 3: Related Offshore Natural Geohazards

	Irregular Seafloor Topography	Seafloor Bedforms	Seafloor Outcrops and Hard Seafloor	Soil Liquefaction	Shallow Gas and Gassy Soils	Gas Hydrates	Gas and Fluid Seepage	Diapirs (e.g. Mud /Salt) and Mud Volcanoes	Earthquakes	Faults	Tsunamis	Slope Failure	Submarine Mass Movement	Wind, Waves and Currents	Seafloor Scour and Sediment Mobility
Irregular Seafloor Topography		x	x							x		x	x	x	x
Seafloor Bedforms	x													x	x
Seafloor Outcrops and Hard Seafloor	x				x		x	x				x			x
Soil Liquefaction					x	x	x	x	x					x	
Shallow Gas and Gassy Soils			x	x		x	x	x		x		x	x		
Gas Hydrates				x	x		x					x	x		
Gas and Fluid Seepage			x	x	x	x		x		x		x	x		
Diapirs (e.g. Mud /Salt) and Mud Volcanoes			x	x	x		x			x		x			
Earthquakes				x						x	x	x	x		
Faults	x				x		x	x	x		x	x	x		
Tsunamis									x	x		x	x	x	x
Slope Failure	x		x		x	x	x	x	x	x	x		x	x	x
Submarine Mass Movement	x				x	x	x		x	x	x	x		x	x
Wind, Waves and Currents	x	x		x							x	x	x		x
Seafloor Scour and Sediment Mobility	x	x	x								x	x	x	x	

Assessment of hazard probability of occurrence and frequency can be based on geomechanical modelling taking into account uncertainty in modelling of site conditions, ground parameter values, ongoing geological processes, actions and applied analysis methods (Clayton and Power, 2002; IOGP, 2009).

The risk of a site hazard is the sum of the product of the probability of a hazard event affecting a structure and damage consequence. The damage consequence can depend on factors such as structure robustness and vulnerability. The information in this document covers the nature of hazards and their potential implications, not the risk. Power et al. (2005) and Galavazi et al. (2006) describe risk analysis methodology.

Risk mitigation can include avoidance (e.g. a certain standoff distance to avoid structure interaction) and design for robustness.

Irregular Seafloor

Seafloor morphology can be irregular as a result of past or present geological processes. Human activities can also affect the seafloor topography. Irregular seafloor may be caused by (or be associated with) a number of natural and man-made phenomena. These include:

- Canyons and channels;
- Boulders (e.g. drop stones);
- Spudcan footprints;
- Anchor scars;
- Trawl marks and ice gouging;
- Drill cuttings.

© Fugro 2014-2020

The scale of morphological features varies (e.g. scour marks, submarine canyons). The impact can differ per structure type and geometry.

Seabed Scour and Sediment Mobility

Seabed scour relates to the erosion of seabed sediments. Such erosion can occur under normal metocean conditions or can be enhanced as a result of a structure or multiple structures interrupting a natural flow regime above seafloor, thereby increasing flow velocities. Scour can be enhanced or initiated by secondary processes such as rocking of a structure.

Especially non-cohesive sandy (and silty) sediments are susceptible to scour. Erosion and transport of fine sand can start at a flow velocity in excess of 0.2 m/s. Local scour pits (or scour holes) can form shortly after installation of a structure. Their dimensions will usually vary in time depending on the flow regime.

Scour can occur in any water depth (from shoreline to deep sea). The flow regime due to wave- and tidal influence is generally stronger in shallow water than in deep water (Soulsby, 1997; Sumer and Fredsoe, 2002). In general, tide- and wave action, in combination with fluvial discharge of fresh water, determine the natural flow regime in coastal areas. Deepwater bottom current activity may result from density differences between water masses and from global thermohaline ocean circulation. Resulting sedimentary accumulations are known as contourite drifts (Faugeres et al., 1999).

Seafloor variation can usually be characterized as some combination of the following (Whitehouse, 1998):

- Local scour and sedimentation; usually a steep-sided scour pit around a structure or structural element;
- Global (or general) scour; a (shallow) scoured basin of large extent around a structure, possibly due to overall structure effects, multiple structure interaction, or wave-soil-structure interaction;
- Overall seabed movement; erosion, deposition, bedform migration that would also occur in the absence of a structure (i.e. regional scour).

Seafloor Bedforms

A seafloor bedform is a morphological feature formed by interaction of wave action and (tidal) currents and cohesionless sediment (i.e. sand/silt). Bedforms are typically found in sandy areas at a continental shelf.

A characteristic of bedforms is their mobility (Table 4). Sand waves tend to move slowly (metres per year) or flex their crests with (tidal) currents. Smaller-scale ripples tend to be more mobile, in the order of metres per day.

Table 4: Seafloor Bedforms

Bedform Type	Related Flow	Wavelength [m]	Amplitude [m]	Time-scale	Migration Rate	Source
Ripple	Instant flow	0.1 to 1	0.01 to 0.1	Hours	> 1 m/day	2, 3, 4
Megaripple	Storm surges	10 to 20	0.1 to 1.5	Days	100 m/year	1, 3
Sand wave	Tidal currents	50 to 1000	2 to 18	Decades	1 m/year to 10 m/year	1, 2, 3, 4
Long bed wave	Unknown	1500 to 2500	1 to 5	Unknown	Unknown	2, 3, 4
Sand bank	Tidal currents	5000 to 10000	5 to 50	Centuries	m/year	2, 3, 4

1. Ashley (1990)
2. Dodd et al. (2003)
3. Morelissen et al. (2013)
4. Reineck and Singh (1980)

For structure design it is important to know which part of the seabed and/or the bedforms is actually mobile. For example, cable trenching can modify bedforms. The rate at which the bedforms recover after cable trenching will depend on sediment transport rate and supply of sediment.

Seafloor Outcrops and Hard Seafloor

Seafloor outcrops and hard seafloor ground conditions commonly include:

- Shell and coral banks, reefs, which are common in shallow waters in the tropical zones;
- Local patches of cemented soil (e.g. hard ground, cap rock). Examples are authigenic carbonates around pockmarks, Kurkar ridges (cemented aeolian dunes) in the eastern Mediterranean Sea, beach rocks (cemented beach sediments) in the Caribbean Sea, sabkha deposits (evaporitic-tidal floodplain deposits) in the Arabian/Persian Gulf and Gulf of Suez;
- Crust composed of precipitated metal sulphides associated with hydrothermal activity (e.g. black and white smokers) in vicinity of tectonic plate boundaries and faults;
- Outcrops of rock. Examples are pre-Quaternary sand- and limestone beds offshore West Africa, sedimentary and metamorphic rocks exposed in the Irish Sea.

It should be noted that seafloor outcrops and hard seafloor may have environmental protection status or legislative implications.

Cementation of soil may result from sub-marine cementation processes. Cementation may also have resulted from past sub-aerial exposure of a continental shelf during low sea level stands under arid climate conditions. Cementation generally occurs in carbonate-rich and hyper-saline environments.

Diapirs and Mud Volcanoes

A diapir is a domal upwelling of sediment, rock or salt that forms in response to tectonic forces, density differences, and high overburden pressures. Diapirs can pierce through a stratigraphic overburden and create an envelope of overconsolidated soils, deformed rock, and sediments around a diaper core (e.g. salt). Generally, a circular dome-shaped topographic feature develops when a diapir approaches the seafloor. Diapirs are commonly associated with radial faulting patterns and locally increased seafloor slopes.

Salt diapirs are known to be present in, for example, the Gulf of Mexico, offshore Brazil and West Africa, and the North Sea.

Mud diapirs and mud volcanoes are usually associated with rapidly-deposited sediments and in situ pore pressure conditions

© Fugro 2014-2020

significantly higher than hydrostatic (overpressured). Additionally, high vertical and horizontal stresses typically apply, caused by faulting, folding and uplift processes.

Mud diapirs and mud volcanoes occur mostly in (historic) delta areas: Nile Delta (offshore Egypt), Absheron Ridge (offshore Azerbaijan, Caspian Sea), Makran Ridge (offshore Iran, Arabian Sea), and Niger Delta (offshore Nigeria).

Release of pressure is commonly provided by faults and folding of the strata. Sediments mixed with over-pressured fluid and gas (mud) migrate upward through the stratigraphic overburden in vertical columnar zones (diapirs). Usually the over-pressured muds enter fault planes, thus causing diapirism along faults. A mud volcano can form when a mud diapir breaks the seafloor.

In general, mud volcanoes are conical, as tall as 65 m and up to 2 km across. The size and shape of a mud volcano depends on the frequency of expulsion and the type of material ejected. This can be unconsolidated soils, overconsolidated material, fractured rock (e.g. breccia), oil, gas, and water (Snead, 1972; Newton et al., 1980; Delisle et al., 2002; Delisle, 2004; Delisle, 2005). Not all offshore mud volcanoes are active. Eruptions are believed to be episodic.

Shallow Gas and Gassy Soils

Gas may be present (trapped) in the seabed (e.g. gassy soils). Shallow gas can comprise a mixture of different gases, such as carbon dioxide, hydrogen sulphide, ethane, and methane. In general, the gases originate from bacterial decay of organic matter (biogenic gases) within a few metres of the seafloor. Gas may also come from sources much deeper in the stratigraphy and migrates upwards through pores and cracks in the soil and rock (petrogenic gases).

Shallow gas may be present dissolved in pore water, as free gas in gas-filled voids or bubbles, and as gas hydrates. Over time, gas in soil may increase the in situ pore pressures and result in excess pore pressures.

Migration of gas in soil can result in accumulation of gas in the seabed below a foundation. Shallow gas in the pore water can have a serious effect on foundation behaviour.

In addition, shallow gas can be toxic to humans, can combust and explode.

Soil property measurements on geotechnical samples containing shallow gas may not be representative of in situ properties.

Gas Hydrates

Gas hydrates are ice-like crystalline solids composed of water molecules surrounding a molecule of gas, generally methane. Gas hydrates can only form when gas is over-saturated in water. Gas hydrates are stable under high pressure and low temperature conditions, and may be present at seafloor and in shallow sediments, generally in deep water environments in excess of 500 m below Mean Sea Level (Rastogi et al., 1999; Von Rad et al., 2000).

Stable gas hydrate acts as cement and increases strength and rigidity of soil.

Natural gas hydrates are regarded as a geohazard when they dissociate, start 'melting'. Both water and gas are released into soil when gas hydrates dissociate. This can result in formation of 'gassy soils'. The addition of water and gas may decrease soil strength and form a weak layer (Orange and Breen, 1992; Judd and Hovland, 2007). Gas hydrate dissociation may be initiated by human activities, e.g. flow of 'hot' hydrocarbons through well production casings, pipelines and flowlines.

Gas hydrates may form as a result of human activity. Gas hydrates can be a by-product of hydrocarbon production, forming hydrate plugs in the wellbore, around leaking joints and in pipelines. If a deep water exploration or production well is leaking, gas introduced into the shallow soils may react with water molecules to form hydrate layers or nodules.

Gas and Fluid Seepage

Gas and fluid seepage at seafloor is commonly associated with pockmarks. Pockmarks are roughly circular or conical depressions in the seafloor, generally 1 m to 350 m wide and up to 35 m deep (Newton et al., 1980; Von Rad et al., 2000; Judd and Hovland, 2007).

Pockmarks form by disruption of a pore pressure environment. This disruption may be triggered by natural or human causes, and can form on time scales of less than a year. Pockmarks can be intermittently active over long periods of time or can grow with explosive eruption events. The sediments in a pockmark are generally variable and may be overconsolidated.

When gas seeps continue over a long period of time, biological processes may cause cementation of the seabed sediments. Formation of authigenic carbonates can take place around the seeps (Judd and Hovland, 2007; Ding, 2008). In some cases, unique ecological habitats form in and around pockmarks. Such habitats may be protected by environmental legislation.

Authigenic carbonates may form thin crusts of weakly cemented sediments (hard grounds). They can be continuous over distances of several hundreds of metres (Von Rad et al., 2000). Locally more massive, competent layers of authigenic carbonates can be present as hard cemented layers or 'lenses'. They may form large build-ups and seafloor mounts (Judd and Hovland, 2007).

Apart from natural seeps, gas seepage may also be induced by drilling activities (e.g. geotechnical drilling, hydrocarbon exploration drilling). The drilling process may cause fracturing of soil and rock, when drilling mud pressures exceed the fracture pressure of the soil or rock (i.e. hydraulic fracturing). These fractures may form pathways for fluid and gas migration into the wellbore and up to seafloor. A wellbore or leaking well casing may form a pathway to the surrounding rock and soil formations, introducing gas into sand layers in the shallow subsurface. Overtime, the introduced gas may affect the geotechnical properties of a soil and have serious effects on foundation behaviour.

Drilling-induced fluid flows (e.g. shallow water flows) occur when a pressurised sand body (aquifer) encapsulated in clay is penetrated by the drilling process. Shallow water flows are common offshore large river deltas, such as the Mississippi Delta (Gulf of Mexico) and the Nile Delta (offshore Egypt). The sand bodies are commonly derived from sediment deposition out of turbidity currents.

Earthquakes

An earthquake, or seismic event, occurs after stresses in the earth's crust that have gradually built up, are suddenly released by movements along a fault. The movement generates seismic waves which propagate away from the earthquake epicentre. Most earthquakes occur along tectonic plate boundaries.

The location, magnitude, and frequency (recurrence) of earthquakes cannot be reliably predicted. The probability of

© Fugro 2014-2020

seismic events can be assessed on the basis of historic records of earthquake activity.

Seismic impact depends on geotechnical conditions at the site and structure design. Seismic activity may induce faulting, soil liquefaction, slope failure, and tsunamis.

Soil Liquefaction

Two types of liquefaction may be distinguished:

- Gravitational (sometimes called static- or flow-) liquefaction, usually occurring in submerged slopes;
- Cyclic liquefaction, usually generated through strong cyclic forces.

Soil liquefaction or cyclic mobility represents a decrease of soil strength and stiffness caused by an increase in pore water pressure in saturated soil. Soil liquefaction usually occurs in response to sudden change in stress condition, causing it to behave like a liquid. Examples of cyclic and dynamic actions include earthquake shaking, storm wave loading, structure displacements upon cyclic load application, pile installation by driving, and vortex vibrations due to fluid flow around a structure.

Liquefaction potential can be significant for loose cohesionless soils present close to ground surface (seafloor) and below the water table. Dense sands, loose unsaturated sands, and some sensitive cohesive materials can also liquefy under some conditions. In addition, the presence of gas in loose sands can change soil behaviour and may potentially cause liquefaction (Grozic, 2003).

Faults

A fault is a planar fracture or discontinuity in a volume of soil or rock along which significant vertical and/or horizontal displacement has occurred (Figure 3) (i.e. faulting). Fault zones are areas where multiple fractures and faults occur in close proximity, with similar moment direction.

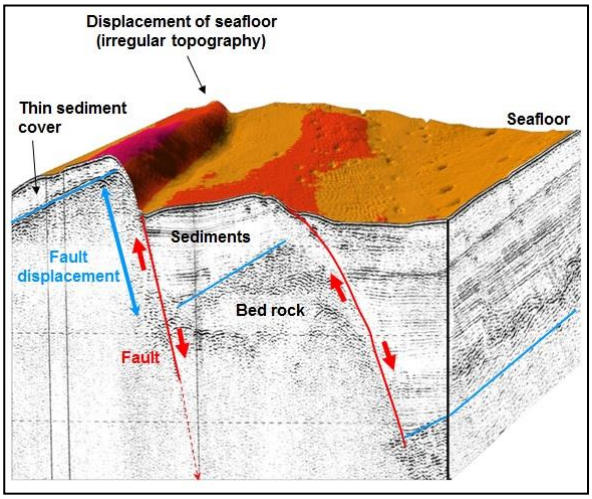

Figure 3: Surface and subsurface expression of fault displacement

Faults can be associated with:

- Tectonic activity (e.g. at tectonic plate boundaries, earthquake zones);
- Laterally variable soil subsidence and compaction;
- Soil contractions (e.g. polygonal faulting in North Sea and West African seabed sediments);
- Diapirism (e.g. radial faulting);
- Slope failure (e.g. headwall scarp, failure planes, tension cracks).

Movement along the fault plane (and hence soil displacement) is a semi-continuous process acting on time scales ranging from years to millions of years. Faults are commonly considered to be inactive if there has been no observed movement or evidence of seismic activity during the last 10,000 years. In this case a fault can be covered by a uniform layer of soil (i.e. without a clear discontinuity surface being present). Depending on crustal stresses and changes therein, apparently inactive faults may be reactivated causing further soil displacements and even seismic events.

Faults may result in a displaced, stepped seafloor and/ or irregular linear topographic features on the seafloor (e.g., headwall scarps). In addition, stratigraphic sequences are displaced in the seabed.

Deep-seated faults, with lengths of hundreds to thousands of metres, may be associated with earthquakes. The build-up of stresses due to differential movement in the earth's crust may be released along these deep-seated faults, whereby large amounts of energy move through rock and soils in the form of pressure waves and shear waves. These deep-seated, earthquake-generating faults are sometimes referred to as seismic faults.

Tsunamis

A tsunami (or surge wave) is a series of ocean waves of long wave lengths which are created when a large volume of water is suddenly displaced by a submarine earthquake, landslide, or volcanic eruption (Figure 4). In the open ocean, tsunami waves travel at high speeds (in excess of 800 km/h) with heights of, say, less than 0.05 m. As they approach the coast the velocity decreases (to approximately 50 km/h) and the wave height increases up to several metres or tens of metres. At the coastline, the force of a tsunami wave can cause loss of life, damage to buildings and infrastructure, large scale erosion (scour) and flooding of low-lying areas.

© Fugro 2014-2020

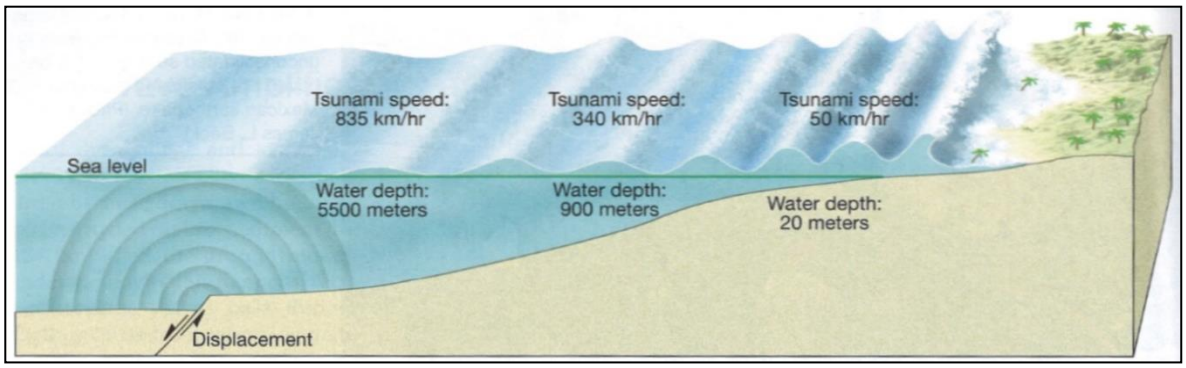

Figure 4: Tsunami generated by fault displacement offshore

Slope Failure

Slope failure occurs when downslope driving forces acting on seabed exceed resistance. In general, slope failure results in the down-slope movement of a soil mass (see section titled 'Submarine Mass Movements'). Slopes may be unstable at any water depth.

Slopes may develop due to tectonics, high sedimentation rates, or incision and erosion by seafloor currents and flows.

Slope failure can be triggered by earthquakes, strong currents, storms (wave actions), tsunamis, volcanism, and human activity (Hampton et al., 1996; Mulder and Cochonat, 1996; Locat and Lee, 2005; Judd and Hovland, 2007; Rogers and Goodbred, 2010).

Usually a combination of two or more factors influences slope failure, e.g. presence of shallow gas and an earthquake (Orange and Breen, 1992; Judd and Hovland, 2007). Slopes can be unstable due to low shear strength and overpressured strata (e.g. shallow gas). Seabed may fail on slight slopes as little as 0.5˚ (Hampton et al., 1996; Judd and Hovland, 2007).

Failure scarps and oversteepened slopes are commonly associated with past slope failures. Past slope failures may be reactivated if a trigger (e.g. pore pressure build-up, earthquake) is present. The seafloor morphology resulting from a slope failure may be irregular and undulating (see section titled 'Irregular Seafloor Topography').

Submarine Mass Movements

A submarine mass movement is a displacement of seabed material driven directly by gravity or other body forces, rather than stresses associated with fluid flow. The deposits of submarine mass movements are commonly referred to as mass transport deposits (MTD).

Submarine mass movements commonly follow from slope failures and include the following processes (Figure 5) (Lee et al., 2007):

- Slides:
  - Translational slide
  - Rotational slide
- Mass flows:
  - Debris flow
  - Debris avalanche
  - Mud flow
  - Liquefaction flow
  - Turbidity current

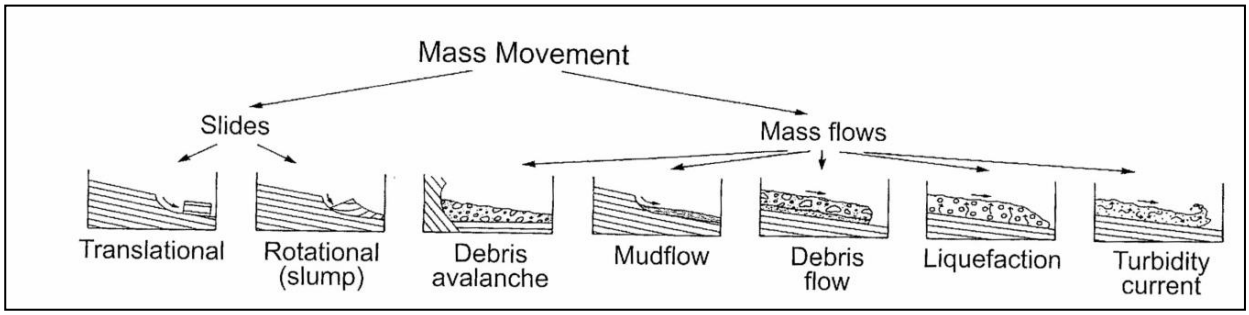

Figure 5: Submarine mass movement classification (after Lee et al., 2007)

Slides are movements of essentially rigid, undeformed masses along discrete failure/slip planes. If slip occurs along a planar surface the slide is referred to as a translational slide. If slip occurs along a curved failure plane and the rigid mass shows rotation, the slide is referred to as rotational.

If moving sediments take a form of viscous fluid, the feature is referred to as mass flow or gravity flow. Mass flow deposits show considerable internal deformation with many invisible or short-lived internal slip surfaces. Submarine slides can become mass flows as the failed material progressively disintegrates, gets entrained with surrounding water and moves downslope.

Debris flows are mass flows in which sediments are heterogeneous and may include larger clasts supported by a fine-grained soil matrix. Mud flows involve predominantly fine-grained (mud) sediments. Turbidity currents involve downslope transport of a relatively dilute suspension of sediment grains that are supported by an upward component of fluid turbulence. Turbidity currents often evolve from disintegration and dilution of debris and mud flows. Liquefaction flows occur when loosely packed sandy sediments collapse under environmental conditions (e.g. cyclic actions by waves or earthquakes; see section titled Soil Liquefaction. Debris avalanches occur where slides collapse and disintegrate into smaller pieces. They move rapidly without following pre-existing channels or valleys.

The potential impact of submarine mass movements on a structure depends upon the location or orientation of the structure in relation to the movement direction (Figure 6).

© Fugro 2014-2020

Mass Movement Mechanism	Profile View	Plan View	Impact		
			Structure	Pipeline / Flowline / Cable	
				Orientation of mass movement	
				Parallel	Perpendicular
Creep	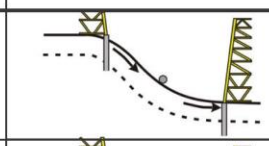	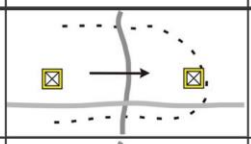	Rotation About Base	Dragging Rupture Spanning	Dragging Rupture Spanning
Translational Slide	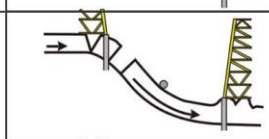	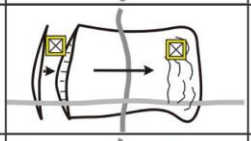	Translation Downdrag at Crest Uplift at Toe	Stretching at Crest Compression at Toe Loss of Support Rupture Spanning	Dragging Loss of Support Rupture Spanning
Rotational Slide	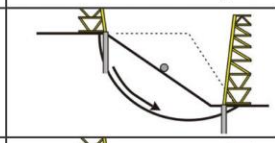	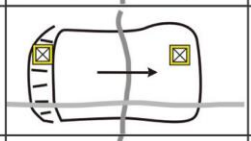	Rotation About Top Downdrag at Crest Uplift at Toe	Stretching at Crest and Toe Loss of Support Rupture Spanning	Dragging Loss of Support Rupture Spanning
Debris Avalanche	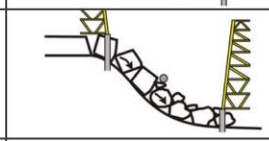	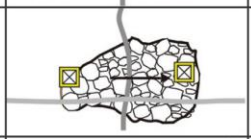	Translation/Rotation +/- Downdrag +/- Uplift	Compression and Stretching Loss of Support Rupture Spanning, Burial	Dragging Loss of Support Rupture Spanning Burial
Debris Flow	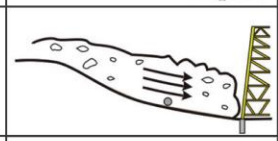	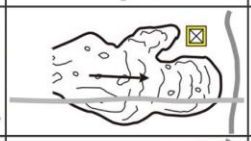	Loading Burial Scour	Compression Burial Loading Scour	Dragging Burial Loading Scour
Liquefied Flow		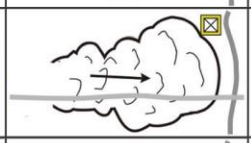	Loading Burial Scour	Compression Burial Loading Scour	Dragging Burial Loading Scour
Fluidised Flow	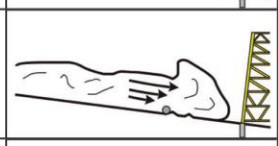	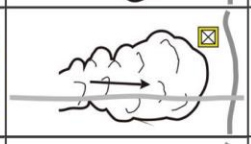	Loading Burial Scour	Compression Burial Loading Scour	Dragging Burial Loading Scour
High Density Turbidity Current	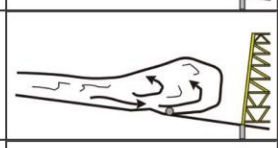	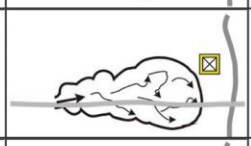	Loading? Burial? Scour	Burial Loading Scour	Burial Loading Scour
Low Density Turbidity Current	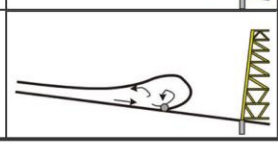		Scour?	Scour	Scour

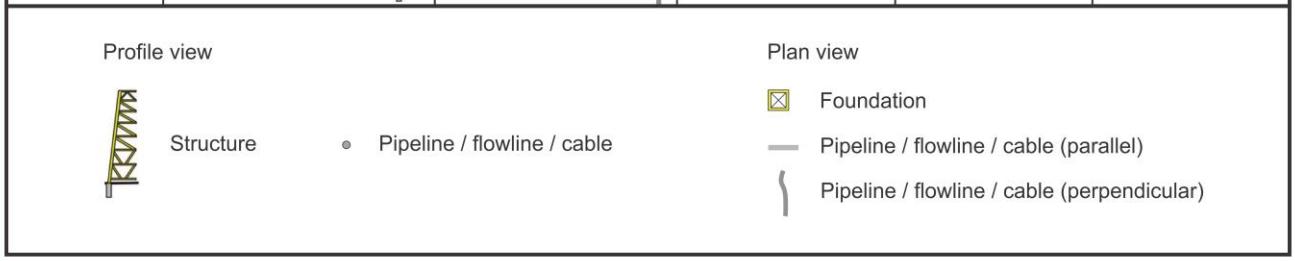

Figure 6: Potential impacts of submarine mass movements on platform foundation and pipeline (modified after Thomas et al., 2009)

Wind, Waves and Currents

Periods of extreme weather conditions, such as (tropical) storms, monsoons, peak wind, waves, and current regimes can cause lateral and cyclic actions on the seafloor and any seabed-supported structure. In addition, adverse weather conditions may complicate structure installation activities.

Peak wave and (seafloor/bottom) current regimes can also cause changes in seafloor conditions due to scour and burial (i.e. sediment remobilisation), winnowing of seafloor sediments (i.e. removal of fine/clay-size materials) and development of irregular seafloor topography.

© Fugro 2014-2020

Tidal variation and atmospheric pressure fluctuations as a result of storms are known to change pore pressure conditions in the seabed, potentially creating circumstances leading to soil failure and liquefaction.

Estimation of environmental actions is relatively inaccurate. It normally involves statistical data for a specific geographic region and various procedures for modelling the interaction of a structure and its environment.

Man-Made Hazards

Human activities and anthropogenic (i.e. man-made/man-induced) features, debris, or obstructions can have an adverse effect on an offshore structure.

Seafloor features and objects have been left by human activities since the dawn of mankind. Shipwrecks can form archaeological sites, war graves, enhance ecological diversity, and may be restricted areas.

In addition, offshore energy activities such as drilling, (jack-up) platform installation and decommissioning and resulting footprints may alter seafloor topography and/or potentially alter seabed conditions (e.g. drill spoils, gas charging as a result of gas migration along exploration wells).

Commonly encountered man-made hazards include:

- Unexploded ordnance (UXO);
- Existing energy facilities (e.g. fixed platforms, pipelines, manifolds, wellheads, power cables etc.);
- Telecommunication cables;
- Shipwrecks;
- Fallen objects (e.g. shipping containers).

These hazards can complicate structure installation and design if not identified at an early stage.

Activities such as hydrocarbon extraction and deep salt mining can change site conditions, for example causing regional subsidence of the seabed and/or trigger fault activity (Barton et al., 1987; Broughton et al., 1998; Broughton et al., 1997, Gebara et al., 2000). Subsidence can range from millimetres to tens of metres. It typically depends on reservoir size, mechanical properties of reservoir and overlying ground, reservoir depth, production rate, pressure drawdown, and duration.

References

American Petroleum Institute [API] (2014a). Geotechnical and foundation design considerations: ISO 19901-4:2003 (modified), petroleum and natural gas industries-specific requirements for offshore structures, part 4-geotechnical and foundation design considerations: addendum 1. (ANSI/API RP 2GEO First Edition, with Addendum) https://www.apiwebstore.org/publications/item.cgi?b6c6e7f5-6da7-46c2-97bb-54bd470f0401.

American Petroleum Institute [API] (2015). *Design, construction, operation, and maintenance of offshore hydrocarbon pipelines (limit state design* (API RP 1111 5th Edition). https://www.apiwebstore.org/publications/item.cgi?3fb25780-bd91-43e0-8959-e064621d198f.

American Petroleum Institute [API] (2014b). *Planning, designing and constructing fixed offshore platforms - working stress design.* (API RP 2A-WSD, 22nd Edition) https://www.apiwebstore.org/publications/item.cgi?b9e32dec-268b-404d-988e-5cda65c27757I.

Ashley, G.M. (1990). Classification of large-scale subaqueous bedforms: a new look at an old problem [research symposium]. *Journal of Sedimentary Petrology*, *60*(1) 160-172 https://doi.org/10.2110/jsr.60.160.

ASTM International (2018)., *Standard guide to site characterization for engineering, design, and construction purposes* (ASTM D420-18). https://www.astm.org/Standards/D420.htm.

Barton, N., Hårvik, L., Christianson, M., Bandis, S.C., Makurat, A., Chryssanthakis, P. & Vik, G. (1987). Rock mechanics modelling of the Ekofisk reservoir subsidence. *Proceedings of the 27th symposium on rock mechanics, Alabama, 1986* (pp. 267-274)

Broughton, P., Aldridge, T.R. & Komaromy, S. (1998). Steel jacket structures for the new Ekofisk complex in the North Sea. *Proceedings of the Institution of Civil Engineers. Civil Engineering*, *126*(2), 54-64. https://doi.org/10.1680/icien.1998.30433

Broughton, P., Aldridge, T.R. & Nagel, N.B. (1997). Geotechnical aspects of subsidence related to the foundation design of Ekofisk platforms. *Proceedings of the Institution of Civil Engineers. Geotechnical Engineering*, *125*(3) 129-140. https://doi.org/10.1680/igeng.1997.29464

Campbell, K.J., Hooper, J.R. & Prior, D.B. (1986). Engineering implications of deepwater geologic and soil conditions, Texas-Louisiana slope. In *Eighteenth annual offshore technology conference, May 5-8, 1986, Houston, Texas: Proceedings, 1, OTC Paper 5105* (pp. 225-232) https://doi.org/10.4043/5105-MS

Clayton, C. & Power, P. (2002). Managing geotechnical risk in deepwater. In M. Cook et al. (eds.) *Offshore site investigation and geotechnics: diversity and sustainability: proceedings of an international conference, 26–28 november 2002* (pp. 425-443). Society for Underwater Technology.

Delisle, G. (2004). The mud volcanoes of Pakistan. *Environmental Geology*, *46*(8) 1024-1029. https://doi.org/10.1007/s00254-004-1089-x

Delisle, G. (2005). Mud volcanoes of Pakistan — an overview: a report on three centuries of historic and recent investigations in Pakistan. In G. Martinelli & B. Panahi (eds.) *Mud volcanoes, geodynamics and seismicity* (pp. 159-169). Springer.

Delisle, G., Von Rad, U., Andruleit, H., Von Daniels, C.H., Tabrez, A.R. & Inam, A. (2002). Active mud volcanoes on- and offshore eastern Makran, Pakistan. *International Journal of Earth Sciences*, *91*(1) 93-110. https://doi.org/10.1007/s005310100203

Ding, F. (2008). *Near-surface sediment structures at cold seeps and their physical control on seepage: a geophysical and geological study in the Southern Gulf of Mexico and at the frontal makran accretionary prism/Pakistan*. [Dissertation] Universität Bremen.

DNV GL AS (2017, August). *Offshore soil mechanics and geotechnical engineering*. *Recommended practice* (DNVGL-RP-C212). https://standards.globalspec.com/std/10183661/DNVGL-RP-C212.

Dodd, N., Blondeaux, P., Calvete, D., De Swart, H.E., Falqués, A., Hulscher, S.J.M.H., Rózynski, G. & Vittori, G. (2003). Understanding coastal morphodynamics using stability methods. *Journal of Coastal Research*, *19*(4) 849-865.

European Committee for Standardization (2009). *Eurocode 7: geotechnical design - part 1: general rules (with corrigendum EN 1997-1:2004/AC, February 2009)* (EN 1997-1:2004). https://standards.cen.eu/dyn/www/f?p=204:110:0::::FSP_PROJECT,FSP_ORG_ID:12442,6231&cs=1D03CC06CB9166EAAA1C6CE997CDA87C2.

© Fugro 2014-2020

European Committee for Standardization (2015). *Petroleum and natural gas industries - pipeline transportation systems ISO 13623:2009 modified)* (EN 14161+A1:2015) https://standards.cen.eu/dyn/www/f?p=204:110:0::::FSP_PROJECT,FSP_ORG_ID:60145,5996&cs=1CB24029A869268F9A5290800D2D8C0A6.

Evans, T.G. (2010). A systematic approach to offshore engineering for multiple-project developments in geohazardous areas. In S. Gourvenec & D. White (Eds.), *Frontiers in offshore geotechnics II: proceedings of the 2nd international symposium on frontiers in offshore geotechnics*, *Perth, Australia, 8-10 November 2010* (pp. 3-32). CRC Press.

Faugères, J.-C., Stow, D.A.V., Imbert, P. & Viana, A. (1999). Seismic features diagnostic of contourite drifts. *Marine Geology*, *162*(1) 1-38. https://doi.org/10.1016/S0025-3227(99)00068-7

Galavazi, M., Moore, R., Lee, M., Brunsden, D. & Austin, B. (2006). Quantifying the impact of deepwater geohazards. In *2006 Offshore technology conference, 1-4 May, Houston, OTC Paper 18083*. https://doi.org/10.4043/18083-MS

Gebara, J.M., Dolan, D., Pawsey, S., Jeanjean, P. & Dahl-Stamnes, K.H. (2000). Assessment of offshore platforms under subsidence—part I: approach. *Journal of Offshore Mechanics and Arctic Engineering*, *122*(4) 260-266. https://doi.org/10.1115/1.1313530

Grozic, J.L.H. (2003). Liquefaction potential of gassy marine sands. In J. Locat & J. Mienert (eds.), *Submarine mass movements and their consequences* (pp. 37-45). Kluwer Academic Publishers.

Hampton, M.A., Lee, H.J. & Locat, J. (1996). Submarine landslides. *Review of Geophysics, 34*(1), 33-59. https://doi.org/10.1029/95RG03287.

International Association of Oil and Gas Producers (2009). *Geohazards from seafloor instability and mass flow.* (IOGP Report No. 425) IOGP.

International Association of Oil and Gas Producers (2017). *Guidelines for the conduct of offshore drilling hazard site surveys* (Version 2.0). (IOGP Report No. 373-18-1) IOGP.

International Organization for Standardization (2014). *Petroleum and natural gas industries – specific requirements for offshore structures – part 8: marine soil investigations* (ISO 19901-8:2014). https://www.iso.org/standard/61145.html.

International Organization for Standardization (2016a). *Petroleum and natural gas industries – specific requirements for offshore structures – part 4: geotechnical and foundation design considerations* (ISO 19901-4:2016). https://www.iso.org/standard/61144.html.

International Organization for Standardization (2016b). *Petroleum and natural gas industries – specific requirements for offshore structures – part 1: jack-ups* (ISO 19905-1:2016). https://www.iso.org/standard/68135.html.

International Organization for Standardization (2017). *Petroleum and natural gas industries - pipeline transportation systems*(ISO 13623:2017). https://www.iso.org/standard/61251.html

International Organization for Standardization (2019a). *Petroleum and natural gas industries – general requirements for offshore structures* (ISO 19900-2019). https://www.iso.org/standard/69761.html.

International Organization for Standardization (2019b). *Petroleum and natural gas industries - specific requirements for offshore structures – part 10: marine geophysical investigations* (ISO/DIS 19901-10:2019). https://www.iso.org/standard/77017.html.

Judd, A.G. & Hovland, M. (2007). Seabed fluid flow: the impact on geology, biology, and the marine environment. Cambridge University Press.

Lee, H.J., Locat, J., Desgagnés, P., Parsons, J.D., McAdoo, B.G., Orange, D.L., Puig, P., Wong, F.L., Dartnell, P. & Boulanger, E. (2007). Submarine mass movements on continental margins. In C.A. Nittrouer et al. (eds.) Continental margin sedimentation: from sediment transport to sequence stratigraphy (pp. 213-274). (Special Publication of the International Association of Sedimentologists, No. 37) Blackwell

Locat, J. & Lee, H.L. (2005). Subaqueous debris flows. In M. Jakob & O. Hungr (eds.), Debris-flow hazards and related phenomena (pp. 203-245). Springer-Verlag.

Morelissen, R., Hulscher, S., Knaapen, M.A.F., Németh, A.A. & Bijker, R. (2003). Mathematical modelling of sand wave migration and the interaction with pipelines. Coastal Engineering, 48(3) 197-209. https://doi.org/10.1016/S0378-3839(03)00028-0

Mulder, T. & Cochonat, P. (1996). Classification of offshore mass movements. Journal of Sedimentary Research, 66(1), 43-57. https://doi.org/10.1306/D42682AC-2B26-11D7-8648000102C1865D

Newton, R.S., Cunningham, R.C. & Schubert, C.E. (1980). Mud volcanoes and pockmarks: seafloor engineering hazards or geological curiosities? In Twelfth annual offshore technology conference, May 5-8, Houston, Texas: proceedings, 1, OTC Paper 3729 (pp. 425-429) https://doi.org/10.4043/3729-MS

Parker, E.J., Traverso, C., Moore, R., Evans, T. & Usher, N. (2008). Evaluation of landslide impact on deepwater submarine pipelines. OTC.08: proceedings 2008 offshore technology conference, 8 May, Houston, Texas, USA, OTC Paper 19459. https://doi.org/10.4043/19459-MS

Peuchen, J. (2012). Site characterization in nearshore and offshore geotechnical projects. In R.Q. Coutinho & P.W. Mayne (eds.) Geotechnical and geophysical site characterization 4: proceedings of the fourth international conference on site characterization ISC-4, Porto de Galinhas-Pernambuco, Brazil, 17-21 September 2012, volume I (pp. 83-111). CRC Press.

Power, P., Galavazi, M. & Wood, G. (2005). Geohazards need not be: redefining project risk. In Offshore technology conference, 2-5 May 2005, Houston, Texas, U.S.A., OTC Paper 17634. https://doi.org/10.4043/17634-MS.

Rastogi, A., Deka, B., Budhiraja, I.L. & Agarwal, G.C. (1999). Possibility of large deposits of gas hydrates in deeper waters of India. Marine Georesources & Geotechnology, 17(1), 49-63. https://doi.org/10.1080/106411999274007.

Reineck, H.-E. & Singh, I.B. (1980). *Depositional sedimentary environments* (2nd ed.). Springer.

Renewable UK (2013). Guidelines for the selection and operation of jack-ups in the marine renewable energy industry: version 2: full technical and regulatory update. RenewableUK.

Rogers, K.G. & Goodbred, S.L. (2010). Mass failures associated with the passage of a large tropical cyclone over the swatch of no ground submarine canyon bay of Bengal. Geology, 38(11) 1051-1054. https://doi.org/10.1130/G31181.1.

Skipp, B.O. & Mallard, D.J. (1995). Site investigations with earthquakes in mind. In A.S. Elnashai (ed.) European seismic design practice: research and application: proceedings of the

© Fugro 2014-2020

fifth SECED conference on european seismic design practice, Chester, United Kingdom, 26-27 October 1995 (pp. 151-161). Balkema.

Snead, R.E. (1972). Mud volcanoes of the Makran Coast. Explorers Journal, 50(1) 22-28.

Soulsby, R. (1997). Dynamics of marine sands: a manual for practical applications. Thomas Telford.

Sumer, B.M. & Fredsøe, J. (2002). The mechanics of scour in the marine environment. World Scientific.

Thomas, S., Hooper, J.R. & Clare, M. (2009). Constraining geohazards to the past: impact assessment of submarine mass movements on seabed developments. In D.C. Mosher et al. (eds.), Submarine mass movements and their consequences: 4th international symposium (pp. 387-398). Springer.

Von Rad, U., Berner, U., Delisle, G., Doose-Rolinksi, H., Fechner, N., Linke, P., Lückge, A., Roeser, H.A., Schmaljohann, R., Wiedicke, M. & SONNE 122/130 Scientific Parties (2000). Gas and fluid venting at the Makran accretionary wedge off Pakistan. Geo-Marine Letters, 20(1) 10-19. https://doi.org/10.1007/s003670000033

Wells, D.L. & Coppersmith, K.J. (1994). New empirical relationships among magnitude, rupture length, rupture width, rupture area, and surface displacement. Bulletin of the Seismological Society of America, 84(4), 974-1002.

Whitehouse, R. (1998). Scour at marine structures: a manual for practical applications. Thomas Telford.

Yuan, F., Wang, L., Guo, Z. & Shi, R. (2012). A refined analytical model for landslide or debris flow impact on pipelines. part I: surface pipelines. *Applied Ocean Research*, *35*, 95-104. https://doi.org/10.1016/j.apor.2011.12.001.

© Fugro 2014-2020

Positioning Survey and Depth Measurement

Introduction

This document describes survey of horizontal and elevation/depth reference points for geotechnical and/or environmental data acquisition in a marine environment.

National and international standards for geotechnical and/or environmental data acquisition (as ASTM, BSI, CEN and ISO) require such surveys. This document summarises common practice.

Procedure

The procedure for positioning survey and depth measurement depends on the agreed project specifications. For example, water level correction and subsurface positioning may not be part of the activities agreed upon. Some or all of the following steps can apply:

- definition of the type of survey and the target location;
- set-up and initial checks of the survey system and depth measurement system;
- surface positioning survey of the reference point, i.e. the determination of grid coordinates;
- subsurface positioning survey, i.e. adjustment of the surface positioning results for underwater offset;
- measurement of the water depth;
- estimation of depth below water level for a data point applicable to the water column;
- estimation of depth below seafloor for a data point applicable to the seabed;
- calculation of elevation of seafloor relative to a vertical datum, e.g. water level correction;
- calculation of elevation of a data point relative to a vertical datum.

This document uses the terms seafloor and seabed. Seafloor is the underwater ground surface, i.e. the plane separating water and ground (soil, rock, made ground). The seabed is the ground below seafloor.

IHO Classification for Horizontal Positioning and Water Depth

Positioning surveys require specific systems and procedures, such as those summarised below for marine applications. The International Hydrographic Organization (IHO, 2019) defines four orders of hydrographic survey (Table 1). The term "depth" refers here to water depth, i.e. the vertical distance between water level and seafloor and referenced to a vertical datum such as Lowest Astronomical Tide LAT. Note that a water level such as LAT depends on the calculation model used for determining the vertical datum.

Table 1: Summary of IHO Classification

Parameter Order	IHO Order			
	2	1b	1a	Special
Area description	Areas where a general description of the seafloor is considered adequate	Areas where under-keel clearance is not considered to be an issue for the type of surface shipping expected to transit the area	Areas where underkeel clearance is less critical but features of concern to surface shipping may exist	Areas where under-keel clearance is critical
Depth – total horizontal uncertainty	20 m + 10 % of depth	5 m + 5 % of depth	5 m + 5 % of depth	2 m
Depth – total vertical uncertainty	a = 1.0 m b = 0.023	a = 0.5 m b = 0.013	a = 0.5 m b = 0.013	a = 0.25 m b = 0.0075
Feature search	Not applicable	Not applicable	100 %	100 %
Bathymetric coverage	4 %	5%	100 %	100 %
Feature detection	Not applicable	Not applicable	Cubic features > 2 m in depths up to 50 m; 10 % of depth beyond 50 m	Cubic features > 1 m

Note: The use of coefficients a and b is as follows:

$$\pm\sqrt{[a^2 + (b * d)^2]}$$

where:

a represents that portion of the uncertainty that does not vary with water depth
b is a coefficient which represents that portion of the uncertainty that varies with water depth
d is the water depth
$b * d$ represents that portion of the uncertainty that varies with water depth.

© Fugro 1994-2020

Figure 1 illustrates the effect of coefficients a and b.

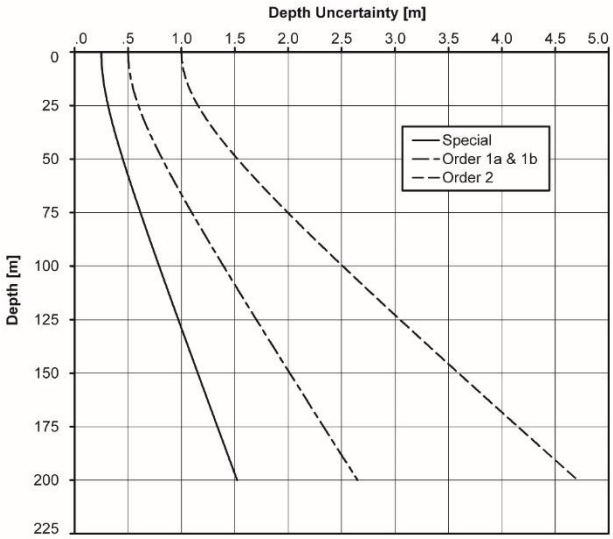

Figure 1: IHO water depth uncertainty

The IHO Special Order Survey is exceptional in geotechnical and/or environmental data acquisition. A Special Order system set-up may be comprised of: RTK DGPS; a multibeam echosounder; a motion compensator, and a conductivity temperature depth (CTD) probe. Subsurface positioning is uncommon in limited water depths.

An IHO Order 1a and 1b survey system set-up may include: high-accuracy DGPS; long baseline (LBL) subsurface positioning; a CTD probe with Digiquartz pressure sensor; a barometer; and a tide gauge.

IHO Order 2 surveys are common in geotechnical and/or environmental data acquisition. Such system set-ups could include: DGPS; ultra short baseline (USBL) subsurface positioning (IMCA, 2017); CTD probe; single beam echosounder or direct sounding by drill pipe; a motion compensator; and predicted tide correction.

These are examples of the simplest set-ups. Independent measurements are often made using a redundant system (IOGP, 2011; ISO, 2019). For example, surface position may be determined by two independent DGPS systems or direct sounding by drill pipe and echosounding.

ISO Classification for Seafloor Mapping

The International Organization for Standardization (ISO, 2019) defines three types of seafloor mapping:

- Reconnaissance seafloor mapping;
- Engineering seafloor mapping;
- Detailed engineering seafloor mapping.

The mapping types are primarily defined by cell sizes for digital terrain models.

ISO Depth Accuracy Classes

ISO (2014) provides depth accuracy classes, as shown in Table 2. These classes apply to depth below seafloor of a data point or measurement point acquired by borehole logging, in situ testing, and physical sampling and laboratory testing. ISO (2014) includes guidance on factors to consider for data point depth uncertainty. One of the factors is the position of a sample or test specimen within a sampler.

Class Z4 applies as default, except for samplers with no fixed seafloor reference, where Z5 applies as default.

Note that ISO (2014) uses accuracy class and application class interchangeably. A definition is given for application class and not for accuracy class. Application classes are defined in terms of "classification of equipment based on achievable level of accuracy". This is interpreted to mean achievable under favourable conditions.

Table 2: Depth Accuracy Classes for Data Point Measurements Relative to Seafloor

Depth Accuracy Class	Maximum Data Point Depth Uncertainty [m]
Z1	0.1
Z2	0.5
Z3	1.0
Z4	2.0
Z5	> 2.0

Guidance on use of Results

General

Use of results should consider that relatively complex uncertainty budgets (uncertainty estimates) can apply. Uncertainty budgets are typically project-specific, for example:

- Horizontal positioning of a tool at seafloor implies use of multiple instruments contributing to the uncertainty budget, e.g. (1) DGPS antenna position and (2) offset between antenna and actual position of the tool at seafloor;
- Soft soils can introduce uncertainty in underwater vertical position. A water pressure measurement tool mounted on an underwater frame may sink into the soil, thus affecting the measurement;
- Insufficient acoustic contrast between water and soft can affect echosounder water depth measurements;
- An irregular or sloping seafloor may affect echosounder measurements. An echosounder determines the earliest arrival of acoustic waves within the beam area. The highest points within the beam are assumed to correlate with the seafloor position, and thus yield the "water depth".

The following sections provide guidance.

Horizontal positioning:

- DGPS - antenna position uncertainty typically in the order of 1 to 2 metres.
- High accuracy DGPS - antenna position uncertainty typically in the order of 0.2 m.
- RTK DGPS – antenna position uncertainty typically in the order of centimetres.
- Gyro compass – uncertainty typically in the order of 0.5° to 1°.

DGPS uncertainty contributions include the geodetic network, vessel dynamics and antenna offset. Continuous logging on location allows some quantification of position uncertainty.

Subsurface positioning:

- LBL system: receiver position uncertainty typically in the order of 1 metre.
- USBL system: uncertainty of typically 0.5 m plus 1 % of distance between transducer and transceiver.

Uncertainty contributions include timing, ray bending, sound absorption, noise and offset.

© Fugro 1994-2020

Water Depth Measurement

Water depth measurement:

- Direct sounding by drill pipe: uncertainty of typically about 1 m plus 0.5 % of measured mean water depth.
- Echosounder: uncertainty of typically about 0.3 m plus 1 % of measured mean water depth.
- Digiquartz probe: probe position uncertainty of typically about 0.2 m plus 0.1 % of measured mean water depth.
- Motion compensator: heave measurements have a typical uncertainty of 0.05 m, and roll and pitch an uncertainty of about 0.1°, relative to the mounting of the unit itself.

The pressure sensor estimates are corrected for atmospheric pressure. The echosounder estimate typically incorporates CTD sound velocity checks, motion compensation, and transducer draught, including vessel squat correction. Vessel squat is a vertical displacement of the hull as a vessel moves, and is determined by water depth and the vessel shape and size. The direct sounding estimate includes uncertainties related to tape measurement, heave, drill pipe length variation due to self-weight and temperature change, drill pipe bending and offset from vertical axis.

Tide Correction

Tide correction:

- Predicted tides: correction uncertainty typically in the order of 0.2 m to 1 m, depending on tidal range and meteorological circumstances.
- High accuracy DGPS: antenna position uncertainty typically in the order of 0.1 m.
- Tide gauge: correction uncertainty typically in the order of 0.1 m.
- RTK DGPS: antenna position uncertainty typically in the order of 0.1 m.

Depth below Seafloor

Peuchen et al. (2005) present the following expression for depth uncertainty assessment for in situ testing, i.e. excluding considerations for sampling and laboratory testing:

$$\Delta z = \pm\sqrt{[a^2 + (b * d)^2 + (c * z)^2]}$$

where:

a	constant depth uncertainty, i.e. the sum of all uncertainties that do not vary with depth below seafloor in metres
b	uncertainty dependent on water depth, i.e. the sum of all uncertainties that are water depth dependent
c	uncertainty dependent on data point depth below seafloor, i.e. the sum of all uncertainties that are data point depth dependent
d	water depth in metres
z	data point depth in metres below to seafloor
Δz	data point depth uncertainty in metres (95 % confidence level)

Tables 3 to 5 present coefficients and accompanying premises.

Table 3: Coefficients for Data Point Uncertainty Assessment – In Situ Testing

Deployment System	Data Point Depth Uncertainty Δz		
	A	b	c
Vessel drilling – favourable	0.4 m	0.003	0.003
Vessel drilling – adverse	1.0 m	0.005	0.004
Non-drilling – favourable	0.2 m	0	0.01
Non-drilling – adverse	0.8 m	0	0.02
Note: resolution estimated at 50 % of uncertainty			

Table 4: Premise to Estimated Data Point Depth Uncertainty – In Situ Testing and Vessel Drilling Deployment

Characteristics	Marine Setting	
	Favourable	Adverse
Vessel - horizontal position	Variation within 5 m of target	Variation within 5 m of target
Vessel heave	1 m at "hook" point	3 m at "hook" point
Tidal variation	1.5 m, with correction for tidal variation by pressure sensor mounted on seabed frame	3 m, with correction for tidal variation by pressure sensor mounted on seabed frame
Seafloor	Firm and level	Very soft seabed soils or very rugged seafloor
Drill pipe checkpoint	Touchdown on seabed frame at borehole start	Touchdown on seabed frame at borehole start
Drill pipe bending	None	Minor
Borehole orientation	Vertical	Inclined at average 2° from vertical from sea level to test depth z

Table 5: Premise to Estimated Data Point Depth Uncertainty – In Situ Testing and Non-Drilling Deployment

Characteristics	Marine Setting	
	Favourable	Adverse
Vessel - horizontal position	Variation within 5 m of target	Variation within 5 m of target
Vessel heave	1 m at "hook" point	3 m at "hook" point
Tidal variation	1.5 m	3 m
Seafloor	Firm and level	Very soft seabed soils or very rugged seafloor
Orientation of Penetration	Vertical at start, with correction for measured inclination	Inclined at average 5° from vertical from seafloor to test depth z

Definition of seafloor is difficult for extremely soft ground. Reaction equipment may penetrate unnoticed into a near-fluid zone of the seabed. Settlement may also continue during testing (Bouwmeester et al., 2009).

Seabed frame settlement is likely to be governed by the following factors:

1. Descent velocity and penetration into seabed, including possible erosion (scouring) caused by seabed frame descent and resulting water overpressures.
2. Non-centric loading during touchdown and testing.
3. Variable on-bottom weight of reaction equipment, because of drilling, sampling and testing activities and because of tensioning and hysteresis forces in a heave compensation system.
4. Consolidation of seabed sediments.

References

Bouwmeester, D., Peuchen, J., Van der Wal, T., Sarata, B., Willemse, C.A., Van Baars, S. & Peelen, R. (2009). Prediction of

© Fugro 1994-2020

breakout forces for deepwater seafloor objects. In *OTC.09: Proceedings 2009 Offshore Technology Conference, 4-7 May, Houston, Texas, USA, OTC Paper 19925* *https://doi.org/10.4043/19925-MS*.

International Association of Oil and Gas Producers & IMCA International Marine Contractors Association (2011). *Guidelines for GNSS positioning in the oil & gas industry.* (Geomatics Guidance Note 19, IMCA S 015, IOGP Report No. 373-19) IOGP & IMCA

International Hydrographic Organization (2019). *IHO standards for hydrographic surveys (S-44)*. 6th ed. Draft 1.7.0. IHO

International Marine Contractors Association (2017). *Guidance on vessel USBL systems for use in offshore survey, positioning and DP operations* (IMCA M 244 (Rev 1)). IMCA (also IMCA S 017).

International Organization for Standardization (2014). *Petroleum and natural gas industries – specific requirements for offshore structures – part 8: marine soil investigations* (ISO 19901-8:2014). https://www.iso.org/standard/61145.html

International Organization for Standardization (2019). Petroleum and natural gas industries - specific requirements for offshore structures – Part 10: Marine geophysical investigations. (ISO/DIS 19901-10). https://www.iso.org/standard/77017.html

Peuchen, J., Adrichem, J. & Hefer, P.A. (2005). Practice notes on push-in penetrometers for offshore geotechnical investigation. In S. Gourvenec and M. Cassidy (Eds.) *Frontiers in offshore geotechnics ISFOG 2005: proceedings of the first international symposium on frontiers in offshore geotechnics, University of Western Australia, Perth, 19-21 September 2005.* (pp. 973-979). Taylor & Francis.

© Fugro 1994-2020

APPENDIX D: SUPPLEMENTARY INFORMATION ABOUT DOCUMENT

CONTENTS

Quality Management Record
Document Issue Record

QUALITY MANAGEMENT RECORD

Report Approval: J. Peuchen
Principal Geotechnical Engineer
and Manager of Engineering

Key team members

Organization	Name	Qualifications	Specialty
FUGRO	Joek Peuchen	Principal Engineer	Integrated marine site characterisation, geology, geophysics, geotechnical engineering
	Roeland Nieboer	Research Geophysicist	Seismic data acquisition, processing and inversion
	Bogusia Klosowska	Principal Geologist	Lead geologist in complex integrated geological, geophysical and geotechnical studies
	Wessel van Kesteren	Principal Geologist	Lead geologist in complex integrated geological, geophysical and geotechnical studies
	Alexandra Cristobal Huerta	Data Scientist	Data sciences, machine learning, data conditioning
TNO innovation for life	Bart Meijninger	Senior Geologist	Geology and geo-statistics; nearshore and offshore site investigations
	Vincent Vandeweijer	Senior Geophysicist and Project Manager	Geology, Geophysics and Project management. High resolution seismic, advanced seismic processing,
	Stefan Carpentier	Senior Geophysicist	Seismic imaging and 4D problems through migration and inversion, machine learning
	Bob Paap	Senior Geophysicist	Integration of geophysical observations with simulations for developing a comprehensive understanding of geological setting and subsurface processes
	Boris Boulanger	Senior Geophysicist	Seismic imaging, deep learning, machine learning
TU Delft Delft University of Technology	Michael Hicks	Professor of Soil Mechanics and Head of Geo-Engineering	Finite elements methods, constitutive modelling, heterogeneity, static liquefaction, strain localisation, stochastic analysis, adaptive mesh refinement and the material point method

DOCUMENT ISSUE CONTROL

Section	Page No.	Plate No.	Issue	Revision
Main Text	All		2	Editorials
Appendix B	All		2	Editorials
Appendix B	10		3	Update figure numbering in Section 2.1
Appendix B	17		3	Update figure numbering in Section 2.3.4
Appendix B	21		3	Update figure numbering in Section 3.1

1) The definitive copy of this document is held in Fugro's information system
2) Document distribution is restricted to project participants approved by the client
3) The *document* issue number is the same as the highest issue number of any individual page
4) Pages of this document are at Issue 1, except those pages listed above
5) The reference at the bottom left-hand corner of each page shows the Fugro document ID and the page issue number (between brackets)

The creative commons license terms 4.0 CC BY apply to this material.
Please take notice of the general terms "Creative Commons Attribution 4.0 International public License" before starting to use the license. These terms can be accessed by clicking on this link https://creativecommons.org/licenses/

This investigation was carried out by Fugro, commissioned by RVO, an agency of the Ministry of Economic Affairs and Climate Policy.

Whilst a great deal of care has been taken in compiling the contents of this investigation, RVO can not be held liable for any damages resulting from any inaccuracies and/or outdated information.

The information in this document is valid at the time of publishing (see month/year). Updates will be published on the website https://offshorewind.rvo.nl/ at the relevant sitemap (Hollandse Kust (west), General Information, submap Revision Log and Q & A. In the Revision Log is indicated which versions are the latest and what the changes are in relation to previous versions. The documents can be found at the relevant sites, indicated in the List of all reports and deliverables.

Contacts
Netherlands Enterprise Agency (RVO)
Croeselaan 15 | 3521 BJ | Utrecht
P.O. Box 8242 | 3503 RE | Utrecht
www.rvo.nl / https://english.rvo.nl

Netherlands Enterprise Agency (RVO) | October 2020